RESONANT COUPLING ENERGY TRANSMISSION TECHNOLOGY AND ITS APPLICATIONS TO IMPLANTED MEDICAL DEVICES

WANG Junhua

Ph.D

The Hong Kong Polytechnic University

2012

The Hong Kong Polytechnic University
Department of Electrical Engineering

RESONANT COUPLING ENERGY TRANSMISSION TECHNOLOGY AND ITS APPLICATIONS TO IMPLANTED MEDICAL DEVICES

WANG Junhua

A thesis submitted in partial fulfillment of the requirements for the degree of Doctor of Philosophy

August 2011

CERTIFICATE OF ORIGINALITY

I hereby declare that this thesis is my own work and that, to the best my knowledge and belief, it reproduces no material previously published or written or material which has been accepted for the award of any other degree or diploma, except where due acknowledgement has been made in the text.

__________________________(Signed)

___WANG Junhua____________(Name of student)

ABSTRACT

Due to the development of power electronics and magnetic materials, replacing conventional wire energy transmission in electrical power systems with non-contact, inductive couplings becomes possible. The technology of transferring energy through electromagnetic field opens the door to a new age of rotating, sliding, and separable couplings. Inductive couplings can offer safe, reliable, and efficient power transmission that is largely immune to the effects of wear and the environment.

Inductive charging transfers energy from the transmitter to the receiver by inductive coupling. A transmitter sends energy through inductive coupling to an electrical device, and then the energy is stored in the batteries. Because there is a gap between the two transmitting and receiving coils, inductive charging falls into one kind of certain-distance wireless energy transfers. The implanted medical devices, including cardiac pacemaker and cardioverter defibrillator, are now increasingly being used in the therapeutic treatment for cardiac arrests. However the power supply arrangement, hitherto, of the implanted medical devices are far from satisfactory.

A new technology called witricity for wireless energy transmission over a fair distance as reported by Massachusetts Institute of Technology (MIT) in July of 2007 provides a new possibility to overcome the above difficulties. The method is based on the well known principle of resonant coupling, which stipulates the coupling between the resonant objects of the same resonant frequency, while reduces the coupling with other off-resonant environmental objects. However, the MIT's receiver has the same size as the transmitter (with a diameter of 600 mm). In implanted medical devices, the receiver must be very small in order to be implanted and housed within the patients' thoracic cavity. In the MIT design, the receiver size cannot be scaled down easily because the receiver dependents on the distributed

capacitance of the coils. Therefore, there are many challenges in the applications of this basic theory to implanted medical devices.

This thesis intends to develop a wireless energy transmission system based on witricity technology for powering and recharging the implanted medical devices. A resonant coupling energy transmission system which is specially designed for implanted medical devices is thus proposed with different geometry structures including circular coil, ring-shaped coil, and rectangular coil have been designed.

Special coils with the same resonant frequency of the transmitter and the receiver have been fixed that the energy transmission efficiency can be greatly increased and the size of the receiver is substantially reduced. Electromagnetic field and electric circuit coupled models have been built based on Ansoft HFSS and Ansoft designer. The experimental prototypes have been constructed to test the performances of the witricity energy transfer system.

In the thesis, three practical witricity systems with different geometry structures have been designed specially for electrical devices. We used the developed program and numerical models to capture the entire behaviors of the system from transmitter to receiver including the power source circuit and charging circuit through co-simulation with the electromagnetic field. The experimental prototypes for the study of electrical energy delivery between an electric implant and an external charger have been constructed. The new energy transmission system has high efficiency, long transfer distance, good robustness, low insensitivity to misalignment and line-of-sight interruption. In vitro performance tests have been realized using a physical thorax phantom to verify its effectiveness.

LIST OF PUBLICATIONS DURING PHD DEGREE

Twelve Journal Papers:

1. *Junhua Wang**, Jiangui Li, S. L. Ho, W. N. Fu, Zhigang Zhao, Weili Yan, and Mingui Sun, "Analytical study and corresponding experiments for a new resonant magnetic charger with circular spiral coils," *Journal of Applied Physics*, 111, 07E704 (2012).
2. *Junhua Wang**, S. L. Ho, W. N. Fu, and Mingui Sun, "FEM simulations and experiments for the advanced witricity charger with compound nano-TiO_2 interlayers," *IEEE Trans. Mag.*, vol. 47, no. 10, pp. 4449-4452, 2011.
3. *Junhua Wang**, Youhua Wang, S. L. Ho, Xiaoguang Yang, W. N. Fu and Guizhi Xu, "Design and FEM analysis of a new distributed vernier traveling wave induction heater for heating moving thin strips," *IEEE Trans. Magn.*, vol. 47, no. 10, pp. 2612-2615, 2011.
4. *Junhua Wang**, S. L. Ho, W. N. Fu, and Mingui Sun, "Analytical design study of a novel witricity charger with lateral and angular misalignments for efficient wireless energy transmission," *IEEE Trans. Magn.*, vol. 47, no. 10, pp. 2616-2619, 2011.
5. Youhua Wang, *Junhua Wang**, Lingling Pang, S. L. Ho, and W. N. Fu, "An advanced double-layer combined windings transverse flux system for thin stripinduction heating," *Journal of Applied Physics*, 109, 07E511 (2011).
6. Youhua Wang, *Junhua Wang**, S. L. Ho, Lingling Pang, and W. N. Fu, "A neural network combined with 3-D FEM applied to optimize eddy current and temperature distributions of travelling wave induction heating system," *Journal of Applied Physics*, 109, 07E522 (2011).
7. S. L. Ho, *Junhua Wang**, W. N. Fu, and Mingui Sun, "A novel resonant inductive magnetic coupling wireless charger with TiO_2 interlayer," *Journal of Applied Physics*, 109, 07E502 (2011).
8. *Junhua Wang**, S. L. Ho, W. N. Fu, Tsz Kit Cheung, and Mingui Sun, "Finite element analysis and corresponding experiments of resonant energy

transmission for wireless transmission devices using witricity," *IEEE Trans. Mag.*, vol. 47, no. 5, pp. 1074-1077, 2010.

9. S. L. Ho, *Junhua Wang**, W. N. Fu, and Mingui Sun, "A comparative study between witricity and traditional inductive coupling in wireless energy transmission," *IEEE Trans. Ma*g., vol. 47, no. 5, pp. 1522-1525, 2010.
10. *Junhua Wang**, S. L. Ho, W. N. Fu, and Y. H. Wang, "Design and analysis of a novel traveling wave induction heating system with magnetic slot wedges for heating moving thin strips ," *IEEE Trans. Mag.*, vol. 20, no. 6, pp. 2175-2178, 2010.
11. S. L. Ho, *Junhua Wang**, W. N. Fu, and Y. H. Wang "A novel crossed traveling wave induction heating system and finite element analysis of eddy current and temperature distributions," *IEEE Trans. Mag.*, vol. 46, no. 10, pp. 4777-4780, 2009.
12. *Junhua Wang**, Jiangui Li, S. L. Ho, W. N. Fu, and Mingui Sun, "Analytical study of a novel PCB circular spiral witricity charger with lateral and angular misalignments analysis," *IEEE Trans. Mag.*, 2012. **(in press)**

One book chapter:

Book: Youhua Wang, *Junhua Wang**, S. L. Ho, and W. N. Fu. One Chapter "Two Novel Induction Heating Technologies: Transverse Flux Induction Heating and Travelling Wave Induction Heating," for *Advances in Induction and Microwave Heating*, 978-953-7619-X-X. INTECH, 2010.

ACKNOWLEDGEMENT

I wish to express my sincere gratitude and appreciation to my chief supervisor Dr. W. N. Fu, for his invaluable guidance, his patience and constant encouragements throughout the challenging path towards a doctoral degree. His enthusiasm and guidance were strong sources of inspiration for me.

I would like to thank my co-supervisor, Professor S. L. Ho, the head of the Department of Electrical Engineering, the Hong Kong Polytechnic University, for his kind support, his valuable comments and discussions on my research project.

I am grateful to my oversea supervisor, Professor Mingui Sun, Bioengineering and Electrical Engineering, Pittsburgh University, USA. His guidance, encouragement and continuous help greatly supported me to finish the project on time during my study in USA.

I gratefully thank the Neurological Surgery team members in Pittsburgh University, USA. I had a very good time there. And I acknowledge to all staffs of the Department of Electrical Engineering in the Hong Kong Polytechnic University for their kind support and help.

Special thanks to my parents for their deep love and encouragement in my life. They are always being supportive.

And I want to offer my deepest thanks to my wife LI Jiangui, Gina. She has contributed much more to my thesis than she can imagine.

The last but not the least, thanks a lot to the financial support provided by a grant from the Hong Kong Research Grants Council (Project No. PolyU 5184/09E).

TABLE OF CONTENTS

LIST OF FIGURES

LIST OF TABLES

CHAPTER 1 INTRODUCTION

1.1 Background and Motivation

To charge a rechargeable battery of electrical device, the most frequently used method is utilizing a traditional charger. However, the traditional plug and socket charging method cannot satisfy the requirements of consumers for safety and fast charging. Traditional chargers have many disadvantages owing to the charger must be physically connected to the load and the charging contacts can be broken or easily interrupted.

Thanks to the development of power electronics, inductive charging, also known as wireless charging, has found much successes and is now receiving more and more attention by merits of its simplicity and efficiency. The most important and distinctive difference between a contactless transformer and a conventional transformer in structure is that the two ‘coils’ in the former one are separated by a large air gap.

To overcome the aforementioned drawbacks, increasing attentions in wireless charging have reemerged [1-4]. The traditional way in wireless energy transfer is through magnetic coupling using a transformer which has a primary coil and a secondary coil. When ac power is applied to the primary coil, ac voltage is induced in the secondary coil through mutual inductance.

Compared with plug and socket (i.e. conductive) charging, the main advantage of the inductive charging approach is that the system can work with no exposed conductors, no interlocks and no connectors, therefore the system can work with much lower risk of electric shock hazards. Because of the charging system is often fully enclosed, wireless charging can be realized in waterproof packages and as such, wireless charging is attractive in situations at which rechargeable devices need to be frequently used near or even in the water as well as in humid conditions. It is also a very attractive option in the medical field when the replacement of batteries for implanted devices is very costly. The risk due to surgical operations is highly reduced if the batteries for the implant devices can be charged externally through wireless charging techniques. After years of effort, wireless charging technology has achieved major breakthroughs both in theory and in practice [5, 6]. Hitherto, most researches focus on mobile devices, especially those who work in harsh operating environment/conditions, such as in electric vehicles, trucks, cranes, underwater or underground equipments [4].

However, there are two major disadvantages of magnetic coupling in wireless power transfer technology regarding physical sizes. Indeed, if the size of the receiver is reduced, the magnetic flux linked to the secondary coil is greatly reduced. In order to ensure the magnetic flux is high enough for efficient energy transfer, a large current must flow in the primary coil. Nonetheless, even if an impractically larger power supply is provided to the device, the transmitting distance is still very short (less than 10 cm) and the efficiency is very low (about 0.01%). Hence magnetic coupling is not practical and not suitable in real-life engineering applications.

Physical separation between the primary and secondary windings incurs proximity-effect winding losses. Weak coupling can result in poor transmission performance and low efficiency. Due to the large air-gap between the primary and secondary windings, contactless transformers have large leakage inductances, small mutual inductance and low efficiency [1-6]. Compared to direct contact charging, inductive charging efficiency is lower and resistive heating is higher. Realization of low frequency inductive charging in electrical devices lead to slow charging and heat generation.

Witricity (short form of wireless electricity), a new resonant coupling energy transmission technology, was reported by a Massachusetts Institute of Technology (MIT) research team in 2007 to transmit power wirelessly over a long distance, which has the order of several times of the physical size of the transmitter/receiver, based on strongly coupled magnetic resonance [7, 8]. Instead of spreading radiative and lossy electromagnetic fields to the environment, the source resonator fills the surrounding with lossless, non-radiative magnetic fields oscillating at MHz frequencies. The non-radiative fields allow efficient power transmission between the source and the device resonators. The resonant essence of the process ensures that the interaction between the source and device is adequately strong and the interaction with non-resonant objects is minimal. In this way, an efficient wireless energy-transmitting channel can be established.

1.2 Research goals, New Contributions, and Methodology

1.2.1 Research Goals

1. The primary goal of this project is to develop a resonant wireless energy transmission system for recharging implanted medical devices. It is based on the witricity principle and has the feature of high energy transfer efficiency.

2. Study the basic principles about the witricity technology with the help of others related works, corresponding simulations and preliminary experiments.

3. To develop accurate numerical models of the proposed implanted medical recharging system using commercial Ansoft HFSS for design validation.

4. To evaluate the performances of the implanted medical recharging system by experiments. Prototypes are fabricated according to the results of the analysis results and are constructed to carry out experiments of electrical energy transmission among the external transmitter coil and the receiver coil.

1.2.2 New Contributions

1. According to the specifications of energy storage and space available, initial implanted medical systems with different geometry structures including round coil,

ring-shaped coil, rectangular coil, thin film coil and array-combination coil have been designed specially for implanted medical devices. Several methods have been utilized to increase the product of the inductance and the capacitance values in the LC tank.

2. An electromagnetic field and electric circuit coupled method for studying witricity devices has firstly developed for high-frequency problems based on Ansoft HFSS and Ansoft designer. When the applied voltage to the transmitter coil is given, the electromagnetic field in solution domain, the currents in the transmitter coil and receiver coil can be directly computed. Then the input power, the output power and the efficiency can be calculated.

3. We used the developed program and numerical models to capture the entire behavior of the system from transmitter to receiver including the power source circuit and charging circuit through co-simulation with the electromagnetic field.

4. Some experimental prototypes for the study of electrical energy delivery between an electric implant and an external charger have been constructed. A variety of witricity energy transfer coils have been constructed to test the performance of the witricity energy transfer system.

5. Three novel chargers, based on coupled mode theory, microwave network theory and witricity technology, have been fabricated for cell phone charging, rats' experiment playground and especially the charger for DBS discussed in Chapter 5.

1.2.3 Methodology and Specific Phases

According to the specifications of energy storage and space available, initial implanted medical systems with different geometry structures including round coil, ring-shaped coil, rectangular coil, thin film coil and array-combination coil have been designed. Each type of the coils can also have different geometrical and electrical parameters.

We have constructed several prototypes of the witricity cell with different coil dimension. As the fundamental witricity theory requires identical resonant frequencies of the transmitter and the receiver, it would therefore be easy for design if the physical sizes of them are comparable. However, for implanted medical devices, the receiver has a much smaller physical size than the transmitter and hence some design studies need to be carried out.

In order to satisfy the fundamental requirement, we utilized several methods to increase the product of the inductance and the capacitance values in the LC tank. We used the entire circumference of the ring-structure to maximize the capacitance value. A gap is intentionally formed within each of the two conductors to break the harmful loop current.

For the convenience of evaluating the resonant frequency, the resonant frequency of the transmitter can also be adjusted by changing the inductance value of the coil. This function has been achieved by increasing the turns of the transmitter coil. In order to reduce the resistance within the LC tank of the receiver, a solid copper and/or silver wire are used to construct the coil and a thicker copper and/or silver strip have been also used to form the conductors within the capacitor. As in the transmitter case, the

LC loop resistance can be reduced by eliminating the wiring connections.

To make the system operate at its highest efficiency, many factors, such as the distributed parameters, geometric shapes and dimensions, material properties, and physical arrangements of the components have been determined precisely.

We used commercial Ansoft HFSS (High Frequency Structure Simulator). It can solve 3-D high-frequency electromagnetic field in frequency domain using Finite Element Method (FEM). It supports parameterized geometry so the dimensions can be swept or optimized. It can compute the s-parameters and resonant frequency directly. Numerical models based on HFSS software for the EM field computation have been built. Since the study of the witricity requires high-frequency analysis involving displacement current and skin conduction effects, full-wave 3-D EM fields in the transmitter, the receiver and the regions around them have been computed. According to the s-parameters of the input port of the transmitter coil and the output port of the receiver coil, an equivalent impedance matrix is obtained. Then an equivalent circuit has been established and the currents in the transmitter coil and the receiver coil was computed. With the numerical models, the design has been studied by means of repeatedly varying the dimensional and structural parameters and comparing the simulation results.

The simulation has been repeated to study the effects on different dimensional and structural parameters to evaluate and compare different design schemes, different physical sizes, different components and materials in order to verify the system performance further.

In the stage of refined design, we carefully analyzed the system and tried to improve its overall performance. As is well-known, the Q value is an important factor in evaluating the energy losses. In order to improve the Q value, the spiral inductor is modified to have either symmetric or step width or patterned floating structures as alternative designs. Copper and/or silver wires have been used for the inductors to maximize their conductance. In order to reduce the resistance in the LC resonant tank further, one can eliminate the traditional wire connections between the inductor and the capacitor using an integrated structure.

An experimental DBS prototype for the study of electrical energy delivery between an electric implant and an external charger has been constructed in Chapter V. This prototype can geometrically resemble the actual situation, simulates the geometry and electrical properties. Each receiver has a volume of approximately a few cm^3 for implementation. It contains an energy receiver and a rechargeable lithium-ion polymer battery for energy storage. An external single coil with large size might be added to increase the energy transmission distance and efficiency. It can also help to reduce the size of the receiver coil.

During the evaluation, the rechargeable battery is put into the prototype model. The external witricity transmitter was placed at different distances and angles from the prototype, and the system performance parameters, including the energy transmission efficiency and Q-factors, have been measured and compared to the results obtained from computer simulation. The relationship among the efficiency of the system, the distance between the transmitter and the receiver are nonlinear. All these have been simulated and tested.

The proposed research project generated a lot of useful knowledge. The final stage of the project involves the collection of results, report on the findings and dissemination of this knowledge to the outside world. The findings of this project, including (i) the modeling, simulation of the implanted medical energy system; (ii) the design program of the transmitters and receivers; (iii) the structures of the novel two-stage energy deliver system; the construction and manufacturing of the devices, and the (iv) overall performance of the device, are extremely useful to both academics and industrial practitioners.

1.2.4 Thesis Organization

The thesis is formed by six text chapters with the abstract, publication list, and the reference. It has been organized as follows.

Chapter 1: Introduction. Chapter 1 provides a background and motivation in terms of witricity study. The research goals, new contributions, and methodology of the research work are also described. The purpose of this chapter is to provide general information about the historical background, as well as what we plan to do and how to do the project in this thesis.

Chapter 2: Literature review of the wireless power transmission technology and the witricity technology, including kinds of power transfer technologies and the developments of wireless energy transmission. Chapter 2 provides an introduction to the working principles of the traditional wireless power transmission technology and witricity for charging electrical devices. Conventional modeling and design approaches are described.

Chapter 3: System Theory &Coupling. Inductance and coupling study has been illustrated in this chapter. Self-inductance, mutual-inductance and coupling coefficiencies for both circular and rectangular coils have been studied. Then coupled-mode theory for resonant couplers is discussed for guiding the corresponding simulation and experiment model designs.

Chapter 4: System Performance and Verification. Witricity transfer with rectangular coils is studied further, including the typical systems, lateral and angular misalignment analysis, and the novel one with TiO_2 compound interlayer. Then we have analyzed the performances of the witricity transfer with circular coils. The output voltages and power, the efficiency, and the model with lateral and angular misalignments have been studied.

Chapter 5: Witricity Charger for Implanted Deep Brain Stimulation (DBS). Wave network theory has been introduced. Based on it and the witricity concept, one application for charging DBS is proposed and studied through simulations and experiments. The performance of the system is analyzed and the design of the structure parameters is discussed. Experimental results are presented to evaluate the performance of the derived prototype. Also, the electric distributions in the head phantom have been illustrated through FEM simulation to verify that the magnetic flux created when charging is safe to the human beings.

Chapter 6: Conclusion and future work. Chapter 6 concludes the whole thesis. A summary of the completed tasks are given. Further development and potential research areas are also discussed.

CHAPTER 2 LITERATURE REVIEW

2.1 Introduction

In 1825, William Sturgeon devised the electromagnet by wrapping a conducting wire around an iron core. The principle of EM induction which was discovered by Michael Faraday in 1831, he argued that a changing magnetic field can induce an electrical current in an adjacent wire. Nicholas Joseph Callan combined these two discoveries together, and he firstly demonstrated the transmission and receiving of electrical energy without wires. Callan's 1836 induction coil apparatus consisted of two insulated coils which is called the primary and secondary windings, both placed around a common iron core. By intermittently connecting a battery to the primary coil, a voltage in induced in the longer secondary causing a spark to jump across its free terminals [15].

The energy transmission takes place by simple electromagnetic coupling through mutual induction in induction coils or electrical transformers, which can have either iron core or air core. In this way, it can transmit and receive energy over a considerable distance. However, to draw significant power with this method, the two inductors must be placed close with each other. Resonant can be used to solve this problem, where inductors are tuned to a mutual frequency, then significant power may be transmitted over many meters away [9-17].

James Clark Maxwell modeled the behavior of electromagnetic radiation mathematically in 1864. Heinrich Hertz had made some early work in the area of wireless transmission via radio waves in 1888 and he also performed experiments that validated Maxwell’s mathematical model. Hertz’s apparatus for generating electromagnetic waves is acknowledged as the first radio transmitter generally. After a few years Guglielmo Marconi worked with a modified form of the Hertz-wave transmitter, the main improvement is the addition of an elevated conductor and a ground connection. To assign the origin of these elements, it is the 1749 work of Benjamin Franklin and Mahlon Loomas in 1864 [15].

Nikola Tesla also investigated radio transmission and reception, Tesla designed his own transmitter which is different from Marconi. It is a transmitter with power-processing capability some five orders-of-magnitude and it is greater than those of its predecessors. And also, he would use this same coupled-tuned-circuit oscillator to implement his conduction-based wireless energy transmission method. Both of these wireless methods use a minimum of four tuned circuits, two at the transmitter and two at the receiver.

2.2 Developments of Wireless Energy Transmission

Many researchers have experimented with the design of Tesla's wireless energy transmission system and made observations that may be inconsistent with a basic tenet of mainstream physics which are presently considered to be nonphysical [18-34].

The Tesla wireless energy transmission system combines electrical power transmission together with broadcasting and wireless telecommunications, and it did not need most of the existing power transmission lines, the electrical generation plants.

One of Tesla's patents [35] said he may have proposed a 25–70 km nodal structure along with lightning observations in his 1899 Colorado Springs experiments in terms of propagating standing waves. That system would replace the local interference of direct and reflected waves involving a nearby mountain range, or between the ground and the ionosphere.

At that time, Tesla did not know many properties of the earth-ionosphere cavity that have subsequently been given in great details, and the earth-ionosphere or concentric spherical shell waveguide propagation parameters. As we know today, it is not realizable that wireless energy transfer by direct excitation of a Schumann cavity resonance mode [36]. *"The conceptual difficulty with this model is that, at the very low frequencies that Tesla said that he employed (1-50 kHz), earth-ionosphere waveguide excitation, now well understood, would seem to be impossible with the either the Colorado Springs or the Long Island apparatus (at least with the apparatus that is visible in the photographs of these facilities)"* [37].

On the other hand, Tesla's concept of a global wireless power transmission grid and telecommunications network based on energy transmission by means of a spherical conductor transmission line with an upper half-space return circuit is not practical but feasible, defying no law of physics. Wireless energy transmission by a spherical conductor "single-wire" surface wave transmission line may be possible, a feasibility study using a sufficiently powerful and properly tuned Tesla coil earth-resonance transmitter being called for.

2.2.1 Traditional Magnetic Inductive Coupling Wireless Power Transmission Technology

Induction chargers create an alternating electromagnetic field by using induction chargers from within a charging base station, and a secondary induction coil in the portable device absorbs power from the electromagnetic field and transforms it back into electrical current to charge the battery. The two induction coils in proximity combine to form an electrical transformer [39, 40]

Inductive charging have no exposed conductors, it takes a much lower risk of electrical shock when compared with conductive charging. Water impermeability is essential here, so the ability to fully enclose the charging connection also makes the approach attractive. For example, inductive charging is used for implanted medical devices that periodic or even constant external power is required, and for electric hygiene devices, they are frequently used near or even in water. Instead of having to connect a power cable, the device of inductive charging can be placed on a charge plate, it makes charging mobile devices more convenient [41].

Compared with direct contact, one disadvantage of inductive charging is its lower efficiency and increased ohmic (resistive) heating. Implementations which use lower frequencies or older drive technologies charge more slowly and generate heat for most portable electronics, however, the technology is commonly used in some electric toothbrushes and wet/dry electric shavers, partly for the advantage that the battery contacts can be completely sealed to prevent exposure to water. Inductive charging also requires drive electronics and coils that increase manufacturing complexity and cost [39, 40].

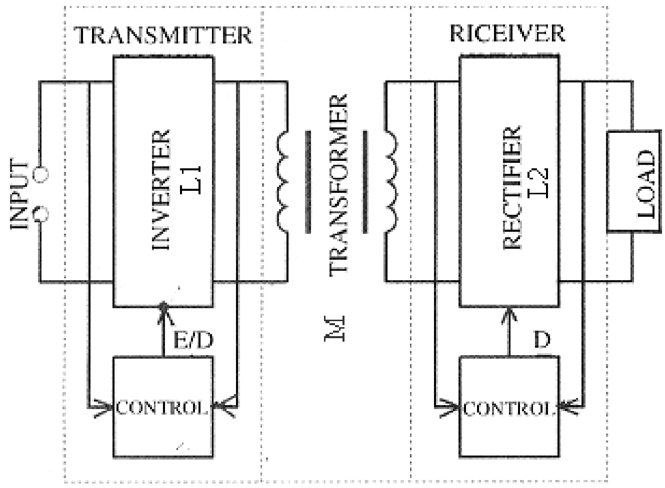

Fig. 2-1 Magnetic inductive coupling

The dominant method in wireless power delivery and communication is the magnetic inductive coupling currently. The primary and secondary circuits of a transformer are not connected directly. The transfer of energy happens by electromagnetic coupling through a process which is called as mutual induction. (An added benefit is the capability to step the primary voltage either up or down.) One example of the use of this principle is that the battery chargers of a mobile phone or the transformers in the street. A transformer-like device consisting of a primary coil and a secondary coil is used (see Fig. 2-1). When an RF signal is applied to the primary coil L_1, current is induced in the secondary coil L_2, through mutual inductance M.

This power wireless transmission mode is based on the modern power electronic energy conversion technology and control theory and electromagnetic induction coupling theory. The non-physical connection for the energy transmission is called "wireless electricity." To achieve the safety, reliability, flexibility and efficiency, it is important to overcome the electric shock, sparks, wear and tear and other defects in energy transfer process of traditional mode of power supply wire. The main disadvantage of coupling induction is the short range. Because of the limitations, the depth and the breadth of current research mainly confined to the smaller power capacity and short-distance researches. So how to increase its power transmission capacity, efficiency, distance, and how to prevent electromagnetic interference become more important, and need to have a further study.

Electric toothbrushes appeared as early as in mid-70s of the 20th century. After that, several U.S. patents were issued for such devices [42, 43] which belongs to discrete wireless power transmission system. When the toothbrush is not in use, cup-shaped base transfers energy to the toothbrush through electromagnetic induction, and this is the process of the battery charging. As the toothbrush should be regularly exposed to water and dust during the wireless energy charging process, there is no contact with bare conductors, it greatly improves the reliability of electric toothbrushes and security. This is the wonderful application for the inductive coupling technology. The toothbrush and other inductive coupling electric devices have been shown in Fig. 2.

At present, there are more research institutes and companies are studying in this area. The identical representative institution for this research is the Power Electronics Research Center, Electronics and Electrical Engineering, University of Auckland, New Zealand. The center mainly focuses on wireless sliding power transmission system studies [44] since the early 90s of the 20th century.

Newer approaches diminish the transfer losses and provide chargers and receivers that are compact, efficient and can be integrated into mobile devices or batteries with minimal change by using ultra thin coils, higher frequencies and optimized drive electronics. [45].

The technology has won some patents for this invention and has achieved important developments both in theory and in practice after 10 years of effort [46-57]. Most researches concentrate on mobile devices, especially in the harsh environment, such as electric vehicles, cranes, trucks, as well as underwater, underground equipments. Currently the technology has been successfully extended to Japan, Germany, the United States [49] and so on.

Fig. 2-2. Inductive coupling electric devices [42, 43]

An electrical distribution system which is based on this method would eliminate the requirement for an inefficient, costly, and capital intensive grid of cables, towers, and substations. The advantages of this system are reducing the cost of electrical energy used by the consumer and ridding the landscape of wires, cables, and transmission towers. There are some areas in the world where the needs for electrical power exists, yet there is no proper method for delivering power and the wireless transmission will solve many of these problems.

The electrical energy can be transmitted without wires economically, so it can help to reduce the loss of transmission and distribution to a great extent. Regarding to the new systems, the market is enormous, because more efficient energy distribution systems and sources are needed by both developed and under developed nations. The increasing demands for electricity in industrial nations are well documented. It has the potential to become a multi-billion dollar per year market.

But due to the weak coupling between the primary and secondary coils, this simple magnetic coupling method has a major shortcoming that the efficiency in power delivery is generally poor (see Fig. 2-1) [58]. This is because intracranial neural implants must be small, limiting the size of the secondary coil. As the coil size decreases, there is a rapid decline in magnetic flux captured by the secondary coil. So, a large current must be delivered to the primary coil to maintain a sufficient amount of power transfer. But this may not so practical, because an external battery must be carried by some patients at all times.

This is an unacceptable scenario in engineering design that when the distance between the two coils increases further, the efficiency becomes so low that even a large external battery becomes impractical. For example, with the choices of typical coil geometries, with a 20 cm coil separation, the power transmission efficiency drops to approximately 10^{-6}, requiring an external power of approximately 1 KW to deliver only 1 mW of power to the implanted device.

The possible biological effect is one criticism of the wireless power system Calculating the circulating reactive power, it was found that the frequency is very small and it is very biologically compatible [59].

2.2.2 The Electromagnetic Resonant Wireless Power Transmission Technology

A new wireless powering technique, called witricity (short form of “wireless electricity”), was reported in *Science* in 2007 by a *MIT* research team, which can wirelessly transmit power over a distance based on strongly coupled magnetic resonance, where the distance between the transmitter and the receiver is larger than several times of the size of the device. At this range, the efficiency of the traditional transcutaneous energy transformer method is very low because the receiver can only collect a very small portion of the transmitted energy. As shown in Fig. 2-3, their witricity system consists of two resonant devices (“Source” and “Device”), a driving loop and an output loop. In their primitive experiments, a 60W light bulb was illuminated wirelessly from a power source more than seven feet away, with an incredibly high efficiency of 40%, which is about one million times higher than that realized using traditional transformer method [60]. The *MIT* group devised a clever method by filling the space around the transmitter with a lossless “non-radiative” field oscillating at mega Hertz frequencies, which differs from the traditional lossy “radiative” field. The energy can be drawn from the non-radiative field efficiently if an object is resonating with the transmitting object. Despite the significant power transfer performance, witricity is shown to be safe for humans and insensitive to line-of-sight interruptible and misalignment of the primary and secondary coils. The discovery of witricity is a significant event because it is the first feasible technique to make possible wireless, efficient and omni-directional midrange energy transfer.

It must be pointed out that this novel scientific breakthrough originates from the well-known concept of resonance. Mechanically, it is known that a team of soldiers must break step when marching over bridges to avoid possible collapse due to resonance. Acoustically, an opera singer singing loudly within a room may break a wine glass if the resonant frequencies of the acoustic wave and the intrinsic frequency of that glass match. Electrical engineers have known for over a century to use resonant circuits in both the primary and secondary sides of a transformer to maximize alternating signal reception. However, the use of resonant coupling in a non-radiative transmitter [26] field for wireless electric power transfer, over a distance, is a novel concept which has great potential applications.

In order to explain further how witricity works, we examine a simulation performed by Soljacic [26, 60] where a pair of dielectric disks forms a witricity system as shown in Fig. 2-4. At the start of energy transfer, only the *Source* produces electric field (left panel). Since the *Device* has the same resonant frequency as the *Source*, it is driven by the *Source* and starts to resonate. The electromagnetic field produced by the *Device* enhances the field produced by the *Source*, which then further couples with the *Device*. This positive feedforward /feedback process continues until the resonance between the *Source-Device* pair reaches the maximum amplitude. At this point a strong link for wireless energy transfer is established by means of a non-radiative field between the transmitter and receiver. This active feature represents a fundamental difference from the traditional methods.

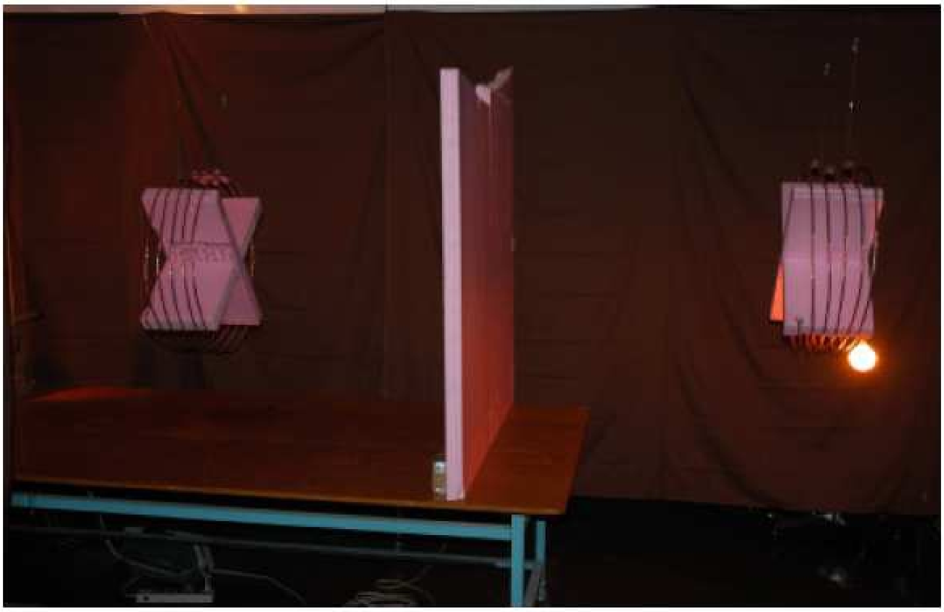

Fig. 2-3. A witricity experiment at MIT which powered a 60-Walt bulb two meters from a wireless transmitter [26, 60]

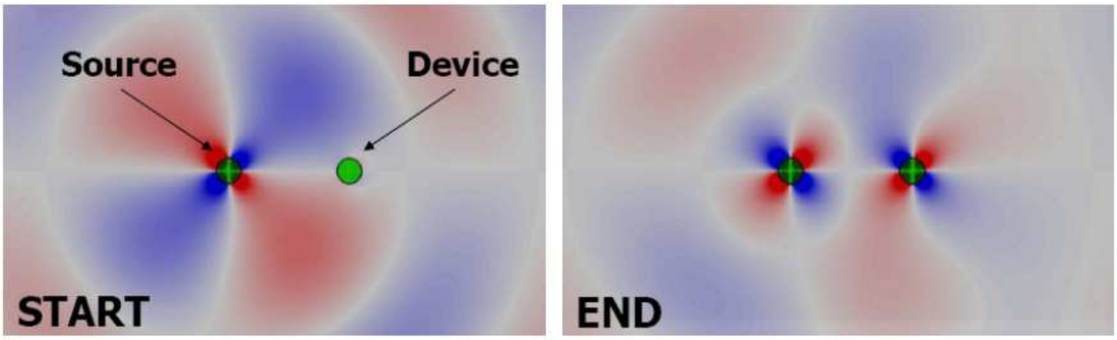

Fig. 2-4. A pair of dielectric disks forms a witricity system [26, 60]

To further analyze the performance of witricity and explore its different structures, a precise mathematical model is necessary. Electromagnetic (EM) field computation has become a most basic method to study EM devices and bioelectric phenomena. Here are some successful examples: an evaluation of the EM fields in the 63-200 MHz frequency range in a human head model in magnetic resonance images (MRI) [61], the biological effect of exposure of the human head to EM fields at 900 MHz from mobile phones [62], the influence of EM fields in the 1-30 MHz range on human subjects exposed to the fields of transmitters [63].

2.3 Potential Applications for Implanted Medical Devices and the Significance

We believe that a dominant problem in the current design of medical implants is providing electrical energy. Energy plays a critical and universal role in essentially all intelligent man-made prosthetic devices, from artificial hearts to brain implants.

More recently, the implanted medical device has been offered to many younger patients, including children and young adults. Typically, the current demands for these applications have been much larger. Thus the need for battery changes can be frequent. In one recent dystonia study, the mean battery life was 30 months [64]. Thus, higher current usage in young patients demands a new approach to deliver sufficiently stable power levels that must be effective, cost-efficient, safe and convenient for the long term.

The power source problem is a dominant factor in the high cost of implanting the current medical devices. Currently, the battery is sealed within the implanted pulse generator (IPG) so that the entire device must be surgically replaced once the battery's power has been depleted. The period between repeated surgeries ranges from less than one year (heavy usage) to several years (light usage). The combined cost of a replacement device, accessories, and surgical procedures is approximately $25,000 for each replacement. Despite the awkwardness of the non-rechargeable battery and the chest implantation, the implanted medical devices have worked well. If all systems from all the implanted medical devices makers are included, the cost figure could be significant higher. Thus, the savings to the health care system is clear if this single power supply improvement were available. Little is known about how hardware placement and replacement affect patient quality of life; however, morbidity associated with hardware replacement is well documented [65-68]. The availability of small implanted medical systems placed entirely within the body, with rechargeable powering, would be a significant advance.

It has been envisioned [69, 70] that this new wireless power source can be used to power a variety of electronic systems without using batteries. For example, a resonant transmitter could be mounted on the ceiling of a room to provide power for each electronic system in the room. Although biomedical applications of witricity have not been envisioned in the literature, we believe that it could become the most effective tool for transmitting electrical power into the human body for the following reasons:

1. As the previous example shows, in using witricity, energy is selectively delivered to the location where a resonant object is present. Since the intrinsic frequency of biological tissue is normally very low, little energy is absorbed by biological matter. It

has been shown [60] that tissue is essentially transparent to witricity, and that the energy transfer system is safe to humans. Clearly, these properties are extremely valuable.

2. Witricity can pass energy in the air or tissue over a long distance while traditional methods cannot.

3. In the previous example, an electromagnetic field was used as the non-radiative field for energy coupling. However, a magnetic field can also be used and is more preferable for biological applications since the magnetic permeability of tissue is similar to that of free space.

4. In either case where the transmitter and receiver are not well aligned or the line of sight is blocked by a non-resonant object, the witricity system can still perform well [60]. This property implies robustness in energy delivery.

CHAPTER 3 SYSTEM THEORIES &COUPLING

3.1 Inductance and Coupling Study

In order to design the wireless devices with primary and secondary coils, it is needed to study how to get the accurate inductance and the coupling rate. The total inductance contains self-inductance and mutual-inductance, which are determined by the shape of the coil loops, the permeability of the medium around, the number of windings and the distributions of the current along the lead's cross section. The mutual-inductance also relates to the positions of the loops [71-73]. In theory, the coupling coefficient is only depends on the above factors except the number of windings.

3.1.1. Circular Coils

3.1.1.1 Self Inductance

Fig. 3-1 shows the diagram of the relative position of the two single-turn coils, where R_1 and R_2 are the radius of the primary coil and the secondary coil, h is the vertical distance of the two coils, and t is the horizontal displacement of the two coils. We have,

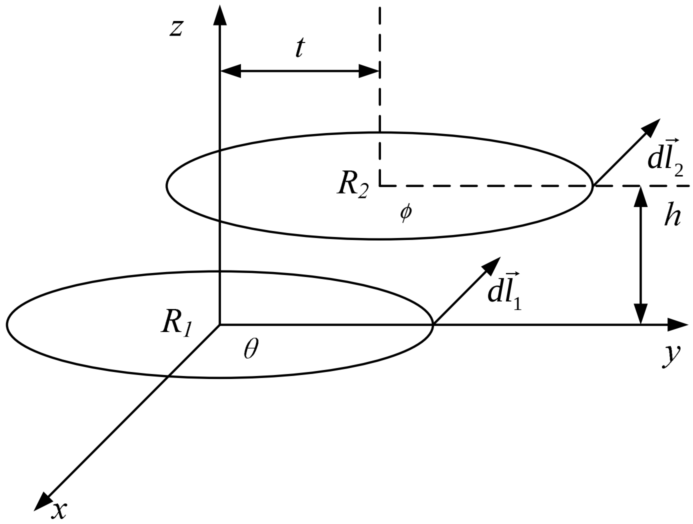

Fig. 3-1 Relative position of the circular coils

Suppose R is the radius of the coil (like R_1 or R_2 in Fig. 3-1) and r is the radius of the wire. The mutual inductance by a filamentary circuit i on a filamentary circuit j is given by the double integral Neumann formula [71]. The external self-inductance is

$$L_e = \frac{\mu}{4\pi}\oint_1\oint_2 \frac{d\vec{l}_1 \cdot d\vec{l}_2}{r} = \frac{\mu}{4\pi}\int_0^{2\pi} d\theta \int_0^{2\pi} \frac{R(R-r)\cos\phi d\phi}{\sqrt{R^2 + (R-r)^2 - 2R(R-r)\cos\phi}} \tag{3-1}$$

Since the radius of the wire is much smaller than the curvature radius of the loop, the current is evenly distributed in the wire cross section. Thus, the internal self-inductance of the coil with one turn is,

$$L_i = \frac{\mu_0}{8\pi}(2\pi R) \tag{3-2}$$

3.1.1.2 Mutual Inductance

$$\vec{R}_1 = R_1 \cos\theta\,\vec{x} + R_1 \sin\theta\,\vec{y}, \vec{R}_2 = R_2 \cos(\theta+\phi)\vec{x} + [R_2 \sin(\theta+\phi) + t]\vec{y} + h\vec{z} \tag{3-3}$$

$$\left|\vec{R}_2 - \vec{R}_1\right| = \sqrt{\left[R_2 \cos(\theta+\phi) - R_1 \cos\theta\right]^2 + \left[R_2 \sin(\theta+\phi) + t - R_1 \sin\theta\right]^2 + h^2} \tag{3-4}$$

$$d\vec{l}_1 \cdot d\vec{l}_2 = R_1 R_2 \cos\phi d\theta d\phi \tag{3-5}$$

According to Neumann formula [71], the mutual inductance between these two coils can be derived by,

$$M = \frac{\mu}{4\pi}\int_0^{2\pi} d\theta \int_0^{2\pi} \frac{R_1 R_2 \cos\phi d\phi}{\left|\vec{R}_2 - \vec{R}_1\right|} \tag{3-6}$$

3.1.2. Rectangular Coils

3.1.2.1 Self Inductance

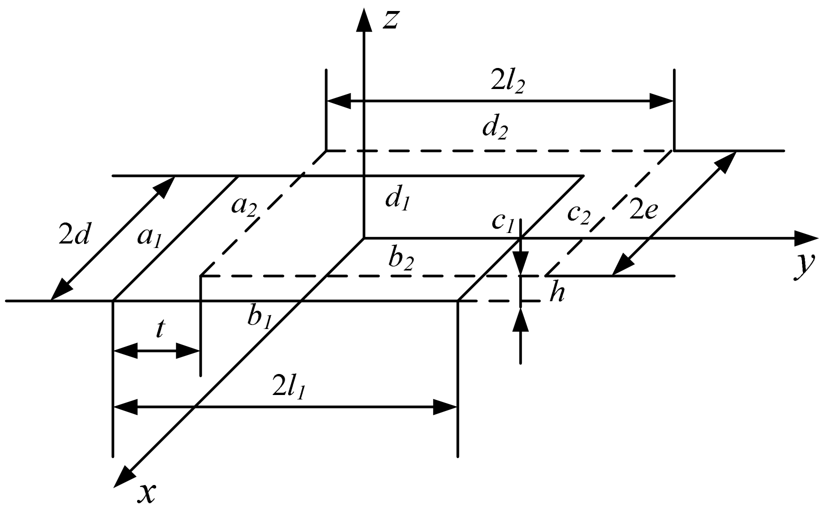

Fig. 3-2 Relative position of the rectangular coils

The self-inductance of a coil can be obtained by the flux method, which integrates the function along the edges of the rectangle. The diagram of the two rectangular coils is shown in Fig. 3-2, where $2l_1$ and $2d$ are the length and width of the primary coil, $2l_2$ and $2e$ are the length and width of the secondary coil, h is the vertical distance of the two coils, and t is the horizontal displacement of the two coils, r is the radius cross-section of the wire, and each coil has one turn.

According to the Biot-Schaffar Law[71-73], the magnetic flux density generated by a straight wire with limited length is given by,

$$B=\frac{\mu_0 I}{4\pi\rho}\left(\frac{d-x}{\sqrt{\rho^2+(d-x)^2}}+\frac{d+x}{\sqrt{\rho^2+(d+x)^2}}\right) \tag{3-7}$$

Thus, the self-inductance of one-turn rectangular coil can be obtained through the flux linkage method,

$$\begin{aligned}L_e=\frac{\mu_0}{\pi}\Bigg\{&2\left(\sqrt{(2d-r)^2+(2l_1-r)^2}-\sqrt{(2d-r)^2+r^2}-\sqrt{(2l_1-r)^2+r^2}+\sqrt{2}r+r\ln\left(\sqrt{2}-1\right)\right)\\&+(2d-r)\left(\ln\frac{\sqrt{(2d-r)^2+(2l_1-r)^2}-(2d-r)}{2l_1-r}-\ln\frac{\sqrt{r^2+(2d-r)^2}-(2d-r)}{r}\right)\\&+(2l_1-r)\left(\ln\frac{\sqrt{(2l_1-r)^2+(2d-r)^2}-(2l_1-r)}{2d-r}-\ln\frac{\sqrt{r^2+(2l_1-r)^2}-(2l_1-r)}{r}\right)\\&-r\left(\ln\frac{\sqrt{r^2+(2l_1-r)^2}-r}{2l_1-r}+\ln\frac{\sqrt{r^2+(2d-r)^2}-r}{2d-r}\right)\end{aligned} \tag{3-8}$$

If the radius of the cross-section of the wire is far smaller than the radius of the coil, the self-inductance can be given by,

$$L_i=\frac{\mu_0}{8\pi}(4l+4d) \tag{3-9}$$

3.1.2.2 Mutual Inductance

According to [71], the mutual inductance can be calculated by the summation of the mutual inductance of individual parts. Therefore, the coil should be divided into small parts, which can be considered as straight wire. Then the Neumann formula can be applied to calculate the inductance.

Primary coil:

$$
\begin{array}{l}
d\vec{l}_1 = dx_1\vec{x} + dy_1\vec{y} - dx_1\vec{x} - dy_1\vec{y} \\
\qquad\ \ \downarrow \qquad\ \downarrow \qquad\ \downarrow \qquad\ \downarrow \\
\qquad\ \ a_1 \qquad\ b_1 \qquad\ c_1 \qquad\ d_1
\end{array} \tag{3-10}
$$

Secondary coil:

$$
\begin{array}{l}
d\vec{l}_2 = dx_2\vec{x} + dy_2\vec{y} - dx_2\vec{x} - dy_2\vec{y} \\
\qquad\ \ \downarrow \qquad\ \downarrow \qquad\ \downarrow \qquad\ \downarrow \\
\qquad\ \ a_2 \qquad\ b_2 \qquad\ c_2 \qquad\ d_2
\end{array} \tag{3-11}
$$

By using the Neumann formula, the mutual inductance between a_1 and a_2 is given by,

$$
\vec{r}_1 = x_1\vec{x} - l_1\vec{y}\ ,\ \vec{r}_2 = x_2\vec{x} - (l_2 - t)\vec{y} + h\vec{z}
$$

$$
|\vec{r}_1 - \vec{r}_2| = \sqrt{(x_2 - x_1)^2 + h^2 + (l_1 - l_2 + t)^2} \tag{3-12}
$$

and $d\vec{l}_1 = dx_1\vec{x}\ ,\ d\vec{l}_2 = dx_2\vec{x}\ ,\ d\vec{l}_1 \cdot d\vec{l}_2 = dx_1 dx_2$

$$
M_{a_1a_2} = \frac{\mu}{4\pi}\oiint_{l_2 l_1}\frac{d\vec{l}_2 \cdot d\vec{l}_1}{|\vec{r}_2 - \vec{r}_1|} = \frac{\mu}{4\pi}\int_{-d}^{d}\int_{-e}^{e}\frac{dx_1 dx_2}{\sqrt{(x_2 - x_1)^2 + h^2 + (l_1 - l_2 + t)^2}} \tag{3-13}
$$

Using the same method, the inductance of other sides can be calculated. Thus, the total inductance can be calculated by,

$$M = M_{a_1a_2} + M_{b_1b_2} + M_{c_1c_2} + M_{d_1d_2} + M_{a_1c_2} + M_{a_2c_1} + M_{b_1d_2} + M_{b_2d_1} \tag{3-14}$$

3.1.3. Coupling Coefficient

In order to study the effects of coil shape and size on coupling characteristics, the coupling coefficient both of the circular coils and rectangular coils are calculated according to method we developed above. In the following analysis, we suppose the each of the coil has one turn and the radius of the wire *r* is 1mm.

3.1.3.1 Coupling Coefficient vs. Horizontal Displacement Based on Different Shapes of the Primary and Secondary Coils

In this part, two cases are to be considered: the coupling coefficient between circular coils, and the coupling coefficient between rectangular coils.

We suppose the lengths of the edges of the rectangular coils are 50 mm, having the same length of the diameter of the circular coils. The vertical distance *h* between the two circular coils is 3 mm. The radii of both wires are 1 mm. The results are shown in Fig. 3-3. It can be seen that the curve of the coupling coefficient of circular coils drops faster than that of rectangular coils while the horizontal displacement increases from 0 mm to 40 mm.

The coupling coefficients between circular coils and between rectangular coils are 0.1494 and 0.2334, separately, as the horizontal displacement is 25mm. Therefore, the square coils have slightly better stability than the circular coils with the horizontal displacement variation.

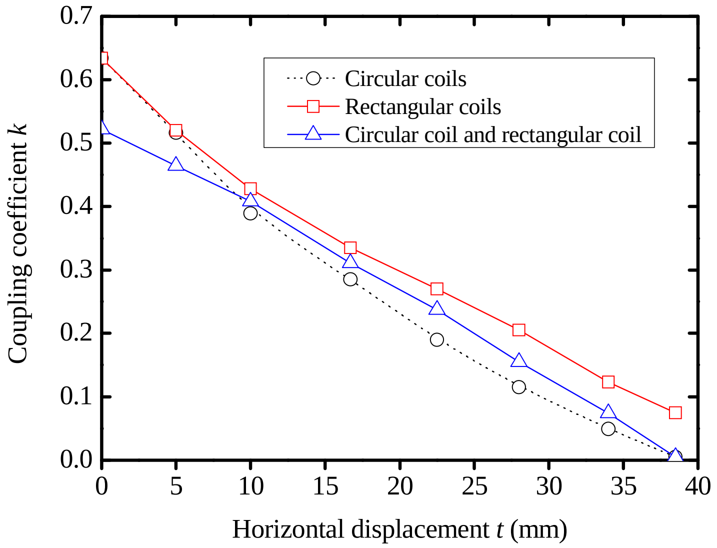

r=1 mm, h=3 mm, 2d=2l_1=2R=50 mm

Fig. 3-3 Coupling coefficient versus horizontal displacement based on different shapes of primary and secondary coil

3.1.3.2 Coupling Coefficient vs. Aspect Ratio of Rectangular Coils

To study the effect of the aspect ratio $m=l/d$ on coupling coefficient, two groups of rectangular coils based on same widths have been analyzed. In each group, the primary coil has the same shape and size with the secondary coil. Then, according to formula (3-10), (3-11), (3-12), (3-13), and (3-14), the curve of aspect ratio versus coupling coefficient is shown in Fig. 3-4 (a), where the aspect ratio $m=l/d$, the coil width $2d$=50 mm, the vertical distance h between the primary coil and the secondary coil in each group is 3 mm. It can bee seen that the coupling coefficient is small while the aspect ratio m is small. The coupling coefficient increases dramatically while aspect ratio m increases, and the growth rate slows down after m is larger than 10 mm. With a further increase in aspect ratio to larger than 50 mm, the coupling coefficient changes gradually levels off. At the points of 50 and 80 of the aspect ratio, the coupling coefficients are 0.6786 and 0.679, respectively.

Next, the widths of the groups of the rectangular coils analyzed above have been changed to 500 mm ($2d$ = 500mm), and the vertical distance h between the primary coil and the secondary coil in each group has been changed to 12 mm. The aspect ratio versus coupling coefficient curve is shown in Fig. 3-4 (b). As the aspect ratio increases beyond 10, the impact of it on coupling coefficient is smaller and smaller.

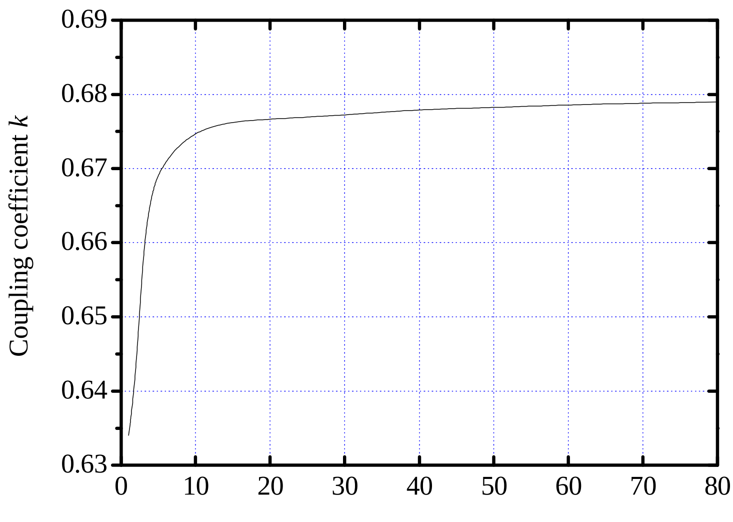

(a) $2d$=$2e$=50 mm, h=3 mm, and r=1 mm

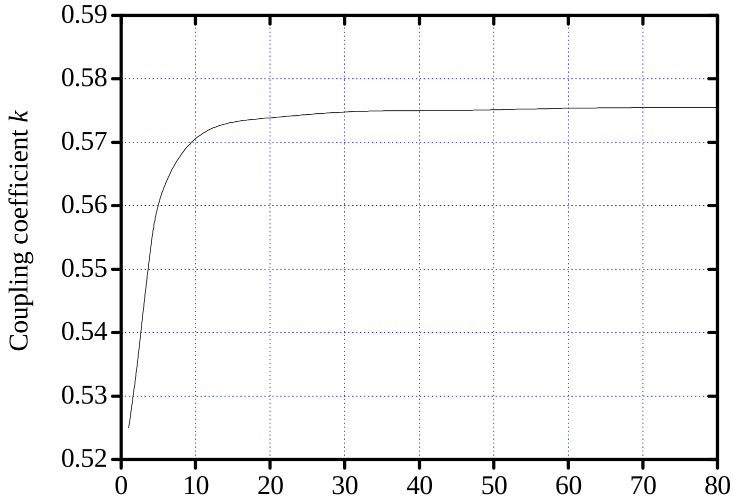

(b) 2*d*=2*e*=500 mm, *h*=12 mm, and *r*=1 mm

Fig. 3-4 Coupling coefficient vs. rectangular coil aspect ratio

3.1.3.3 Coupling Coefficient vs. Horizontal Displacement Based on the Same Widths or Lengths

Letting the coil length 2*l*=100 mm, and the vertical distance *h*=10 mm, curves of the coupling coefficient *k* versus horizontal displacement *t* to coil length ratio are calculated while 2*d*=25 mm, 50mm, 100 mm and 200 mm, as shown in Fig. 3-5. It shows that the smaller width 2*d* is, the coupling coefficients decrease more slowly with horizontal displacement increases. With a displacement of 20 mm, the coupling coefficient decreased by 0.31 while 2*d*=100 mm and 0.22 while 2*d*=25 mm. At *t*=0 mm, that means there is no displacement at all, the wider the coil is, the better the coupling coefficient is resulted.

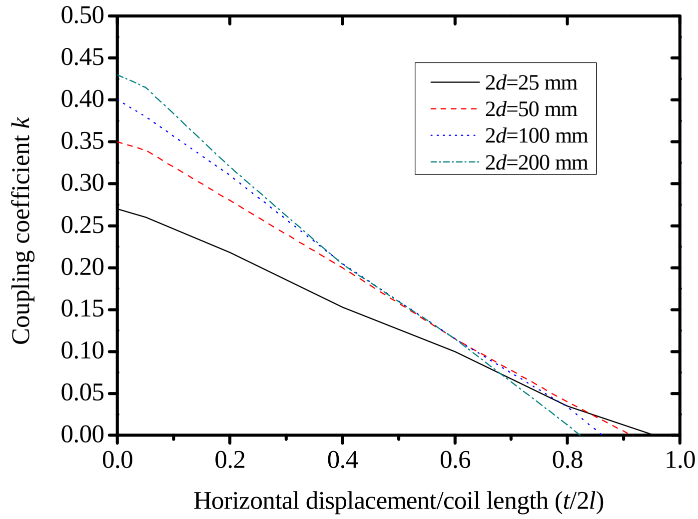

2l=100 mm, h=10 mm, and r=1 mm

Fig. 3-5 Coupling coefficient vs. horizontal displacement to coil length ratio based on the same lengths

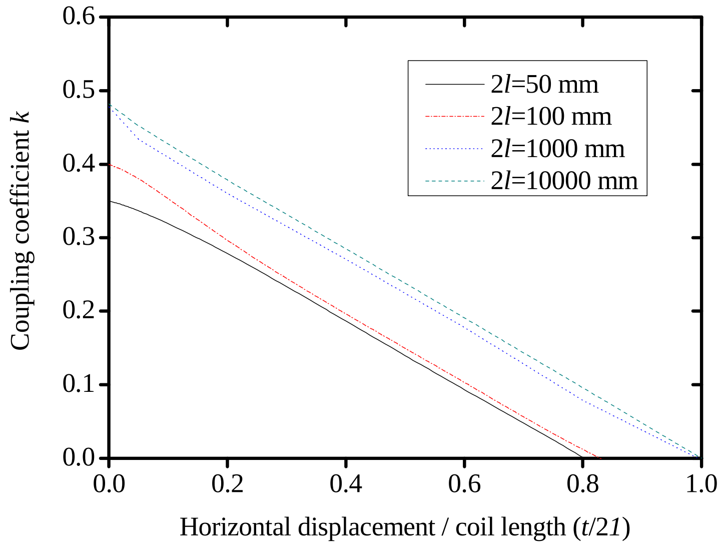

2d=100 mm, h=10 mm, and r=1 mm

Fig. 3-6 Coupling coefficient versus horizontal displacement to coil length ratio based on same widths.

With coil width $2d$=100 mm, h=10 mm, the coupling coefficient versus the horizontal displacement to coil length ratio curves with $2l$=50 mm, $2l$=100 mm, $2l$=1000 mm and $2l$=10000 mm are shown in Fig. 3-6. As can be seen from the figure, the curves with $2l$=50 mm, $2l$=100 mm, $2l$=1000 mm and $2l$=10000 mm are straight lines paralleled with each other, and they decrease at the speed rate as the horizontal displacement increases. It also can be seen that the longer the coils, the higher is the coupling coefficient.

3.1.3.4 Coupling Coefficient vs. Horizontal Displacement Based on the Same Secondary Lengths or l_1/l_2 Ratios

The afore-analyzed primary coils and secondary coils have the same lengths. In this part, rectangular coils with different lengths are studied. Firstly, three curves of coupling coefficient versus horizontal displacement are shown in Fig. 3-7, where the ratios of the primary coil length to the secondary coil length l_1: l_2 are 1.5, 2 and 4, respectively. In theses curves, the lengths of the secondary coils are all 50 mm ($2l_2$=50 mm) and the distance h=3 mm. While the secondary coils are moved from the center of the primary coil to the ends, the coupling coefficients remain at high levels before the secondary coils exceed the boarder of the primary coil and the coupling coefficients drops rapidly after that.

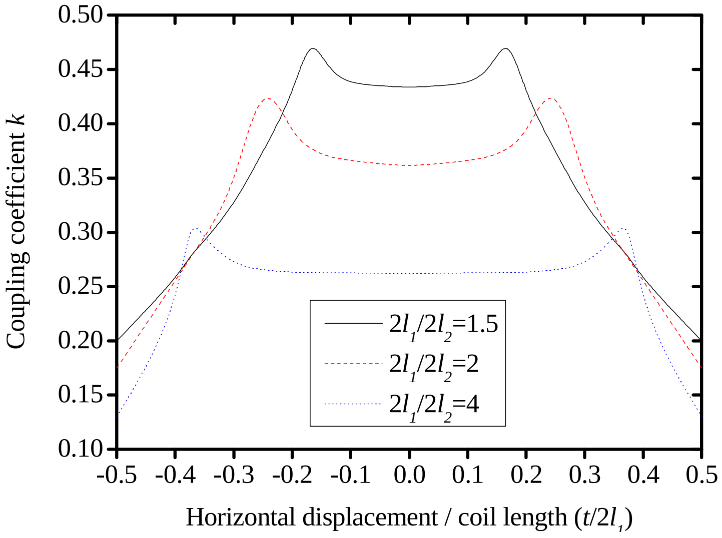

$2d$=$2e$=50 mm, $2l_2$=50 mm, h=3 mm, and r=1 mm

Fig. 3-7 Coupling coefficient vs. horizontal displacement to coil length ratio based on the same secondary coil lengths

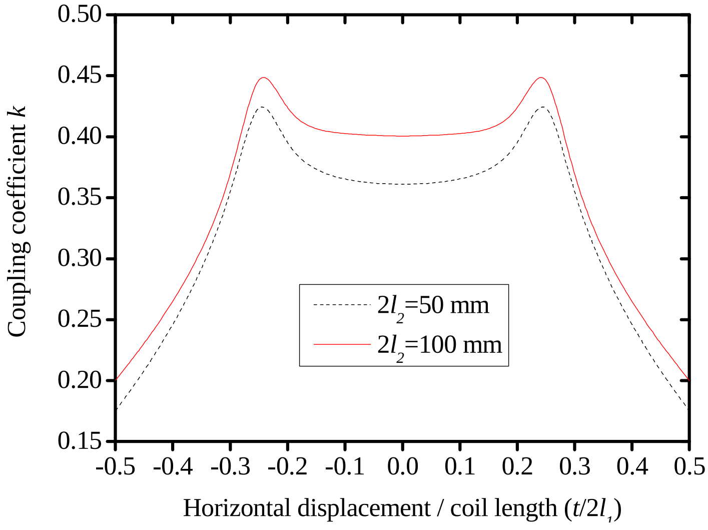

$2d$=$2e$=50 mm, l_1/l_2=2, h=3 mm, and r=1 mm

Fig. 3-8 Coupling coefficient vs. horizontal displacement to coil length ratio based on the same l_1/l_2 ratio

The coupling coefficients versus the horizontal displacements characteristics have been studied via two groups of coils with the same l_1/l_2 ratio but different actual lengths. The results are shown in Fig. 3-8, where the l_1/l_2 ratios are 2, and the lengths of the secondary coils are 50 mm and 100 mm, respectively. The widths of the secondary coils are 50 mm ($2l_2$=50 mm) and the distance is 3 mm (h=3 mm). It should be noticed from the figure that the high level areas of these two curves have the same width. Also, the group with longer coils has higher coupling coefficient and better stability.

3.2 Coupled-Mode Theory for Resonant Couplers

3.2.1. Basic Coupled-Mode Theory

The well-known coupled-mode theory (CMT) is used as the analytical framework for modeling this resonant wireless power transfer process. We choose a simple LC circuit example, shown in Fig. 3-9, to illustrate the meaning of the physical parameters used [74, 75]. The equations are as below

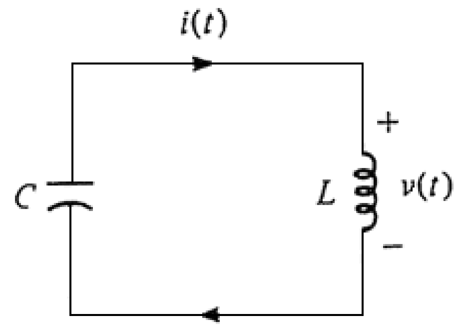

Fig. 3-9 A simple LC circuit

$$v = L\frac{di}{dt} \tag{3-15}$$

$$i = -C\frac{dv}{dt} \tag{3-16}$$

Then the second-order differential equation for the voltage can be derived from the two first-order differential equations above.

$$\frac{d^2v}{dt^2} + \omega_0{}^2 v = 0 \tag{3-17}$$

where,

$$\omega_0{}^2 = \frac{1}{LC} \tag{3-18}$$

Two uncoupled first-order differential equations have been derived by defining the complex variables

$$a_{\pm} = \sqrt{\frac{C}{2}}\left(v \pm j\sqrt{\frac{L}{C}}i\right) \tag{3-19}$$

The following equations can be attained through addition and subtraction of (3-15) and (3-16)

$$\frac{da_+}{dt} = j\omega_0 a_+ \tag{3-20}$$

$$\frac{da_-}{dt} = -j\omega_0 a_- \tag{3-21}$$

Because,

$$v(t) = |V|\cos(\omega_0 t + \phi) \tag{3-22}$$

$$i(t)=\sqrt{\frac{C}{L}}|V|\sin(\omega_0 t+\phi) \tag{3-23}$$

where $|V|$ is the peak amplitude of the voltage and ϕ is the phase, $\phi=\arg V$. So

$$a_+=\sqrt{\frac{C}{2}}\left[|V|\cos(\omega_0 t+\varphi)+j|V|\sin(\omega_0 t+\varphi)\right]=\sqrt{\frac{C}{2}}Ve^{j\omega_0 t} \tag{3-24}$$

Because $a_+(t)$ has the dependence $\exp(j\omega_0 t)$, it can be normalized as

$$|a_+|^2=\frac{C}{2}|V|^2=W \tag{3-25}$$

where W is the energy in the circuit. a_+ is the positive-frequency component of the mode amplitude. Here coupled differential equations have been replaced by two uncoupled equations. Since only the positive frequencies have been set for calculation based on the Michelson interferometer [74], the + will be dropped in the following equations.

Now we consider that the circuit is lossy and we use a conductance G in parallel with L and C to showcase the loss.

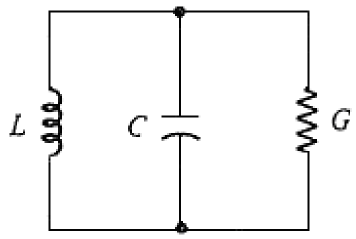

Fig. 3-10 An LC circuit with loss

If the loss is small, equation (3-20) can be derived as

$$\frac{da}{dt} = j\omega_0 a - \frac{1}{\tau_0} a \quad \text{(3-26)}$$

where $1/\tau_0$ is the decay rate. It can be calculated based on the condition that $|a|^2$ decays as exp $\left(-2t/\tau_0\right)$ and the time rate of the circuit energy decrease with the dissipation power P_d

$$\frac{dW}{dt} = -\frac{2}{\tau_0} W = -P_d \quad \text{(3-27)}$$

When the loss is small, P_d can be regarded to be a perturbation and the time averaged-loss is

$$P_d = \frac{1}{2} G|V|^2 = \frac{G}{C}|a|^2 \quad \text{(3-28)}$$

Then we combined (3-25) and (3-26)

$$\frac{P_d}{\omega_0 W} = \frac{G}{\omega_0 C} = \frac{2}{\omega_0 \tau_0} = \frac{1}{Q_0} \quad \text{(3-29)}$$

If we compute the equations of the circuit from the beginning ones, we can obtain the formulation below

$$s = -\frac{1}{\tau} + j\omega = -\frac{G}{2C} + j\sqrt{\frac{1}{LC} - \frac{G^2}{4C^2}} \quad \text{(3-30)}$$

We have used the perturbation approach to evaluate the decay rate. And the correction to the frequency $\omega_0 = \sqrt{\dfrac{1}{LC}}$ is of second order in $\dfrac{G}{C}$. It is just a rigorous mathematical step to reduce the second-order differential equations to two uncoupled first-order differential equations.

3.2.2. Basic Theory About The Resonant Power Transmission System

The electromagnetic fields of the charger which include two resonant coils, a transmitter and a receiver can be approximated by

$$\mathbf{F}(r,t) \approx a_S(t)\mathbf{F_S}(r) + a_D(t)\mathbf{F_D}(r) \tag{3-31}$$

where $\mathbf{F_S}(r)$, $\mathbf{F_D}(r)$ are the respective eigenmodes of the transmitter and the receiver alone. Then the fields a_S and a_D can be shown [60] to satisfy,

$$\dot{a}_S = (j\omega_S - \Gamma_S)a_S(t) + j\kappa_{SD}a_D(t) + f(t) \tag{3-32}$$

$$\dot{a}_D = (j\omega_D - \Gamma_D)a_D(t) + j\kappa_{DS}a_S(t) \tag{3-33}$$

The eigen-frequency is

$$\begin{aligned}\omega = &\frac{\omega_S + \omega_D + \sqrt{4\kappa^2 - (\Gamma_S - \Gamma_D + j\omega_D - j\omega_S)^2}}{2} \\ &+ j\frac{\Gamma_S + \Gamma_D}{2}\end{aligned} \tag{3-34}$$

where $\omega_{S,D}$ are the transmitter and the receiver's eigenfrequencies, $\Gamma_{S,D}$ are the resonance widths depending on the intrinsic losses, and $\kappa_{S,D}$ are the coupling coefficient.

When the system is at resonance, we can get $\kappa_S = \kappa_D = \kappa$, $\omega_S = \omega_D = \omega_0$, and the working frequency is the real part of the eigen-frequency as follows

$$\omega = \omega_0 \pm \sqrt{\kappa^2 - \left(\frac{\Gamma_S - \Gamma_D}{2}\right)^2} \tag{3-35}$$

Moreover,

$$\frac{|a_D|^2}{|a_S|^2} = \frac{\kappa^2}{(\omega - \omega_0)^2 + \Gamma_D{}^2} = \frac{\kappa^2}{\kappa^2 - \left(\frac{\Gamma_S - \Gamma_D}{2}\right)^2 + \Gamma_D{}^2} \tag{3-36}$$

The system is under strong coupling when the coupling rate is much faster than the whole loss rates. We can use the ratio $\kappa / \sqrt{\Gamma_S \Gamma_D}$ to represent that condition. If $\kappa / \sqrt{\Gamma_S \Gamma_D} >> 1$, we can call the desired regime as strong-coupling regime.

Figs. 3-11 and 3-12 are the simple model given by MIT group [26, 60]. The conducting wires have a radius *r*, and the distance between the two coils is *H*. For the rate of energy transfer between the two coils *S* and *D* with a distance *H*, we give κ through the frequency splitting of the combined system.

$$\kappa = \omega M / 2\sqrt{L_1 L_2} \tag{3-37}$$

where *M* is the mutual inductance of the two coils, and it is $M \approx \pi / 2\mu_0 (r_S r_D)^2 / H^3$ in Fig. 3-12. That means $\omega / \mathbf{2}\kappa \sim \left(H / \sqrt{r_S r_D}\right)^{\mathbf{3}}$.

It is important to be aware of the difference between such a resonant-coupling inductive scheme and the well-known non-resonant inductive scheme for energy transfer. Using CMT it is easy to show that, keeping the geometry and the energy stored in the source fixed, the resonant inductive mechanism allows for more power delivered for work at the device than the traditional non-resonant mechanism. Capacitively-loaded conductive loops are actually being widely used also as resonant antennas (for example in cell phones), but those operate in the far-field regime, and the radiation Q's are intentionally designed to be small to make the antenna efficient, so they are not appropriate for energy transfer [76-78].

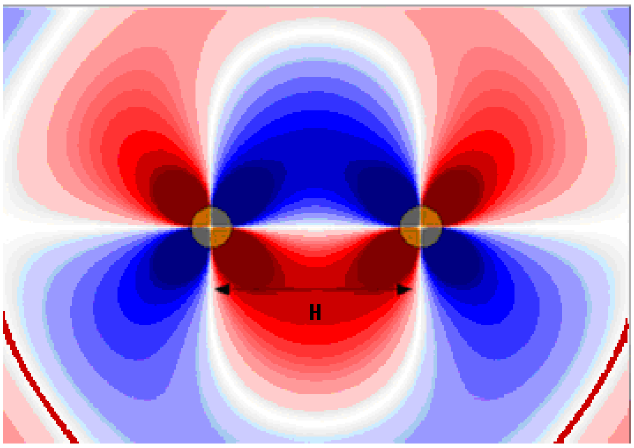

Fig. 3-11 System of two same 2D disks of radius *r* for medium-distance *H* coupling between them [60]

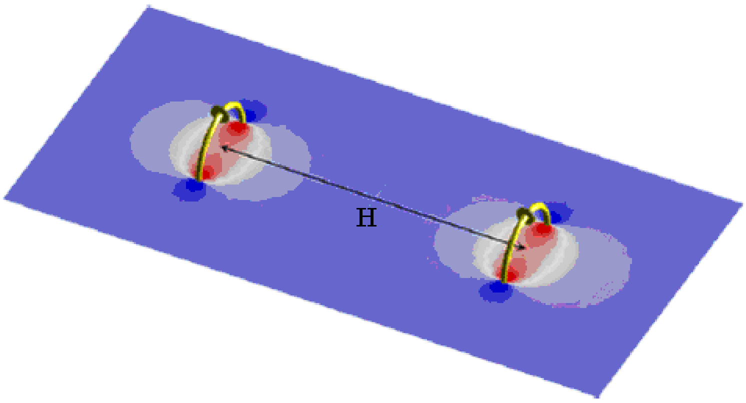

Fig. 3-12 System of two same wire loops connected to parallel plates for medium-distance *H* coupling between them [60]

3.3 Summary

In this chapter, the self-inductance and mutual-inductance of the circular spiral and rectangular coils are studied, and the relationship between them and the shape of the coil loops, the permeability of the medium around, the number of windings and the distributions of the current along the lead's cross section has also been presented. The coupling coefficient, which depends on the above factors except the number of windings, is illustrated through related equations.

Then the CMT has been applied to build the analytical framework for modeling this resonant wireless power transfer. And corresponding formulations have been deduced for study. In the last part, the theory about the resonant power transmission system is shown for the further simulations and experiments.

CHAPTER 4 SYSTEM PERFORMANCE AND VERIFICATION

4.1 Introduction

In this chapter, some novel structures with rectangular or circular coils based on witricity is firstly proposed for charging rechargeable batteries. The first resonator receives energy from an external power supply. It also includes a second resonator which is physically separated from the first resonator to supply useful working power to an external load. The distance between the two resonators can be larger than the characteristic sizes of each resonator. It transfers non-radiative energy between the first resonator and the second resonator through the coupling of their resonant-field evanescent tails [26, 60].

Also based on this novel technology, a resonant wireless energy transfer system, also called witricity system, for powering and recharging electrical devices is then studied. The general block diagram of the witricity systems is shown in Fig. 4-1. A two-stage energy transfer system is analyzed using 3-dimensional (3-D) FEM analysis. Simulation and experimental results show that the system is effective in transferring power to wireless devices. The energy transfer efficiency with respect to system dimensions and the distance between the source and receiving cells of the system are also studied experimentally.

And in both traditional magnetic coupling and advance witricity systems for implantable devices, the transmitter and receiver coils are separated by a layer of skin and tissue, in the range of 1 cm to 5 cm. The coils are usually misaligned, due to anatomical constraints and hence the coupling efficiency is inevitably impaired. For traditional magnetic coupling system, low power inductive links are characterized by very unfavorable coil coupling conditions to result in large coil separation or a very small pickup coil diameter. The coupling factor can be as low as l % and may vary in a very unpredictable manner due to coil misalignments. But for witricity systems, the resonant nature of the process ensures that the interaction between the source and device is sufficiently strong and the interaction with non-resonant objects is minimal. In this manner, an efficient wireless channel for power transmission can be established and the efficiency is up to 60%-90% with a distance of about 1-5 cm between the transmitter and the receiver. Consequently the witricity system still has relative high efficiency when misalignment occurs due to the operating conditions in practice. Because of changes in the coupling rate, lateral misalignment and angular misalignment may cause fluctuations in output voltage, output power and transmission efficiency, leading to instability in the whole system. These effects must be fully addressed in order to enhance the stability of the system. Careful parameter design is also necessary, especially for energy transmission over a relatively large distance.

It is known that the coil dimensions and the shape substantially affect the magnitude of the magnetic field and the magnitude of the magnetic field is closely related to the efficiency of the inductive link. The third contribution of this chapter is to introduce a novel power transfer function to address misalignments of the witricity coils. The analyzed results for the resonant power transfer developed allow the designer to optimize the efficiency of the link and predict the effect of coil characteristics and misalignment on the coupling factor. An interpolative FEA modeling simulation is introduced to study the performance of witricity systems with lateral and angular misalignments. Fig. 4-2 shows the equivalent circuit of the witricity system.

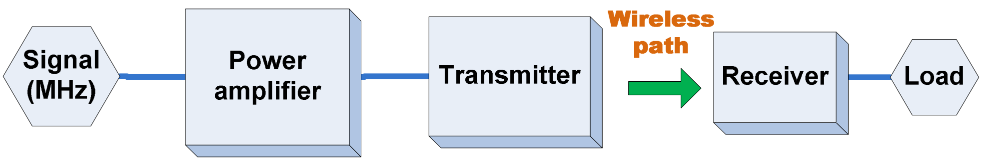

Fig. 4-1. Block diagram of the witricity system

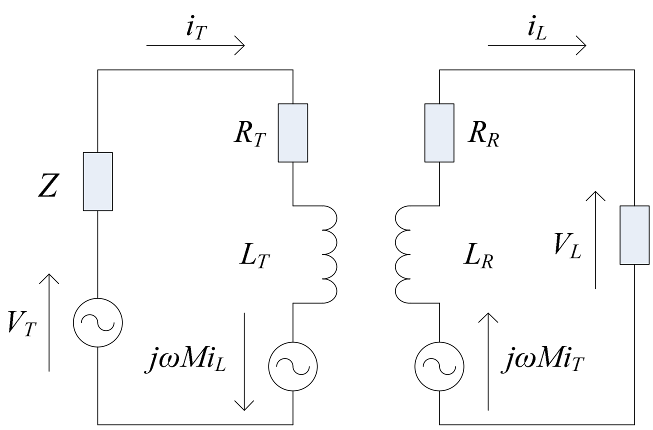

Fig. 4-2 Equivalent circuit for the inductive link representing the two resonant coils

4.2 Witricity Transfer with Rectangular Coils

4.2.1 Finite Element Analysis and Corresponding Experiments for Typical Systems

As a new wireless power transfer technology, witricity is based on the concept of near-field and strongly coupled magnetic resonance. The fundamental principle is that resonant objects can exchange energy efficiently, while non-resonant objects only interact weakly. The geometry and operating frequency are the two key attributes that define the power link. In this section, the link is designed around these two attributes to maximize the voltage transfer efficiency and minimize the power loss in the transmission process.

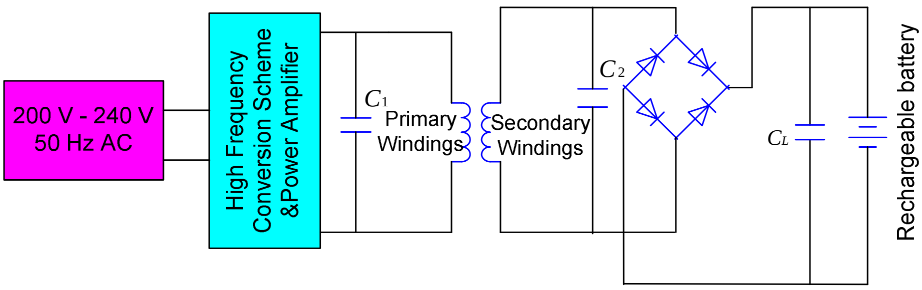

Fig. 4-3 The schematic diagram of the witricity system

Fig. 4-3 shows the basic design of the witricity system consists of source and device resonators, a driving loop, and an output loop. The source resonator is coupled to the driving loop which is linked to an oscillator that supplies energy to the system. The device resonator coil is coupled to the output loop to provide the power to an external load.

Due to its large physical separation, wireless inductive coupling transformers have large leakage inductances and small mutual inductance. Thus the coupling rates are very small, quite often less than 0.1, while those for conventional transformers are between 0.95~0.98 [79]. Judging on this aspect, inductive coupling technology is impractical. For the witricity system, the coupling rate can however be as high as 0.7~0.9 by virtue of the strong resonant frequency coupling between primary and secondary windings.

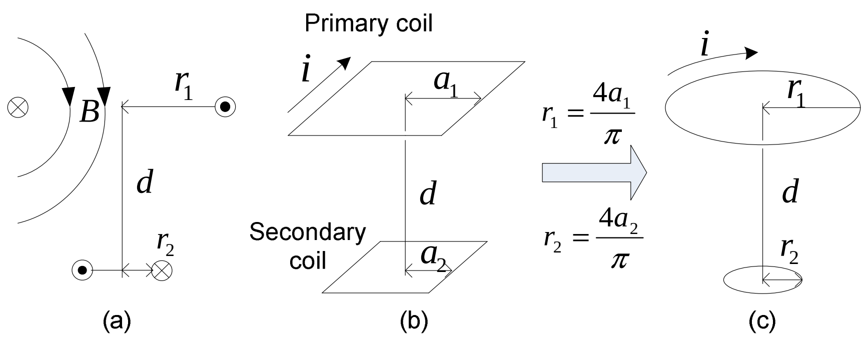

Fig. 4-4 (a) Cross-sectional view for the direction of the magnetic flux density vector. (b) Placement and dimensions of the two rectangular coils in the power link. (c) Placement and dimensions of the two equivalent circular coils in the power link

Energy transfer over mid-range distance is most efficient using resonant coupling. It is also important to note that regular coils should be designed at some chosen operating frequencies for applications such as implantation in human subjects. Such application is very different from traditional inductive energy transfer technology, as it is necessary to design the system firstly based on practical needs before the operation frequency is determined. Therefore, the link used two flat rectangular spiral inductors to create an inductively coupled link. Fig. 4-4 (a) shows the magnetic field generated by the primary coil is penetrating through the area of the secondary coil.

Because the coil inductance is mainly dependent on the length of the wires or the tapes, the flat rectangular spiral coils here are equivalent to the flat circular spiral coils in order to use traditional transformer theory as a reference starting point when such coils are designed. The effects of changing the coil shapes are ignored. The original and the equivalent coil dimensions are given in Figs. 4-4 (b) and 4-4 (c) respectively.

To achieve high coupling rate and transmission efficiency, sources with certain resonant frequency (in the MHz range) is fed to the primary windings. Common formulas in the low frequency range to predict the performance of the system are inapplicable as the values of inductances and resistors vary greatly as frequency changes, especially at high frequency. The equivalent geometry of the link is described in 3-D for the radii of the two coils and spacing between the coils. The separation distance d is determined by actual demand. With the attributes pre-defined, the radius of the transmitter and the receiver coils are the remaining dimensions to be determined.

The coupling coefficient, k, between the transmitter and the receiver, represents the fraction of flux, created in the primary coil coupled into the secondary coil. It can be maximized by selecting the radius of the coils.

When the flux generated by the transmitter coil is confined to itself and there is no common flux between the two coils, the coupling coefficient k is zero. k is equal to one when all of the fluxes created by the transmitter coil is in the receiver coil. In contrary to traditional wireless energy transmitting technology, the coupling coefficient of the RWET system is not only dependent on the geometry of the link; it also relies on the same intrinsic frequency of the transmitter and the receiver. Therefore, k is dependent on the design dimensions. An equation relating the inductances to the coupling coefficient is

$$k = \frac{M}{\sqrt{L_1 L_2}} = \frac{M_0 n_1 n_2}{\sqrt{n_1^2 L_{10} n_2^2 L_{20}}} = \frac{M_0}{\sqrt{L_{10} L_{20}}}, \qquad (4\text{-}1)$$

where; M is the mutual inductance between the coils; L_1 and L_2 are the self-inductances of the coils; n_1 and n_2 are the number turns of the transmitter and the receiver coils, respectively; M_0 is the single turn mutual inductance; L_{10} and L_{20} are the single turn inductance of the transmitter and the receiver, respectively.

From (4-1) it can be seen that the mutual inductance needs to be maximized in order to maximize the coupling coefficient. The mutual inductance of the two coupled coils is computed using

$$M = R\sqrt{r_1 r_2}\,, \qquad (4\text{-}2)$$

and $r_1 = \frac{4a_1}{\pi}, r_2 = \frac{4a_2}{\pi}$, then

$$M = R\sqrt{r_1 r_2} = \frac{4R\sqrt{a_1 a_2}}{\pi}, \tag{4-3}$$

where; r_1 and r_2 are the equivalent radii of the transmitter and receiver coils; a_1 and a_2 are the side lengths of the two coils; R is a factor dependent on the design dimensions and the number of turns in either coils.

The side length of the receiver coil has been designed to be the same as those of the transmitter (a_1=a_2 =a) in order to use a simple structure to obtain relatively practical performance parameters and (4-3) is simplified as

$$M = \frac{4Ra_1}{\pi} = \frac{4Ra_2}{\pi} = \frac{4Ra}{\pi}. \tag{4-4}$$

TABLE 4-I. DIMENSION PARAMETERS OF THE TWO SYSTEMS

Primary winding / Secondary winding	Shape	Rectangular spiral winding
	Turns	6 turns
	Thickness of copper	0.04 mm
	Width of copper	6.35 mm
	Copper track separation	2 mm
	Maximum length	208 mm
	Minimum length	106 mm
Copper strip	Shape	Rectangle
	Number	4
	Thickness	0.04 mm
	Width	25.4 mm
	Length	50 mm

In the case being studied, the coupling rate has a relatively large value (about 0.81) when the distance is 5 cm for witricity. It decreases gradually as the physical separation distance increases. This is easy to understand as magnetic flux coupled to another winding is expected to decrease markedly as separation distance becomes longer.

The system includes a source loop, a transmitter resonant cell, a receiver resonant cell, and a device loop. The transmitter cell, consisting of a 6-turn coil tape in one layer and 4 strips in the other layer, is a square with a maximum length of 208 mm. There is an insulation layer to separate the two layers. The dielectric constant of the insulator is 3.74. The two device cells have the same structure. Both cells are made of copper tapes with a thickness of 40 μm. The width of the wires for the coil tapes and the width of the strips are 6.35 mm and 25.4 mm, respectively. The system inductance is offered by the 6-turn copper tapes and the capacitance is provided by the 6-turn coil tape layers and the 4 strip layers together. Table 4-I shows the parameters of the novel charging system which has identical parameters as those in a conventional system with the exception of the additional copper strips. Fig. 4-5 represents the schematics of the system.

The exciting voltage is given by an amplifier at the frequency range from 0.01 MHz to 10 MHz. The induced electric field in the receiver is generated by variations in the magnetic flux produced by the transmitter coil. Particular attention is paid to the analysis of the voltage received by the receiver with different distances and different frequencies in order to find the energy transfer pattern.

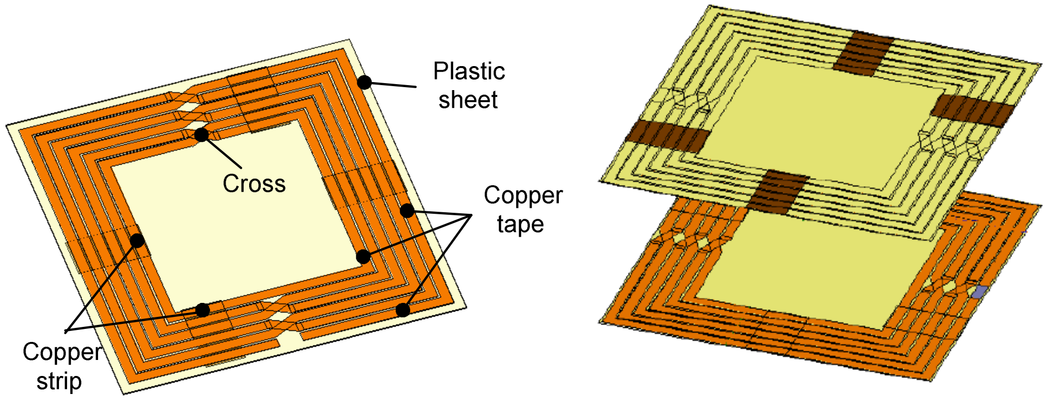

Fig. 4-5 FEM schematics of the system

The system has a relatively large electric field value when the frequency is at 4.8 MHz, which is near to the resonant frequency of the coil. The electric field strength also increases when the frequency is near to the resonant frequency, from 1.2 MHz to 3 MHz, and it decreases when the frequency is up to 8 MHz. This is accomplished mainly because of the application of resonant technology to create the magnetic fields that are largely governed by the electric distributions. When the transmitter and the receiver resonate with each other, most of the energy is transferred from the primary coil to the secondary coil.

For the witricity system, the receiver output voltage drops regularly with an increase in physical separation distance between the transmitter coil and the receiver coil, and Fig. 4-6 shows the trend. When the distance is near to zero, the receiver attains the highest voltage; the voltage values drop to about 14 V and 8 V when the distance increases to 10 cm and 15 cm, respectively. Although the output voltage becomes lower when the distance is increased, the system is more meaningful for practical applications. Hence it is essential to select an optimal distance based on practical requirements in order to balance efficiency and practical requirement.

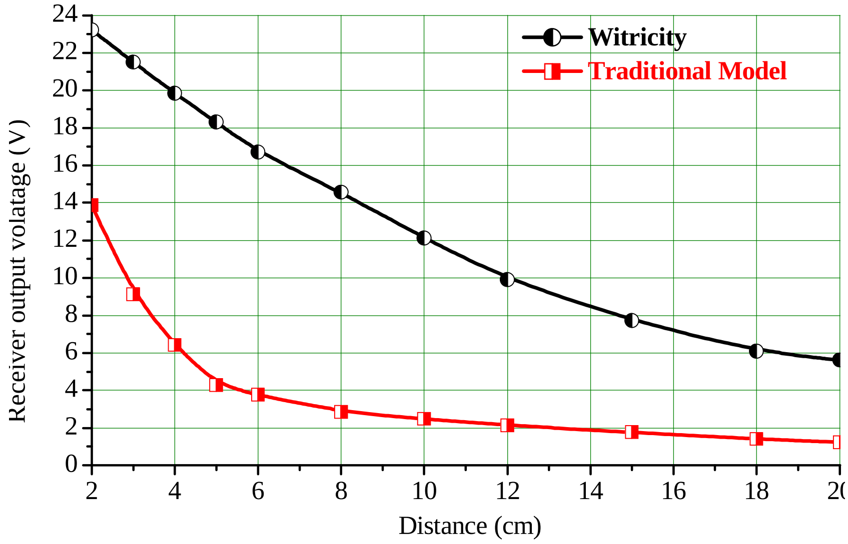

Fig. 4-6 Receiver output voltage vs. distance at a frequency of 4.8 MHz

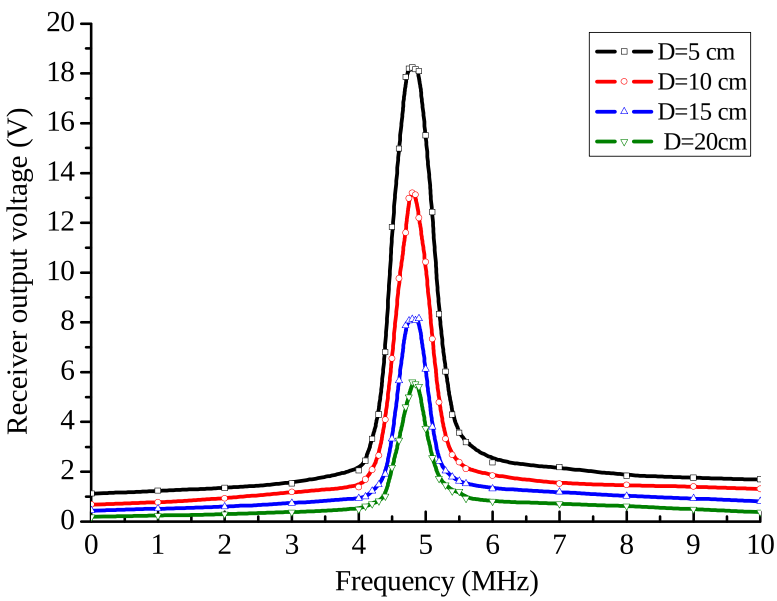

Fig.4-7 Receiver output voltage vs. frequency

Fig. 4-7 shows the receiver's output voltage values at frequencies ranging from 0.01 MHz to 10 MHz, when the distance between the transmitter and the receiver is 5 cm, 10 cm, 15 cm and 20 cm, respectively. It can be seen that all of the four wave lines have a large peak value when the frequency is at about 4.8 MHz, 18.23 V for 5 cm, 13.15 V for 10 cm, 8.12 V for 15 cm and 5.61 V for 20 cm. The appearance of these peak values is because of the resonant condition, which makes the transmitter coil and the receiver coil coupled strongly.

Based on the FEM findings, there is a good chance that the scheme can lead to strong coupling between the two coils for efficient energy transfer over non-negligible distances, and this is important for efficient wireless energy transfer over relatively long distances.

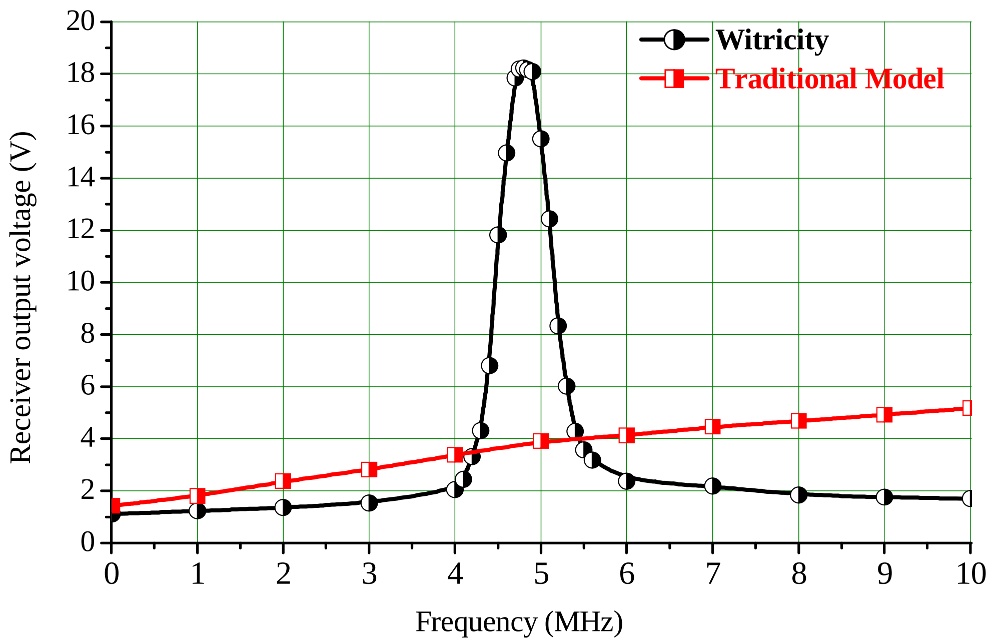

Fig. 4-8 Receiver output voltage vs. frequency with a distance of 5 cm.

Fig. 4-8 shows the receiver output voltage (with a distance of 5 cm) versus frequency for both witricity system and the traditional one. The frequency is varied between 0.01 MHz to 10 MHz. It can be seen that the induced voltage of the witricity system has a large peak value of 18.23 V at a frequency of about 4.8 MHz. For the traditional magnetic coupling model, the receiver output voltage only increase slightly when the frequency rises from 0.01 MHz to 10 MHz.

According to the principle of resonant wireless charging, an experimental prototype of the energy transfer system is built in the laboratory. Function generator and power amplifier are connected in series with the primary coil as shown in Fig. 4-9.

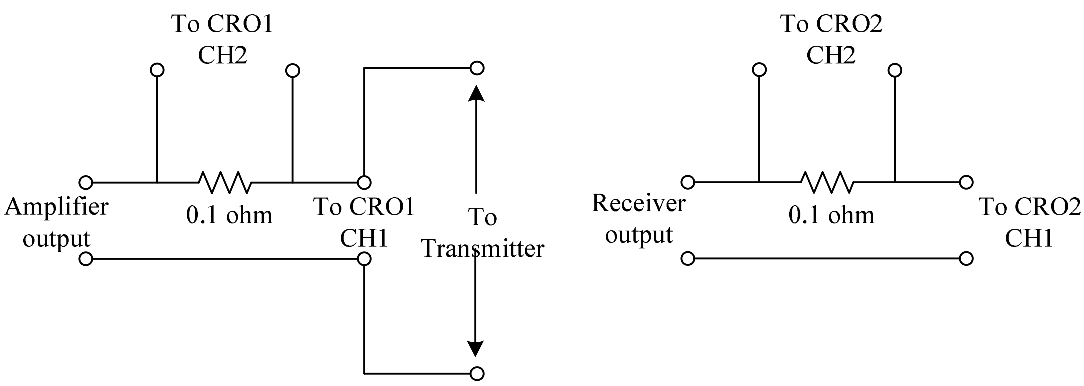

Fig. 4-9. Schematics of the system for experiment

The power signal source is a function generator, and a power amplifier that outputs a MHz sine wave to the source loop is used. A resistor is used as a load and the consumed power is calculated based on the measured voltage across the resistor. A second 0.1 Ω resistor is connected in series with the source to measure the power supplied. The measured resonant frequencies for the transmitter and the receiver are, respectively, 5.05 MHz and 5.02 MHz and their corresponding loaded *Q* factors are 62.1 and 69.5. By checking the voltage across the 0.1 Ω resistor at 5.03 MHz, the source current and therefore the power supplied are measured. Then, the following equations are used to calculate the efficiency:

$$\eta = \frac{S_t \cdot \cos\theta_t}{S_r \cdot \cos\theta_r} = \frac{U_t \times \frac{U_{Rt}}{R_t} \cdot \cos\theta_t}{U_r \times \frac{U_{Rr}}{R_r} \cdot \cos\theta_r} = \frac{U_{Rt} U_t R_r \cdot \cos\theta_t}{U_{Rr} U_r R_t \cdot \cos\theta_r} \tag{4-5}$$

where S_t, θ_t, U_t, R_t, and U_{Rt} are the transmitter's output apparent power, phase difference, output voltage, measured resistor, measured voltage on the resistor, respectively; S_r, θ_r, U_r, R_r, and U_{Rr} are the receiver's output apparent power, phase difference, output voltage, measured resistor, measured voltage on the resistor, respectively.

From Table 4-II, it can be seen that the energy transferred decreases when the distance becomes larger. At a distance of 2 cm, the output voltage is higher than 17 V, and the output current is about 0.479 A along with about 8.5 VA power and 84% efficiency. When the distance is up to 10 cm, these four values are about 12 V, 0.46 A, 5.8 VA and 56%, respectively. All the values drop dramatically as the distance between the transmitter and the receiver become longer and longer.

TABLE 4-II RECEIVER OUTPUT VOLTAGES AND CURRENTS OF THE TWO SYSTEMS

Distance (cm)	Witricity		Traditional model	
	Voltage (V)	Current (A)	Voltage (V)	Current (A)
2	17.590	0.479	13.07	0.412
3	17.160	0.477	10.34	0.327
4	16.800	0.476	8.76	0.212
5	16.200	0.476	6.01	0.196
6	15.300	0.475	4.13	0.161
7	14.670	0.471	3.35	0.133
8	13.800	0.466	3.17	0.116
9	13.200	0.464	2.85	0.107
10	12.350	0.459	2.62	0.104
11	11.600	0.455	2.48	0.101
12	9.400	0.446	2.24	0.0985
13	8.520	0.438	2.1	0.0962
14	7.260	0.408	1.96	0.0938
15	6.210	0.391	1.87	0.0941
16	5.600	0.365	1.65	0.0926
17	4.650	0.349	1.52	0.0932
18	4.250	0.342	1.41	0.0927
19	3.920	0.332	1.23	0.0913
20	3.430	0.322	1.09	0.0922

The trends of the secondary apparent power for the two systems as a function of distances are shown in Fig. 4-10. Though both of them decrease when the distance increases, the apparent power of the witricity system are much higher than that of the traditional model, especially in the distance range of 2 cm to 10 cm. In general, the secondary apparent power in traditional inductive magnetic coupling model decreases very rapidly as the distance increases.

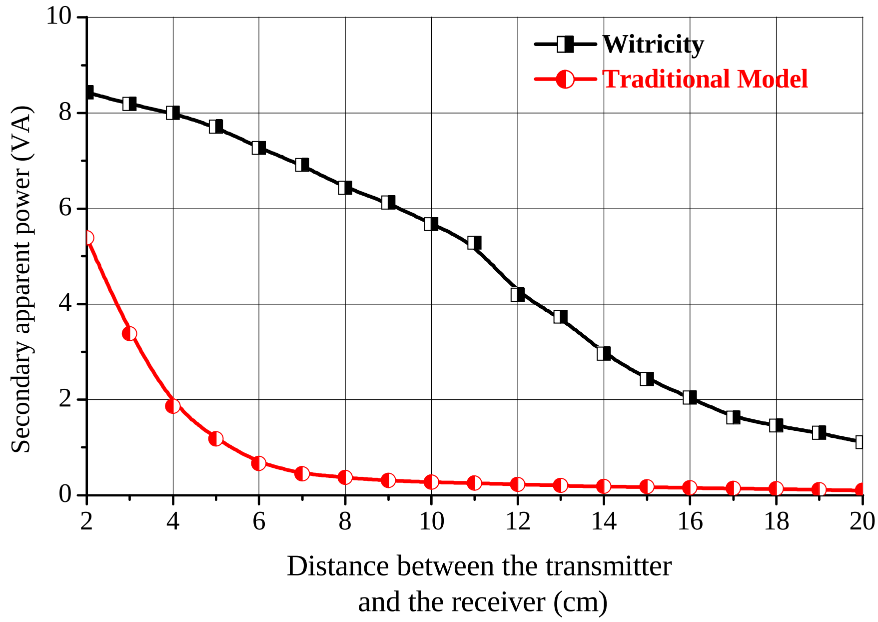

Fig.4-10 Secondary apparent power versus distance

The most important parameters among these results are the efficiency against distance as shown in Fig. 4-11. Although the efficiency is seen to decrease when the distance increases from 2 cm to 20 cm, this system offers a much more efficient power delivery possibility compared to traditional magnetic inductive coupling transmissions.

It can be seen from Fig. 4-11 that the efficiency of witicity is 73% at 5 cm and 24% at 15 cm. In comparison, when the traditional inductive coupling method is used, the physical separation distance must be limited to less than 1 cm and 4 cm, respectively, in order to realize the same efficiencies. The studies indicate that witricity is a suitable and practical technology for providing wireless power to charge a wealth of electrical devices.

Fluctuations of the output voltage, output power and efficiency of the transmission, which may lead to instability in the whole system, appear because of changes in the coupling rate. Therefore this point must be fully addressed to enhance the stability of witricity systems. Carefully parameter design is also necessary, especially for energy transmission over a relatively large distance.

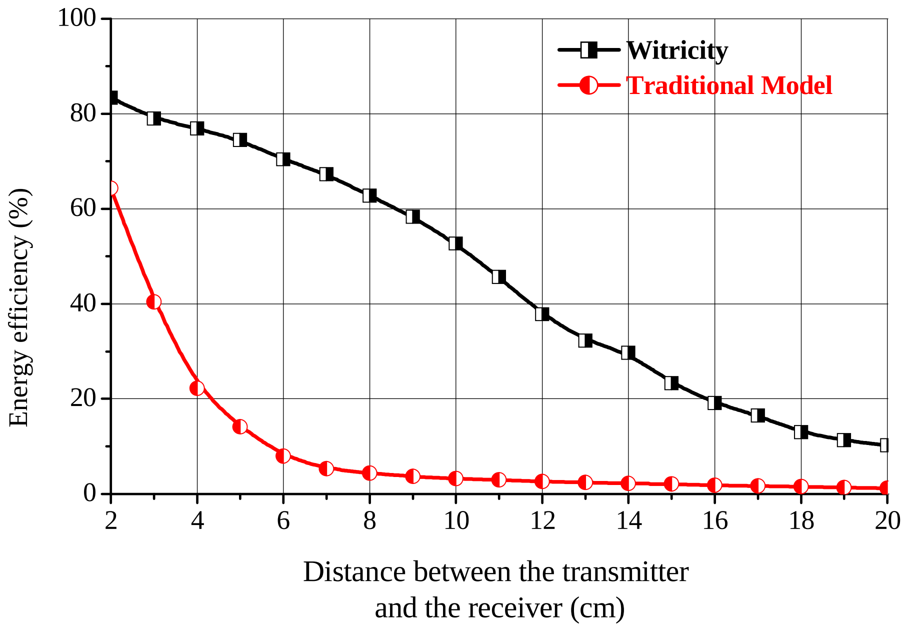

Fig. 4-11 Efficiency comparison between the two systems

The relatively small discrepancies of the resonant frequency and the output voltage between the FEM simulation results and measurement results can be explained for one part by measurement tolerances, especially at high frequencies. On the other hand, the ground plane is assumed to be homogeneous in the simulation model. Actually, there is a layer of glue between the copper layer and the insulation layer. The thickness and conductivity of this glue layer is not known very well and this also contributes to some inaccuracies.

4.2.2 Lateral and Angular Misalignment Analytical Study for Witricity Chargers with One Single-Coil Upgrading the Voltage Rate

The analysis presented in this part is evaluated based on a rectangular witricity model, since such coil shape is particularly well suited for mid-distance inductive power transfer. The extended model geometries for several turns of the transmitter coil and the receiver coil are also proposed with lateral and angular misalignments.

Based on the Biot-Savart law, the induced magnetic field at the receiver can be expressed as

$$\vec{H}_{induced} = \frac{I \cdot n_T}{4\pi} \oint \frac{d\vec{l} \times \vec{r}}{r^3} \tag{4-6}$$

where; n_T is the number of turns; $d\vec{l}$ is the tangential vector along the circular coil; r is the distance from the center of the receiver to the edge of the transmitter.

The proposed witricity charger includes a source loop, a transmitter resonant cell, a receiver resonant cell, and a device loop. The transmitter cell, consisting of a 20-turn coil tape in one layer and 4 strips in the other layer, is a square with a maximum length of 162 mm. There is an insulation layer to separate the two layers. The dielectric constant of the insulator is 3.74. The device cell also has the same structure. Both cells are made of copper tapes with a thickness of 40 μm. The width of the wires for the PCB coil tapes and the width of the strips are 2.9 mm and 25.4 mm, respectively. The system inductance is offered by a 20-turn copper tape and the capacitance is provided by a 20-turn coil tape layer and the 4 strips layer together. Fig. 4-12 shows the schematics of the proposed system.

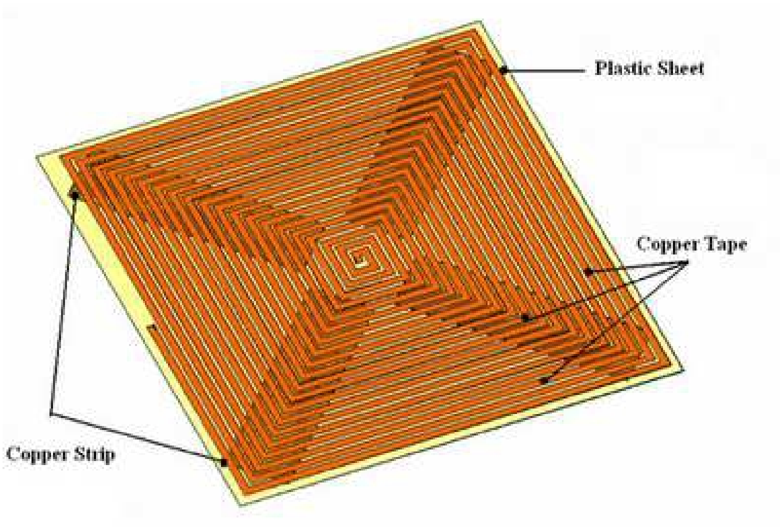

Fig. 4-12 FEM schematics of the witricity charger

The amplitude of the exciting voltage, which is given by an amplifier, is 25 V at the frequency range from 0.01 MHz to 10 MHz and the power rating is 8 W. The induced electric field in the receiver is generated by variations in the magnetic flux produced by the transmitter coil. Particular attention is paid to the analysis of the voltage received by the receiver when misalignments occur with different distances and different frequencies in order to find the energy transfer pattern. It is different from the former model and we used extra single-coil to provide excitation to the transmitter through short-distance magnetic coupling. That can make the transmitter just like a booster transformer, which will dramatically upgrade the voltage rate from 25 V near to 200 V.

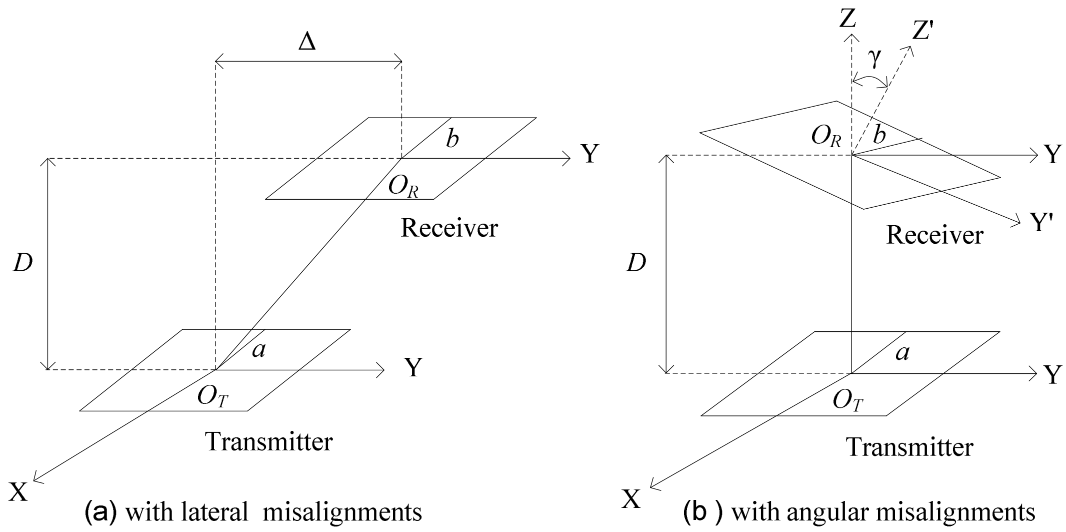

Fig. 4-13 Configurations of the witricity model with lateral and angular misalignments

Configurations of the witricity model with lateral and angular misalignments are shown in Figs. 4-13 (a) and (b), and the corresponding parameters are presented in Table 4-III. A set of design formula is given below, and the FEM analysis has been carried out to showcase the system performance. Because the coil inductance is mainly dependent on the length of the wires or the tapes, flat rectangular spiral coils are taken to be equivalent to flat circular spiral coils in order to use similar theory as a reference starting point for the design of such coils. The effects of changing the shapes of coils are ignored, and the number of turns and coil radius for both the transmitter and the receiver are the same.

TABLE 4-III. COIL AND CONSTRUCTION PARAMETERS

Quantity	Symbols
Coil radius	a, b
Distance between the two coils	D
Lateral misalignment	Δ
Angular misalignment	γ
Number of turns	n_T, n_R
Transmitter excitation current	i_T
Ohmic losses in the coils	R_T, R_R
Free-space permeability	μ_0
Magnetic permeability of ferrite core	μ_r

In the lateral misalignment case the transmitter and the receiver coils are located in parallel planes and their centers are offset by a distance Δ. The *x* and *y* components of the magnetic field vector can be ignored because they are parallel to the plane of the transmitter coil [12]. The component along the z axis is

$$H_{z-induced} = \frac{\frac{a}{\pi}\sqrt{2m}}{\left(\frac{a}{\pi}\Delta\right)^{2/3}} \left(\Delta K(m) + \frac{\frac{4a}{\pi} m - (2-m)\cdot\Delta}{2-2m} \cdot E(m) \right) \quad (4\text{-}7)$$

where; *K(m)* and *E(m)* are the complete elliptic integrals of thefirst and second kind, respectively; *m* is the modulus($0 \le m \le 1$).

$$m=\left[\frac{\left(\frac{16a}{\pi}\Delta\right)}{(\frac{4a}{\pi}+\Delta)^2+D^2}\right] \tag{4-8}$$

The distance between the two coils is fixed to 5 cm. Fig. 4-14 (a) shows the receiver's output voltage values at the frequency range from 0.01 MHz to 10 MHz, when the lateral misalignment between the transmitter and the receiver is 0 mm, 10 mm, 20 mm and 30 mm. It can be seen that all of the four wave lines have a large peak when the frequency is at about 2.03 MHz which are, namely, 146.84 V for 0 mm, 106.92 V for 10 mm, 66.03 V for 20 mm and 44.88 V for 30 mm. The appearance of these peak values is because of the resonant condition, which makes the transmitter coil and the receiver coil coupled strongly.

The output voltage of the receiver are recorded in Fig. 4-14 (b) at the frequency of 2.03 MHz according to the FEM simulation, when the lateral misalignment is 10 mm and the distance between the transmitter and the receiver is changed from 2 cm to 20 cm. It can be seen that there are large peaks when the frequency is at about 2.03 MHz, which are 109.35 V for 5 cm, 57.19 V for 10 cm, 31.84 V for 15 cm and 17.76 V for 20 cm. The appearance of these peak values is, once again, because of the resonant condition, which makes the transmitter coil and the receiver coil coupling strongly.

In the angular misalignment case the transmitter and the receiver coils are tilted to form an angle of γ. The x and y components of the magnetic field vector can be ignored due to the circular symmetry at the center of the receiver coil [80]. The component along the *z*-axis is

$$H_{z-induced} = \frac{\frac{16a^2}{\pi} \cdot \cos\gamma}{\left(\left(\frac{4a}{\pi}\right)^2 + D^2\right)^{3/2}} \tag{4-9}$$

Fig. 4-15(a) shows the output voltage of the receiver at the frequency range from 0.01 MHz to 10 MHz, when the angular misalignments between the transmitter and the receiver are 10°, 15°, 20°and 30°. The distance between the two coils is also fixed to 5 cm. All the four waves have large peak values when the frequency is at about 2.03 MHz which are, namely, 146.84 V for 0°, 124.32 V for 10°, 98.14 V for 20° and 62.75 V for 30°.

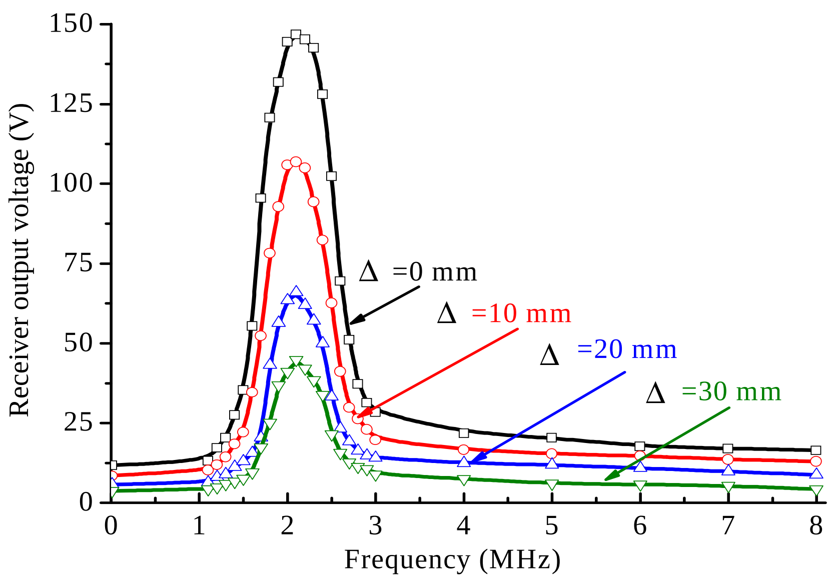

(a) vs. frequency

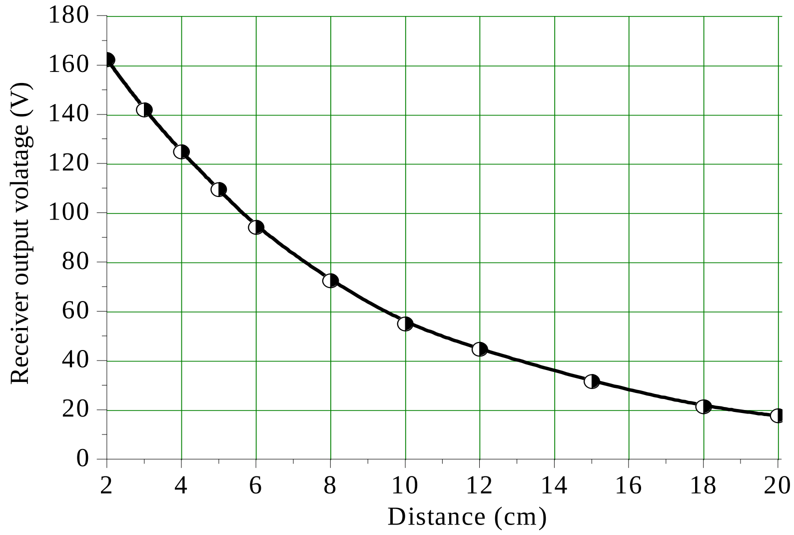

(b) vs. distance

Fig. 4-14 Receiver output voltages with lateral misalignments

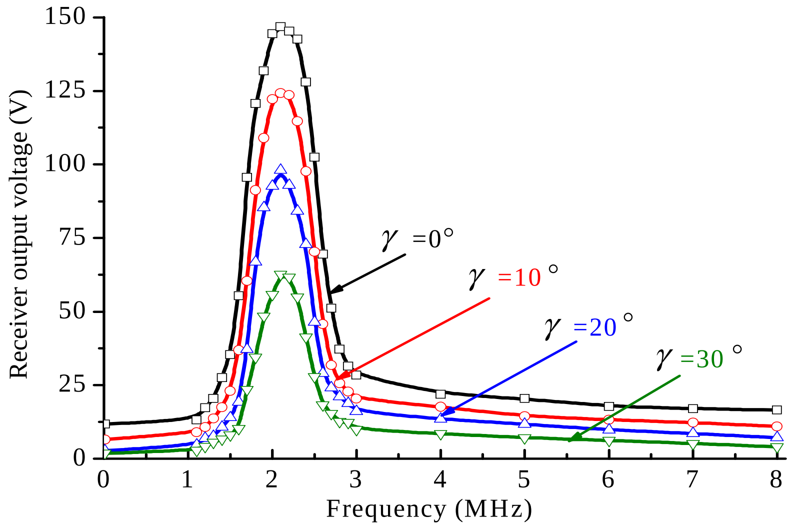

(a) vs. frequency

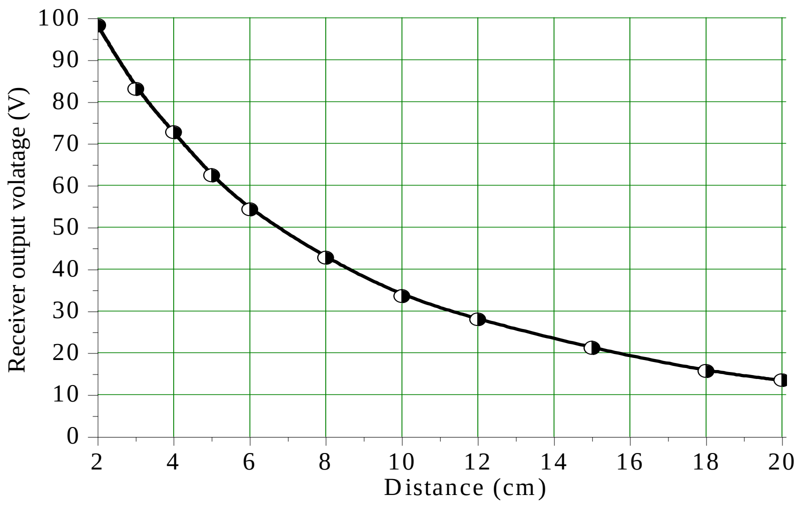

(b) vs. distance

Fig. 4-15 Receiver output voltages with angular misalignments

When the angular misalignment between the transmitter and the receiver is fixed at 30°, the receiver's output voltage values decrease from its peak value of 98.14 V to 13.42 V at the resonant frequency of 2.03 MHz as shown in Fig. 4-15(b). From these results, it can be seen that the energy being transferred for coils with small angular misalignments is reduced gradually when compared with other models with no misalignments.

To verify the simulation result, a prototype model is built and corresponding experiments have been carried out based on the FEM simulation results. The distance between the two coils is fixed at 5 cm and the resonant frequency is 2.34 MHz, which is slightly different from the FEM results.

The most important parameters among these results are the efficiency against distance as shown in Fig. 4-16. It provides very useful information about the witricity system in relation to lateral misalignments and angular misalignments. It can be seen that even though the efficiency decreases when misalignments occur, this system offers a much more efficient power delivery possibility compared to traditional magnetic inductive coupling transmissions.

For many charging applications such as implantable medical devices, mobile phones, and even TVs, a distance of 5 cm is long enough. Even when the lateral misalignment is 30 mm and the angular misalignment is 30°, the efficiency at 5 cm is up to 52.3% according to the test results of the system. It should be noted that by using traditional magnetic inductive coupling methods, the distance must be kept much shorter in order to obtain the same efficiency. Therefore, the witricity system provides a novel power delivery mechanism with a much higher and more attractive efficiency even with lateral or angular misalignments.

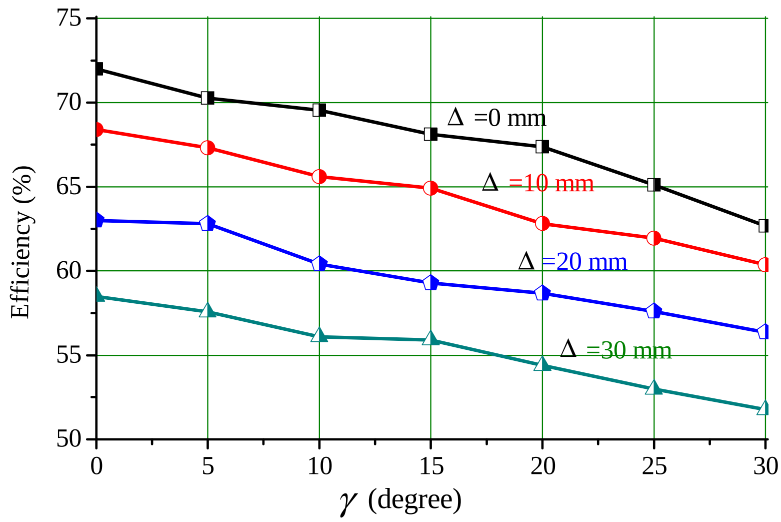

Fig. 4-16 The system efficiency versus distances with lateral and angular misalignments

4.2.3 Two Witricity Charger with TiO_2 Compound Interlayer

As the present witricity works at the MHz range, some undesirable problems become inevitable. First is that high frequency devices are much more expensive than their low frequency counterparts. High-frequency circuits and digital circuits are often sharing the same circuit board, constituting the so-called mixed signals or cross talks. High-frequency circuits are sometimes unstable as the digital circuits start up as the noise generated by the digital circuit affects the normal actions of high frequency circuits. Also, realization of inductive charging at high frequencies in electrical devices results in relatively more radiation and quick heat generation. Such problems require new methods to design the transmitter and the receiver in order to make it work at lower resonant frequencies.

(a)

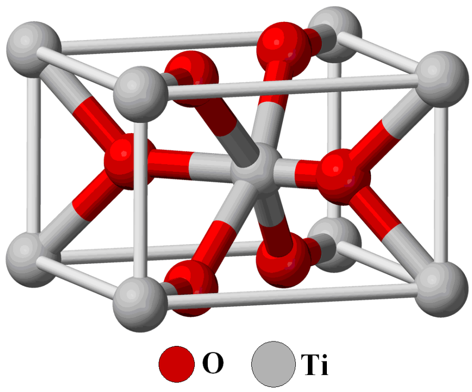

(b)

Fig. 4-17 (a) TiO_2 nano-powder material; (b) The structural model of rutile TiO_2

To reduce the resonant frequencies, new methods are necessary to design the transmitter and the receiver. In this part, two novel witricity chargers with TiO_2 nano-powder and $(C_4H_6O_2)_x$ latex combined interlayer is proposed. Finite element analysis (FEA) and corresponding experiments have also been carried out to showcase the performance of the charger.

Titanium exists in a number of crystalline forms and the most common two are anatase and rutile. Pure titanium dioxide does not occur in nature but can be derived from ilmenite or leuxocene ores. Figs. 4-17 (a) and (b) show the photos of rutile TiO_2 nano-powder material and its structural model. Because of the relatively poor mechanical properties of sintered titania, their applications are limited. It does however find a number of electrical applications in sensors and electro-catalysis [81-83].

For the proposed T-witricity system, the effective inductance L and the effective capacitance C for each coil can be defined as follows [60]

$$L = \frac{\mu_0}{4\pi|I_0|}\iint d\mathbf{r}d\mathbf{r}'\frac{\mathbf{J}(\mathbf{r})\cdot\mathbf{J}(\mathbf{r}')}{|\mathbf{r}-\mathbf{r}'|} \tag{4-10}$$

$$\frac{1}{C} = \frac{1}{4\pi\varepsilon_0|q_0|^2}\iint d\mathbf{r}d\mathbf{r}'\frac{\rho(\mathbf{r})\cdot\rho(\mathbf{r}')}{|\mathbf{r}-\mathbf{r}'|} \tag{4-11}$$

where $\mathbf{J}(\mathbf{r})$ is the spatial current and $\rho(\mathbf{r})$ is the charge densities. The energy W contained in the coil is

$$W = \frac{1}{2}L|I_0|^2 = \frac{1}{2C}|q_0|^2 \tag{4-12}$$

Based on this relation and the equation of continuity, the resulting resonant frequency is

$$f_0 = 1 / \left[2\pi (LC)^{1/2} \right] \tag{4-13}$$

The coil can be treated as a standard oscillator in coupled mode theory by defining

$$a(t) = 1 / \left[(LC)^{1/2} \right] I_0(t) \tag{4-14}$$

According to the equations (4-10)-(4-14), the resonant frequency of the proposed witricity system and other witricity systems, also known as eigenfrequency, is determined by the following equations:

$$\omega_{trans} = 1 / \sqrt{L_{trans} C_{trans}} \tag{4-15}$$

$$\omega_{rec} = 1 / \sqrt{L_{rec} C_{rec}} \tag{4-16}$$

where; L_{trans} and C_{trans} are the transmitter coil's equivalent inductance and equivalent capacitance, respectively; L_{rec} and C_{rec} are the receiver coil's equivalent inductance and equivalent capacitance, respectively.

Stray capacitances between the turns of the coils are negligible because of the small face-to-face areas and the relatively long airgaps. Thus,

$$C_{trans} = \frac{\varepsilon_{trans} \cdot S_{trans}}{d_{trans}} \tag{4-17}$$

$$C_{rec} = \frac{\varepsilon_{rec} \cdot S_{rec}}{d_{rec}} \tag{4-18}$$

where the subscripts *trans* and *rec* refer to transmitter coil and receiver coil, respectively; ε_{trans} and ε_{rec} are the permittivities; S_{trans} and S_{rec} are areas; d_{trans} and d_{rec} are the distances between the coils and the four copper tapes, respectively.

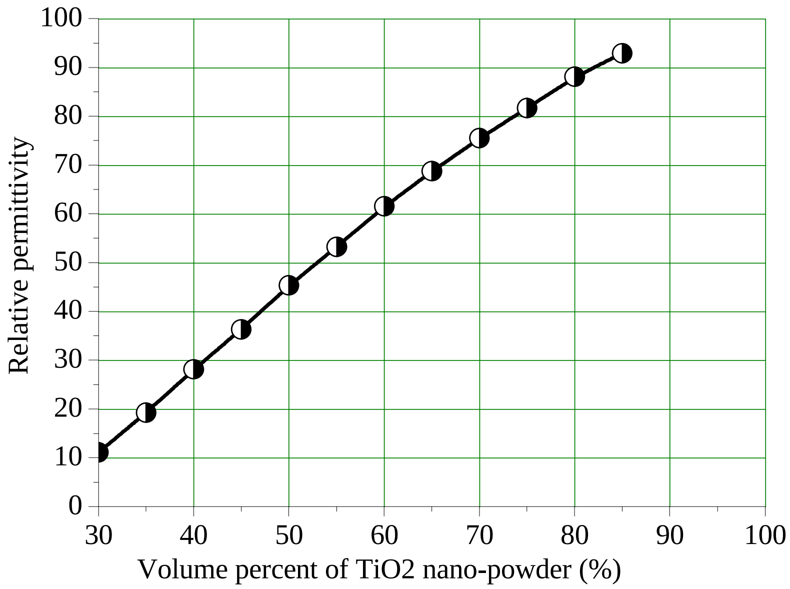

(a)

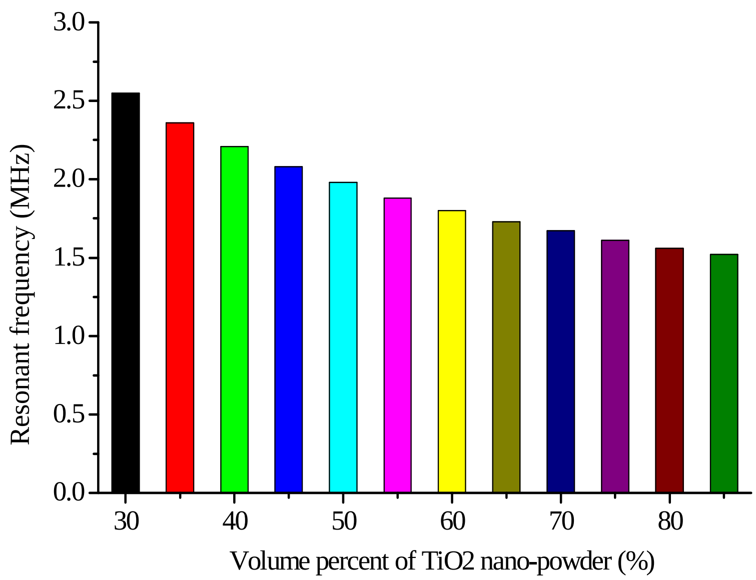

(b)

Fig. 4-18 (a) Relative permittivity of the combined materials. (b) Coils' resonant frequency of the proposed witricity charger

It can be seen from equations (4-17) and (4-18) that the resonant frequency will decrease by tuning the capacitance down. Through selecting materials with high permittivity, the capacitance can obviously be increased. Based on that observation, new interlayers consisting of 99.9% TiO_2 nano-powder and $(C_4H_6O_2)_x$ latex are fabricated. As the compound material composes of TiO_2 nano-powder and $(C_4H_6O_2)_x$ latex, it offers significant advantages over conventional dielectric materials. Since the compound is boned with high-purity TiO_2 nano-powder, it has a high permittivity and this is needed for lowering the systems' eigenfrequency. Figs. 4-18 (a) and (b) show the relative permittivity of the combined materials and the corresponding resonant frequencies of the T-witricity charger.

The relative permittivity of the interlayer selected in this design is 76, which represents a compromise on mechanical properties and taking advantages of the high relative permittivity of the compound. Both cells are made of copper tapes with a thickness of 40 μm. The inductance is offered by the copper tapes and the capacitance is provided by the coil tape layer and the strip layer together.

4.2.3.1 6-Turn Rectangular Spiral Model with TiO_2 Compound Interlayer

The proposed T-witricity charger contains a source loop, a transmitter resonant cell, a receiver resonant cell, and a device loop. There is an insulation layer, which is one of the proposed interlayers, to separate the coil and the four copper tapes for both the transmitter and the receiver. Coils for the transmitter and for the receiver have the same size and the same structure.

TABLE 4-IV. DIMENSION PARAMETERS OF THE 6-TURN T-WITRICITY CHARGER

Primary winding / Secondary winding	Shape	Rectangular spiral
	Turns	6 turns
	Thickness of copper	0.04 mm
	Width of copper	2 mm
	Copper track separation	1.5 mm
	Maximum length	208 mm
	Minimum length	106 mm
Copper strips with TiO_2 interlayer	Shape	Rectangle
	Number	4
	Thickness of copper strips	0.04 mm
	Thickness of TiO_2 interlayer	0.36 mm
	Width of copper strips with TiO_2 interlayer	25.4 mm
	Length of copper strips with TiO_2 interlayer	5 mm
	Relative permittivity	76

The relative permittivity of the interlayer selected is 76, which represents a compromise of mechanical properties and relative permittivity. The larger capacitance leads to lower resonant frequencies if other parameters are the same, as shown in Fig. 4-18(b). Both cells are made of copper tapes with a thickness of 40 μm. The inductance is offered by the copper tapes and the capacitance is provided by the coil tape layer and the strip layer together.

In order to uphold the performance of the proposed T-witricity charger, an interpolative FEA modeling method is introduced. T-witricity charger has a relatively high electric field when compared with those of the traditional magnetic coupling devices at the resonant frequency of 1.67 MHz at which efficient energy transfer is expected to occur in the proposed charger. At that point, most of the energy is transferred from the primary coil to the secondary coil. Fig. 4-19 shows the receiver output voltage (with a distance of 4 cm) versus frequencies for the T-witricity charger, the witricity charger and the traditional one. The frequency is varied between 0.01 MHz to 10 MHz. It can be seen that the induced voltage of the T-witricity charger has a peak value, i.e. 16.46 V at a frequency of about 1.67 MHz and that of the witricity charger is 18.23 V at a frequency of about 4.8 MHz when the input voltage is 25 V. Voltages of the traditional magnetic coupling model only increase slightly when the frequency rises.

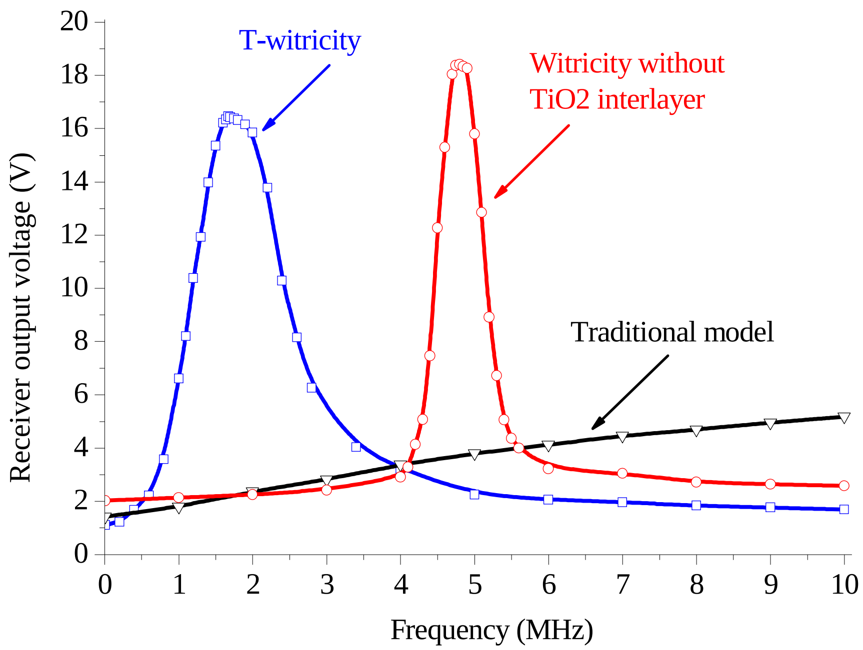

Fig. 4-19 Receiver output voltage vs. frequency with a distance of 5 cm

A noticeable characteristic of T-witricity charger that needs to be considered is the wider band of near resonant fields, from 0.8 MHz to 3.5 MHz. This characteristic is helpful, in some cases, in the design of resonant wireless charger that can work at limited resonant frequencies. But the witricity one only has a narrow frequency band about 0.7 MHz, from 4.5 MHz to 5.2 MHz. That may cause system failure when the frequencies fluctuate.

Output voltages of both the T-witricity charger and the witricity charger decrease steadily with an increase in the physical distance between the transmitter coil and the receiver coil. Although the value is also relatively high at the beginning, the decreasing trend becomes much more noticeable for the traditional magnetic coupling model as the physical distance is increased as shown in Fig. 4-20.

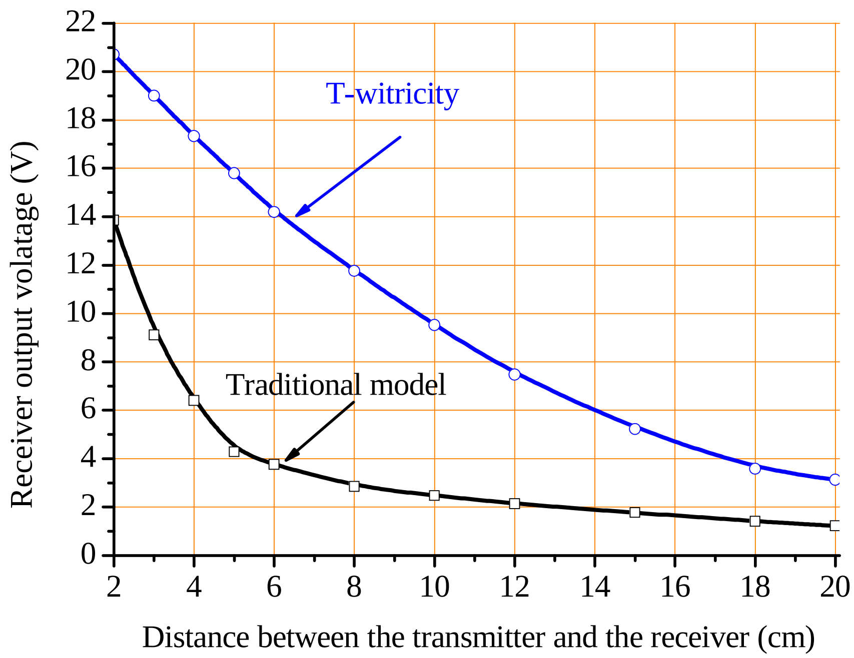

Fig. 4-20 Receiver output voltage vs. distance at the frequency of 1.67 MHz

For the T-witricity charger, the peak value of the receiver output voltages is slightly lower than that of the witricity charger. But the advantages are quite attractive when considering the operating resonant frequency and the wider band near the resonant fields. In addition, the designed resonant frequency should be low at about 600 kHz if the thickness of TiO_2 combined interlayer is the same with the non-TiO_2 interlayer, but it is impossible in practice due to the limitation of the mechanical process.

Based on the design experience of witricity chargers, a T-witricity charger is prepared using laboratory means with the same size of transmitter and receiver. The material of interlayers is produced from 70 volume percent of TiO_2, and 30 volume percent of $(C_4H_6O_2)_x$ latex based on the theoretical analysis and FEM simulation results. Then a function generator is connected to a power amplifier which generates a sinusoidal, 1.67 MHz, 9 W power supplies. The middle layer, made from polymers, serves as a skeleton framework and the proposed TiO_2 combined interlayers act as the electrical isolation between each coil and the four lower copper tapes. The magnetic field is generated by the upper layer which is fabricated by affixing spiral-type conductors consisting of 6 square turns with a separation distance of 4.0 mm between the conductors. The lower copper tapes consist of several conductive strips in parallel with the radial direction of the cell, forming capacitors with the overlapped parts of the upper coil.

The power signal source is a function generator, and a power amplifier that outputs a MHz sine wave to the source loop is used. A 0.1 Ω resistor is used as a load and the consumed power is calculated based on the measured voltage across the resistor. A second 0.1 Ω resistor is connected in series with the source to measure the power supplied. The measured resonant frequencies for the transmitter and the receiver are, respectively, 5.05 MHz and 5.02 MHz and their corresponding loaded Q factors are 62.1 and 69.5. By checking the voltage across the 0.1 Ω resistor at 5.03 MHz, the source current and therefore the power supplied are measured. Then, the following equations are used to calculate the efficiency:

The trends of the secondary apparent power for the three chargers as a function of distances are shown in Fig. 4-21. Though voltages for all of them decrease when the distances increase, the apparent powers of the proposed T-witricity charger and witricity partner are much higher than that of the traditional model, especially in the distance range of 2 cm to 10 cm. But the resonant frequency of the T-witricity charger is 1.74 MHz, only one third of that of the witricity. In general, the secondary apparent power decreases very rapidly as the distance increases in traditional inductive magnetic coupling model.

It can be seen from Fig. 4-22 that the efficiency of T-witricity charger is 70.6% at 5 cm and 26.3% at 15 cm. If the traditional inductive coupling method is used, the physical separation distance must be limited to less than 1 cm and 4 cm, respectively, in order to realize the similar efficiencies. The studies indicate that T-witricity is a suitable and practical technology for providing wireless power to charge a wealth of electrical devices, especially over relative large distance and slightly variable frequencies.

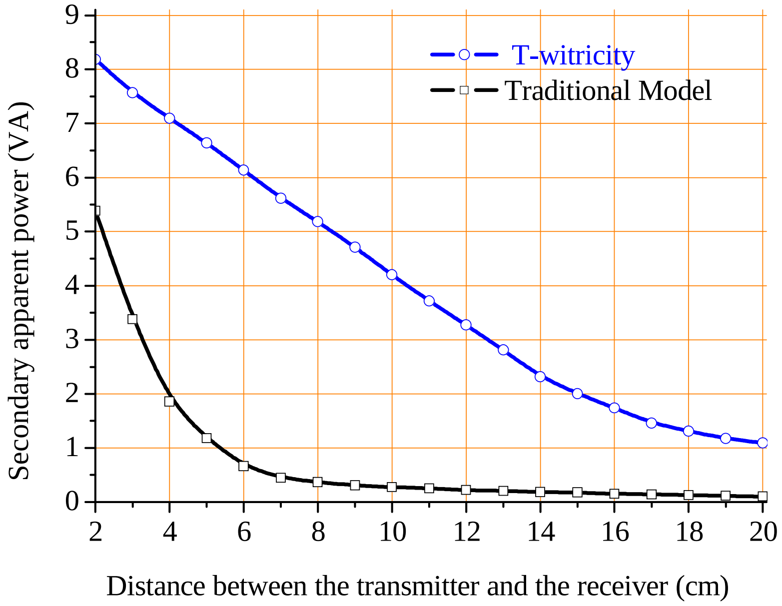

Fig. 4-21 Secondary apparent power versus distance

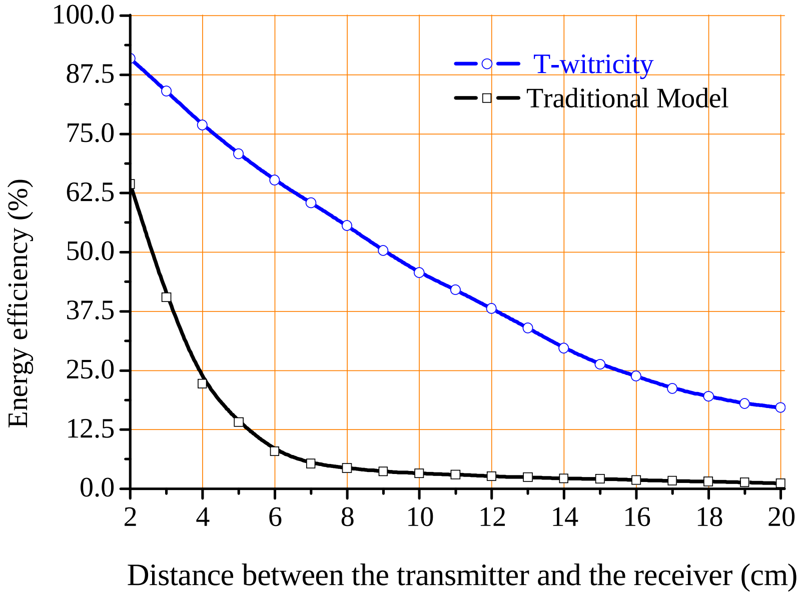

Fig. 4-22 Efficiency comparison between the T-witricity and the traditional magnetic coupling charger

Fluctuations of the output voltage, output power and efficiency of the transmission, which may lead to instability in the whole system, will appear because of changes in the coupling rate. Therefore this point must be fully addressed to enhance the stability of the T-witricity chargers. Careful parameter design is also necessary, especially for energy transmission over a relatively large distance.

4.2.3.2 20-Turn Rectangular Spiral Model with TiO_2 Compound

In order to uphold the optimal performance of the proposed system, an interpolative FEA modeling method is introduced. The T-witricity charger consists of a source loop, a transmitter resonant cell, a receiver resonant cell, and a device loop. There is an insulation layer, which is one of the proposed interlayers, to separate the coil and the four copper tapes for both the transmitter and the receiver. Coils for the transmitter and for the receiver have the same size and structure. Dimensional parameters are presented in Table 4-V.

The proposed charger has a relatively high electric field when compared with those of the traditional magnetic coupling devices at the resonant frequency of 681.2 kHz at which efficient energy transfer is expected to occur. At resonance, most of the energy is transferred from the primary coil to the secondary coil. Fig. 4-23 shows the receiver output voltage (with a distance of 4 cm) versus frequencies for the T-witricity system, the typical witricity charger and a traditional charger. The input voltage is 200V. It can be seen that the induced voltage of the proposed charger has a peak value, i.e. 153 V at a frequency of about 681.2 kHz and that of the typical witricity charger is 171 V at a frequency of about 2.38 MHz. Voltages of the traditional magnetic coupling model only increase slightly when the frequency rises. The output voltages of the proposed charger and the typical witricity charger both decrease steadily with an increase in the physical distance between the transmitter coil and the receiver coil.

TABLE 4-V. DIMENSION PARAMETERS OF THE 20-TURN T-WITRICITY CHARGER

Primary winding / Secondary winding	Shape of winding	Spiral
	Number of turns	20 turns
	Thickness of copper	0.04 mm
	Width of copper	2 mm
	Copper track separation	1.2 mm
	Maximum length	160 mm
	Minimum length	24 mm
Copper strips with TiO_2 interlayer	Shape of strips	Rectangle
	Number of strips	6
	Thickness of copper strips	0.04 mm
	Thickness of TiO_2 interlayer	0.32 mm
	Width of copper strips with TiO_2 interlayer	25.4 mm
	Length of copper strips with TiO_2 interlayer	5 mm
	Relative permittivity	76

Output voltages of both the T-witricity charger and the typical witricity charger decrease steadily with an increase in physical distance between the transmitter coil and the receiver coil. Although the output voltages are relatively high at the beginning for all chargers, Fig. 4-24 shows the decreasing trend becomes much more pronounced for the traditional magnetic coupling model as the physical distance increases.

For the T-witricity charger, the peak value of the receiver output voltages is slightly lower than that of the witricity charger. This characteristic is quite attractive when considering the lower operating resonant frequency and the wider band near the resonant fields of the proposed system. In other words, the system will continue to operate efficiently even if there are small perturbations in the resonance frequency. Indeed, the designed resonant frequency could be as low at about 300 kHz if the thickness of TiO_2 combined interlayer is the same as that of the non-TiO_2 interlayer, but currently it is difficult to fabricate such thickness due to the facility limitation of our laboratory.

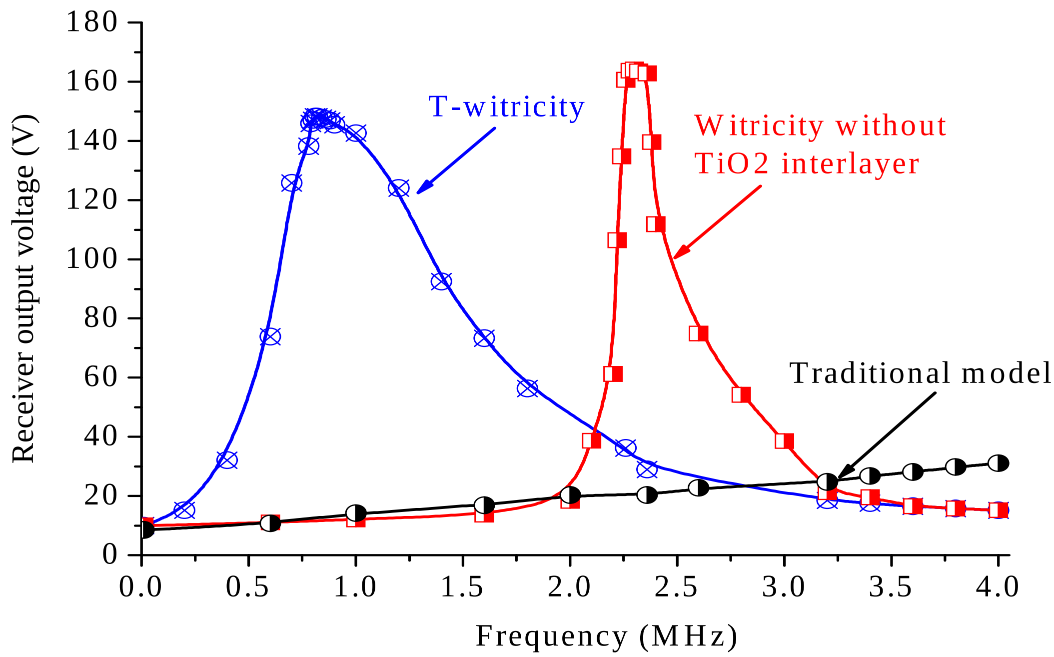

Fig. 4-23 Receiver output voltage vs. frequency with a distance of 4 cm

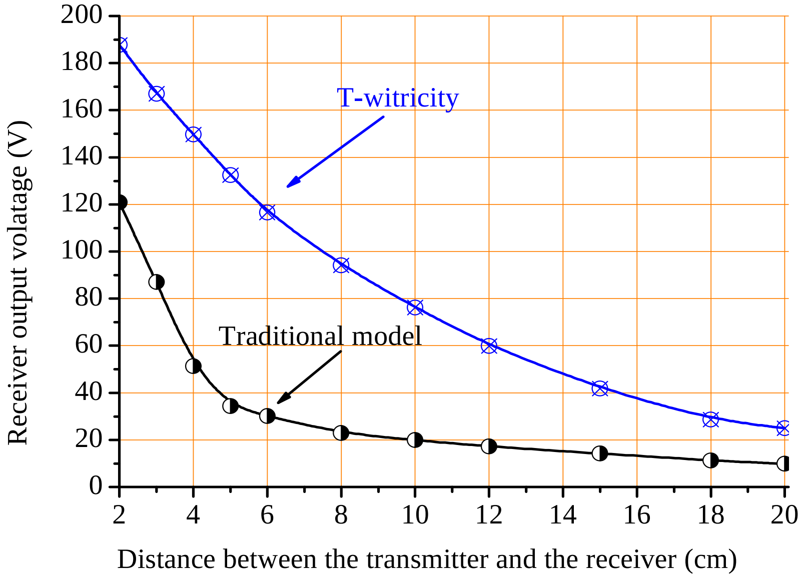

Fig. 4-24 Receiver output voltage vs. distance at the frequency of 681.2 kHz

The preferred resonant frequency should be as low as about 300 kHz if the thickness of TiO_2 combined interlayer can be made thin enough, but it is impossible to fabricate such thickness due to the limitation of our mechanical facilities.

The experimental setup comprises of a function generator together with a power amplifier that outputs a MHz sine wave to the source loop. The measured resonant frequencies for the transmitter and the receiver are, respectively, 693.7 kHz and 693.9 kHz and their loaded *Q* factors are 67.7 and 66.3. By checking the voltages at 693.7 kHz, the source current and therefore the power supplied are measured.

The trends of the secondary apparent power for the T-witricity and traditional magnetic coupling chargers as a function of distances are shown in Fig. 4-25. Though voltages for both of them decrease when the distances increase, the apparent power of the T-witricity charger is much higher than that of the traditional model, especially in the distance range of 2 cm to 10 cm. But the resonant frequency of the proposed charger is about 693.8 kHz, which is only one third of that of the typical witricity charger. In general, the secondary apparent power decreases very rapidly as the distance increases in traditional inductive magnetic coupling model.

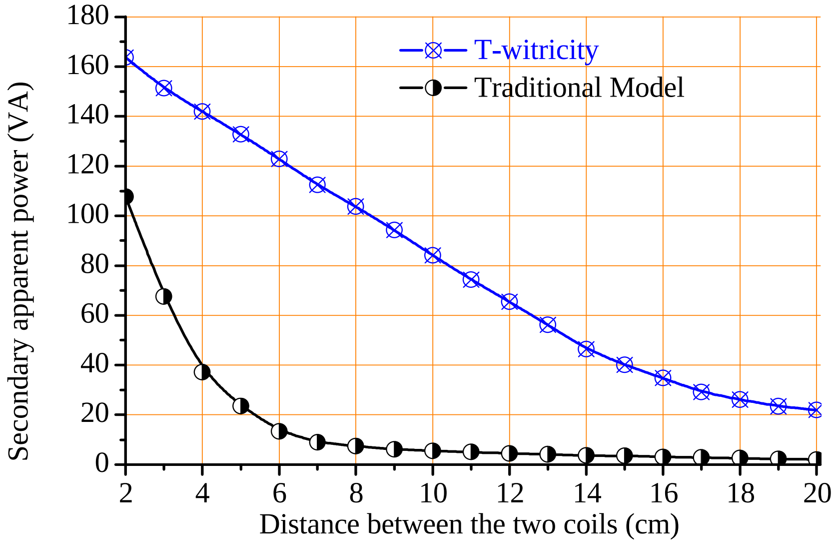

Fig. 4-25 Secondary output apparent power of the T-witricity charger and the traditional magnetic coupling charger

It can be seen from Fig. 4-26 that the efficiency of the proposed charger is 68.7% at 5 cm and 32.2% at 15 cm. If the traditional inductive coupling method is used, the physical separation distance must be limited to less than 1 cm and 4 cm, respectively, in order to realize similar efficiencies. The studies indicate that proposed charger is a suitable and practical technology for providing wireless power transfer to charge a wealth of electrical devices, especially over relative large distance and slightly variable frequencies.

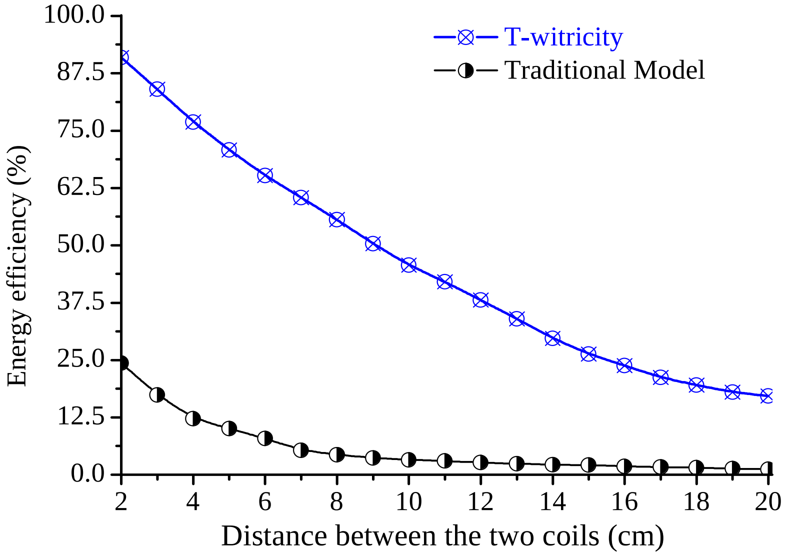

Fig. 4-26 Efficiency comparison between the T-witricity charger and the traditional magnetic coupling charger

Fluctuations of the output voltage, output power and efficiency of the transmission, which may lead to instability in the whole system, will appear because of the changes in the coupling rate. Therefore this point must be fully addressed in order to enhance the stability of the T-witricity chargers. Careful parameter design is also necessary, especially for energy transmission over a relatively large distance.

4.3 Witricity Transfer with Circular Coils

4.3.1 New Resonant Magnetic Charger with Circular Spiral Coils

Based on the witricity novel technology [26, 60], a new resonant magnetic charger with circular spiral coils for powering and recharging electrical devices is studied. Temporal coupled mode theory (CMT) for modeling and simulation is introduced to study the performance of the proposed system. Simulation and experimental results show that the system is effective in transferring power to wireless devices. The energy transfer efficiency with respect to system dimensions and the distance between the source and receiving cells are also studied analytically and experimentally. Figs. 4-27 and 4-28 illustrate the block diagram and the circuit diagram, respectively, of a resonant magnetic charger with circular spiral coils.

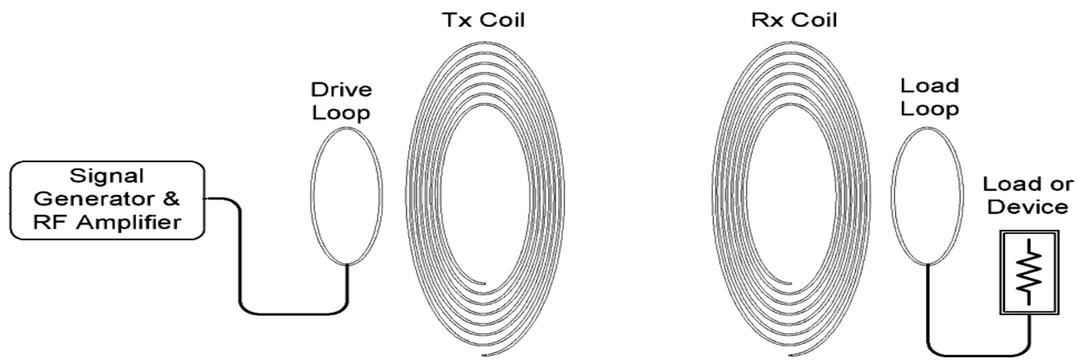

Fig. 4-27 Block diagram of the proposed resonant magnetic charger with circular spiral coils

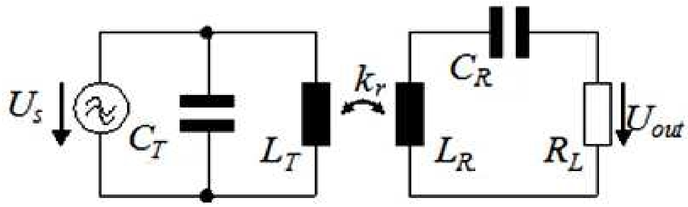

Fig. 4-28 Circuit diagram of a resonant magnetic charger

TABLE 4-VI. DESIGN PARAMETERS FOR RECTANGULAR SPIRAL COILS

Primary winding / Secondary winding	Shape	Circular spiral
	Turns	10 turns
	Thickness of copper	0.02 mm
	Width of copper	3.2 mm
	Copper track separation	1.4 mm
	Maximum diameter	132 mm
	Minimum diameter	40 mm
Copper strips	Shape	Rectangle
	Number	4
	Thickness of copper strips	0.04 mm
	Width of copper strips	25.4 mm
	Length of copper strips	50 mm
	Relative permittivity	3

Resonant coupling is the most efficient energy transfer process over mid-range distance. It is one of the key features in the design of regular coils in order to operate at specific resonating frequencies and to use the coils in applications in, for example, implant systems in the medical field. This technology is very different from traditional inductive energy transfer know-hows, because it is necessary to design the system firstly based on practical needs in terms of the area of the implant sites, for example, before the operation frequency is determined. In our study, the coupling uses two flat circular spiral inductors to create an inductively coupled link. Fig. 4-29 shows an analytical model for a new resonant magnetic charger with circular spiral coils. The design parameters are shown in Table 4-VI.

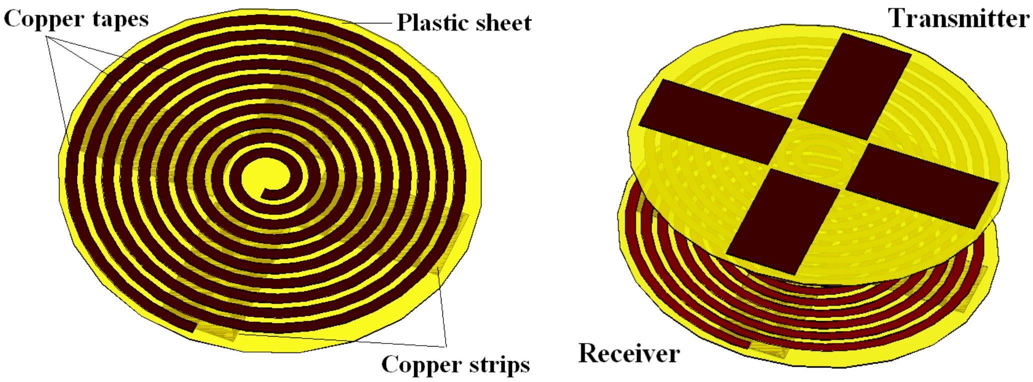

Fig. 4-29 FEM schematics of the resonant magnetic charger

Based on simulation results, the electric field distributions of the proposed charger at frequencies of 0.5 MHz, 3 MHz, 3.4 MHz and 5 MHz with a distance of 5.5 cm are given studied. There is a relatively large electric field when the frequency is at 3.4 MHz, which is near to the resonant frequency of the coils. The electric field strength also increases from 0.5 MHz to 3.4 MHz when the frequency approaches the resonant frequency of the coil. It decreases gradually when the frequency is increased beyond

3.4 MHz. This is accomplished mainly because of resonance which creates magnetic fields that are largely governed by the electric distributions. When the transmitter and the receiver resonate with each other, most of the energy is transferred from the primary coil to the secondary coil.

To evaluate the functionality of the proposed system, one practical model is designed and experimented. Fig. 4-30 presents the structure and one photo of the coils. The magnetic field is generated by the transmitter's upper layer which is fabricated by affixing spiral-type conductors consisting of 10 spiral turns with a separation distance of 1.4 mm between the conductors. The lower layer consists of several conductive strips in parallel with the radial direction of the cell, forming capacitors with the overlapped parts of the upper layer. The receiver picks up the transmitted power through induced eddy currents. The output voltages of the receiver at different frequencies and various distances are given in Fig. 4-31.

The receiver's output voltages are collected at frequencies ranging from 1 MHz to 8 MHz, when the distance between the transmitter and the receiver is adjusted to 3 cm, 5.5 cm, and 10 cm. It can be seen from Fig. 4-31 that all of the three wave lines have a large peak value when the frequency is at about 3.4 MHz, and they are 36.2 V for 3 cm, 25.7 V for 5.5 cm, and 9.3 V for 10 cm. The appearance of these peak values is because of the resonant condition, which electrically couples the transmitter coil and the receiver coil strongly.

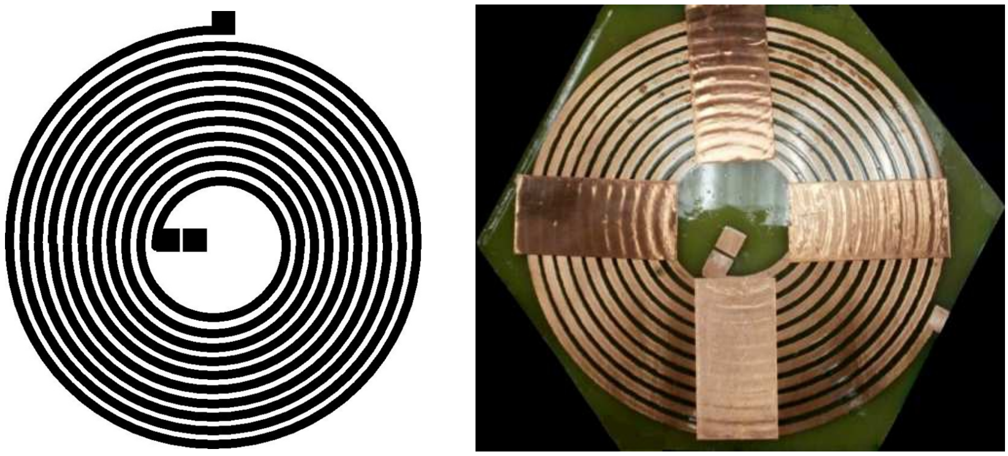

Fig. 4-30 Photos of the proposed charger coils

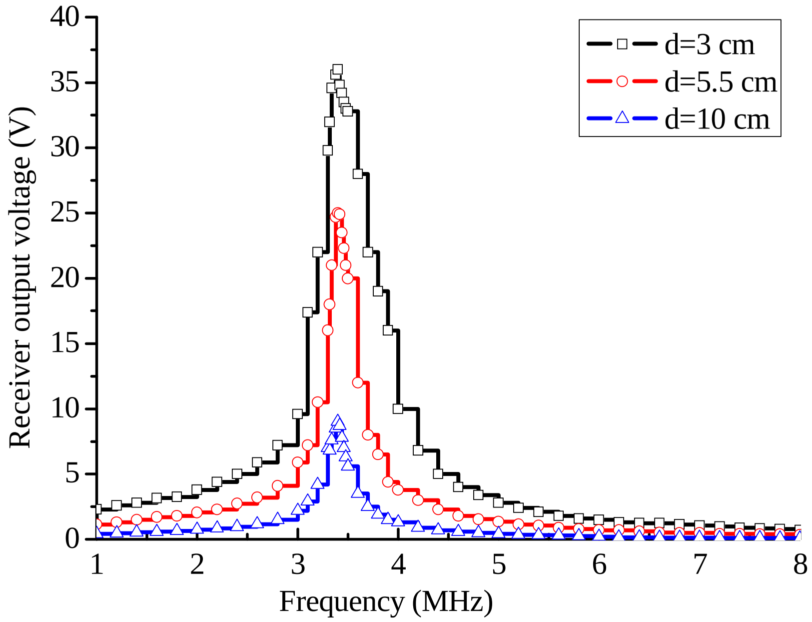

Fig. 4-31 Receiver output voltage at different frequencies

For the proposed resonant coupling system, the receiver output voltage drops regularly with an increase in physical separation distance between the transmitter coil and the receiver coil. Fig. 4-33 shows the receiver's output voltages at frequencies 2

MHz, 3.4 MHz, 3.5 MHz, and 5 MHz, when the distance between the transmitter and the receiver is ranging from 3 cm to 10 cm. When the distance is near to 3 cm, the receiver attains the highest voltage; the voltage values is observed to have dropped to about 25.7 V, 20 V, 2.5V and 2 V at the four afore-mentioned frequencies when the distance is increased to 5.5 cm. Although the output voltage becomes lower when the distance is increased, the proposed system nonetheless is meaningful for practical applications in that a reasonable voltage can still be picked up, with relatively high efficiency, by the receiver with a separation of a few cm.

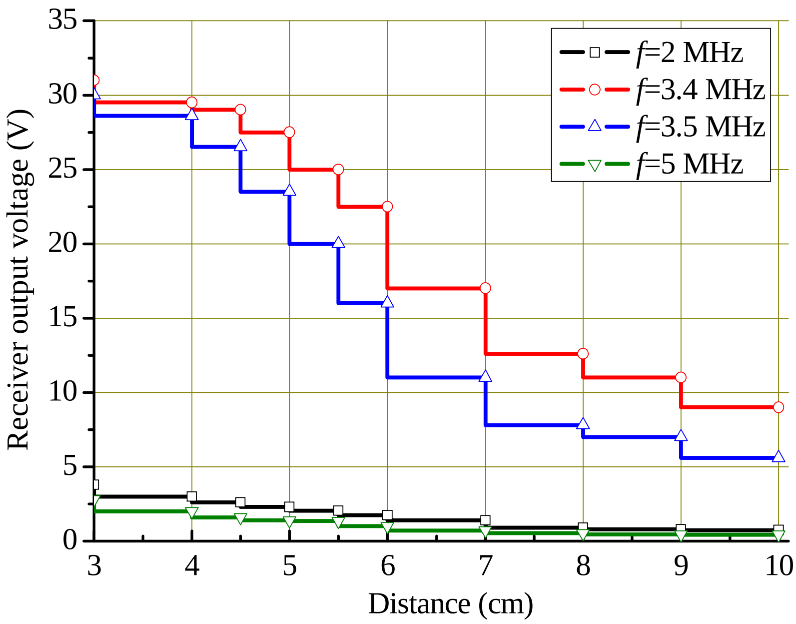

Fig. 4-32 Receiver output voltage vs. distance at the frequency of 3.4 MHz

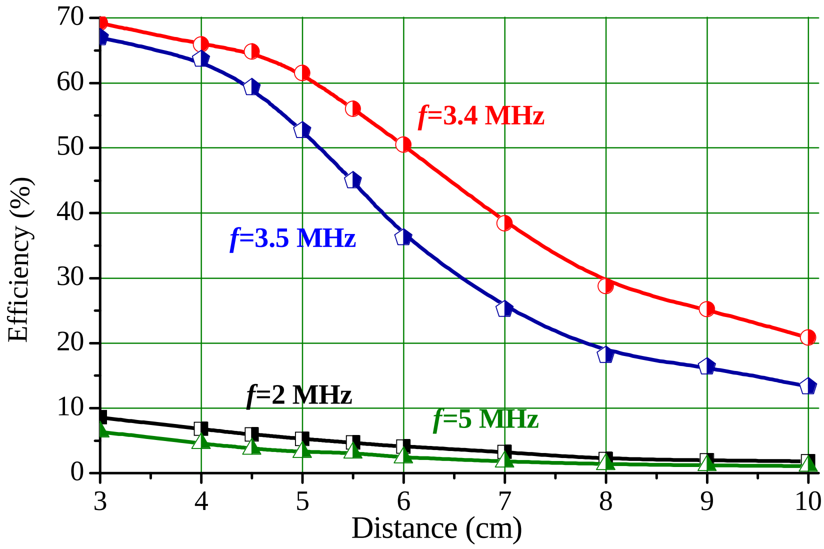

Fig. 4-33 The system efficiency at 2 MHz, 3.4 MHz, 3.5 MHz and 5 MHz with different distances

The energy transmission efficiency of the charger has also been evaluated and shown in Fig. 4-33. At transmitter-receiver separations from 3 cm to 10 cm, the input and output power values are measured by a network analyzer, a high-frequency multimeter and an oscilloscope in the laboratory. The efficiency with separation distances of 3 cm and 5.5 cm are up to 69% and 55% at the resonant frequency of 3.4 MHz. When the operating frequencies are 2 MHz and 5 MHz, which are not the resonant frequency, the efficiencies are only about 7% and 4% with the same distances.

4.3.2 Analytical Study of the PCB Circular Spiral Witricity Charger with Lateral and Angular Misalignments Analysis

In both traditional magnetic coupling and advance witricity systems for implantable devices, the transmitter and receiver coils are separated by a layer of skin and tissue, in the range of 1 cm to 5 cm. The coils are usually misaligned, due to anatomical constraints and hence the coupling efficiency is inevitably impaired. For traditional magnetic coupling system, low power inductive links are characterized by very unfavorable coil coupling conditions with large coil separations or a very small pickup coil diameter. The coupling factor can be as low as l% and may vary in a very unpredictable manner due to coil misalignments. But for witricity systems, the resonant nature of the process ensures that the interaction between the source and device is sufficiently strong and the interaction with non-resonant objects is minimal. In this manner, an efficient wireless channel for power transmission can be established and the efficiency can be as high as 60%-90% with a distance of about 1-5 cm between the transmitter and the receiver. In other words, the witricity system works with a relative high efficiency even if there is misalignment due to the operating conditions in a practical situation.

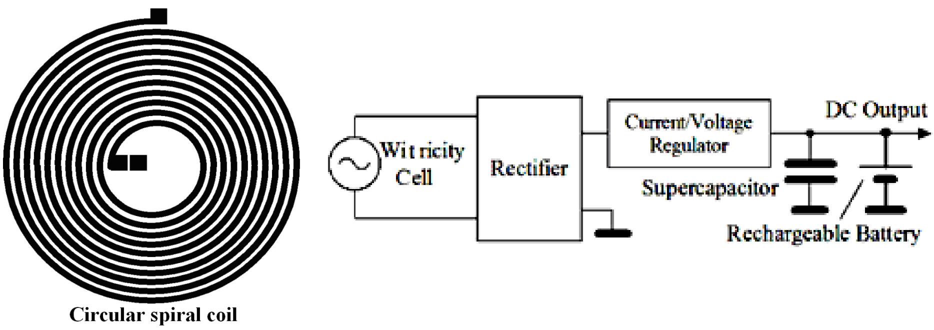

Fig. 4-34 Block diagram of the witricity system

Because of changes in the coupling rate, lateral misalignment and angular misalignment may cause fluctuations in output voltage, output power and transmission efficiency, leading to instability in the witicity system. These effects must therefore be fully addressed in order to enhance the stability of the system. Careful parameter design is also necessary, especially for energy transmission over a relatively large distance.

It is known that coil dimensions and coil shapes substantially affect the magnitude of the magnetic field and the magnitude of the magnetic field is closely related to the efficiency of the inductive link. The contribution is to introduce a novel power transfer function to address misalignments of the witricity coils.

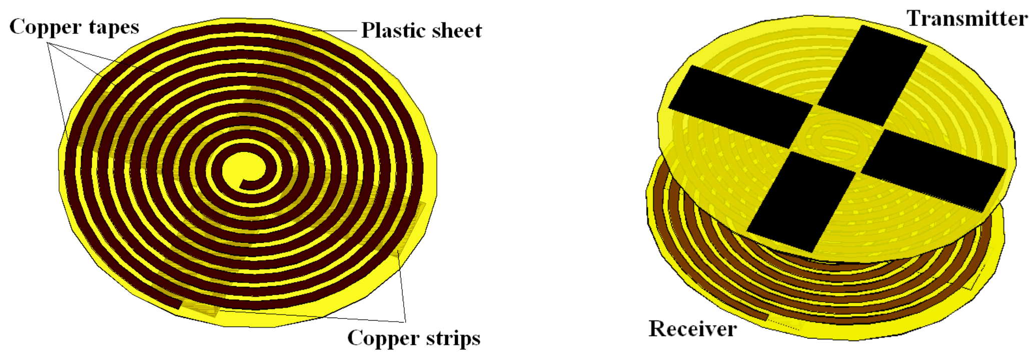

(a) The spiral circular coil; (b) Normal witricity system

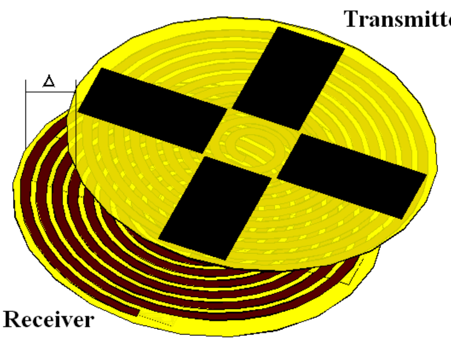

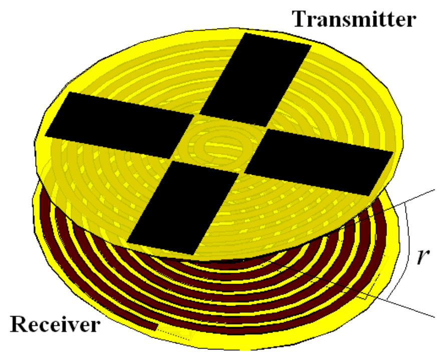

(c) With lateral misalignments Δ; (d) With angular misalignments γ.

Fig. 4-35 FEM schematics of the resonant magnetic charger

The relationship between the energy transfer efficiency and several key parameters of the system is analyzed using FEM. The analyzed results for the resonant power transfer being developed will allow the designer to optimize the efficiency of the link and predict the effect of coil characteristics and misalignment on the coupling factor. An interpolative FEA modeling simulation is introduced to study the performance of witricity systems with lateral and angular misalignments. Experiments have also been carried out to facilitate quantitative comparison. Fig. 4-34 are block diagram of the proposed charger.

The analysis presented is evaluated based on a circular spiral witricity model, since such coil shape is particularly well suited for mid-distance inductive power transfer. The extended model geometries for several turns of the transmitter coil and the receiver coil are also proposed with lateral and angular misalignments.

The proposed witricity charger includes a source loop, a transmitter resonant cell, a receiver resonant cell, and a device loop. The transmitter cell, consisting of a 10-turn coil tape in one layer and 4 strips in the other layer, is a circular spiral with a maximum diameter of 116 mm. There is an insulation layer to separate the two layers. The dielectric constant of the insulator is 3. The device cell also has the same structure. Both cells are made of copper tapes with a thickness of 40 μm. The width of the wires for the PCB coil tapes and the width of the strips are 2.9 mm and 25.4 mm, respectively. The system inductance is offered by a 10-turn copper tape and the capacitance is provided by a 10-turn coil tape layer and the 4 strips layer together. Fig. 4-35 shows the FEM schematics of the proposed system.

The amplitude of the exciting voltage, which is given by an amplifier at the frequency range from 0.01 MHz to 8 MHz. The induced electric field in the receiver is generated by variations in the magnetic flux produced by the transmitter coil. Particular attention is paid to the analysis of the voltage received by the receiver when misalignments occur with different distances and different frequencies in order to find the energy transfer pattern.

Configurations of the witricity model are presented in Table 4-VII, and the FEM analysis has been carried out to showcase the system performance. Because the coil inductance is mainly dependent on the length of the wires or the tapes, flat circular spiral coils are taken in order to use similar theory as a reference starting point for the design of such coils. The effects of changing the shapes of coils are ignored, and the number of turns and coil radius for both the transmitter and the receiver are the same.

TABLE 4-VII. DESIGN PARAMETERS FOR CIRCULAR SPIRAL COILS

Primary winding / Secondary winding	Shape	Circular spiral
	Turns	10 turns
	Thickness of copper	0.02 mm
	Width of copper	2.9 mm
	Copper track separation	1.1 mm
	Maximum diameter	116 mm
	Minimum diameter	36 mm
Copper strips	Shape	Rectangle
	Number	4
	Thickness of copper strips	0.04 mm
	Width of copper strips	25.4 mm
	Length of copper strips	50 mm
	Relative permittivity	3

In the lateral misalignment case the transmitter and the receiver coils are located in parallel planes and their centers are offset by a distance Δ. The *x* and *y* components of the magnetic field vector can be ignored because they are parallel to the plane of the transmitter coil [80].

The receiver's output voltages are collected at frequencies ranging from 1 MHz to 8 MHz, when the distance between the transmitter and the receiver is adjusted to 2 cm, 5 cm, and 10 cm. It can be seen from Fig. 4-36 that all of the three wave lines have a large peak value when the frequency is at about 4.2 MHz, and they are 49.3 V for 2 cm, 35.2 V for 5 cm, and 12.4 V for 10 cm. The appearance of these peak values is because of the resonant condition, which electrically couples the transmitter coil and the receiver coil strongly.

Fig. 4-37(a) shows the receiver's output voltage values at the frequency range from 0.01 MHz to 8 MHz and the distance between the transmitter and the receiver is 5 cm, when the lateral misalignment between the transmitter and the receiver is 0 mm, 10 mm, 20 mm and 30 mm. It can be seen that all of the four wave lines have a large peak when the frequency is at about 4.2 MHz which are, 35.2 V for 0 mm, 25.95 V for 10 mm, 16.01 V for 20 mm and 10.89 V for 30 mm. The appearance of these peak values is because of the resonant condition, which makes the transmitter coil and the receiver coil coupled strongly.

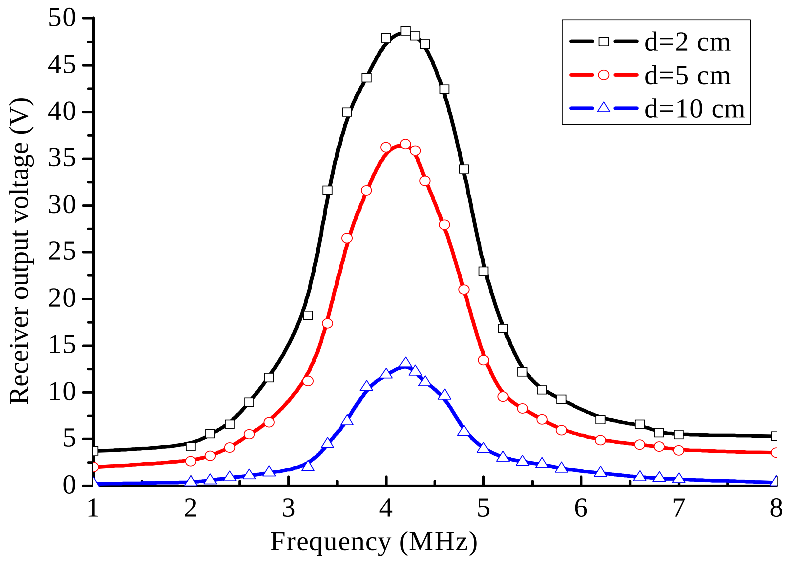

Fig. 4-36 Receiver output voltage at different frequencies

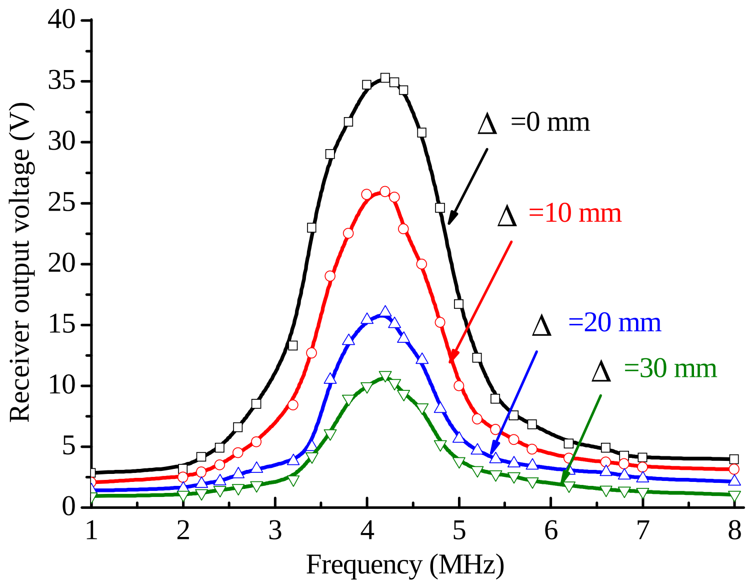

(a) vs. frequency at the distance of 5 cm

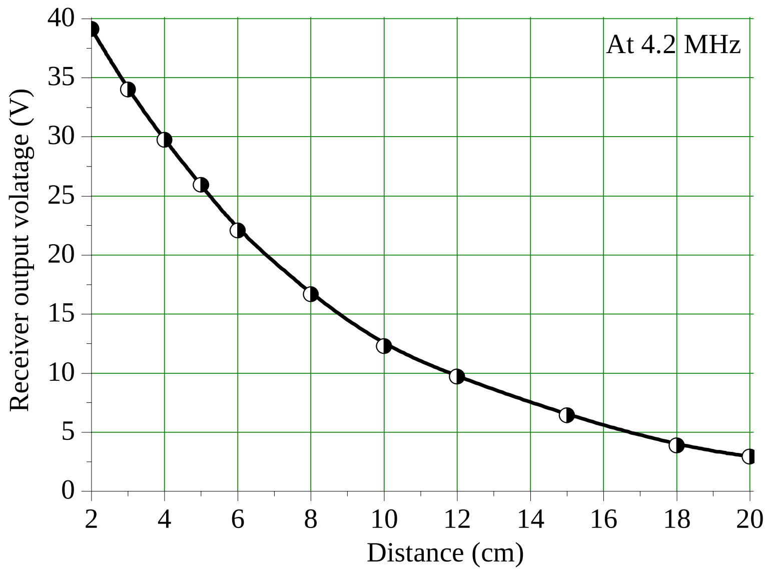

(b) vs. distance when the lateral misalignment is 10 mm

Fig. 4-37 Receiver output voltages with lateral misalignments

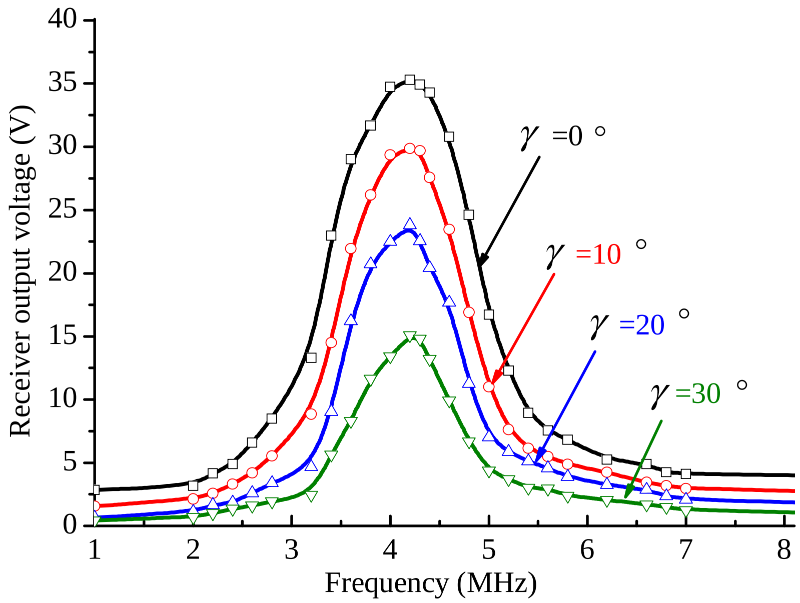

(a) vs. frequency at the distance of 5 cm

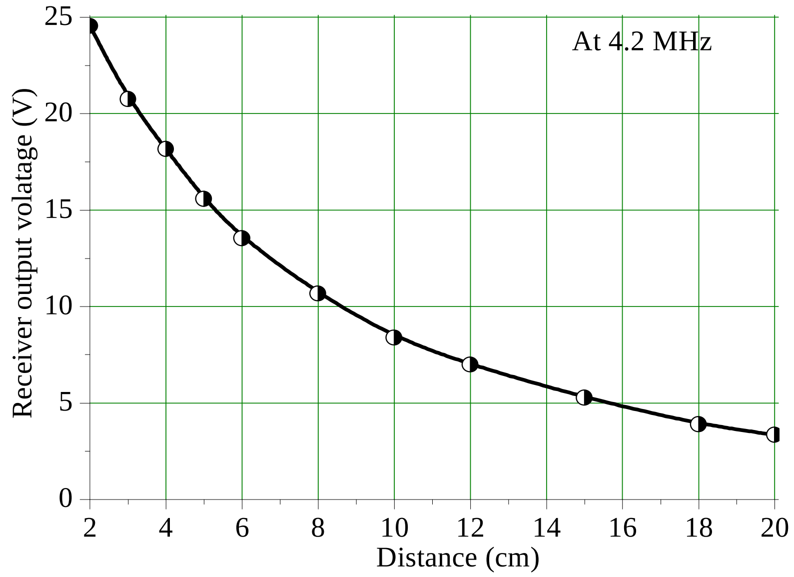

(b) vs. distance when the angular misalignment is 30º

Fig. 4-38 Receiver output voltages with angular misalignments

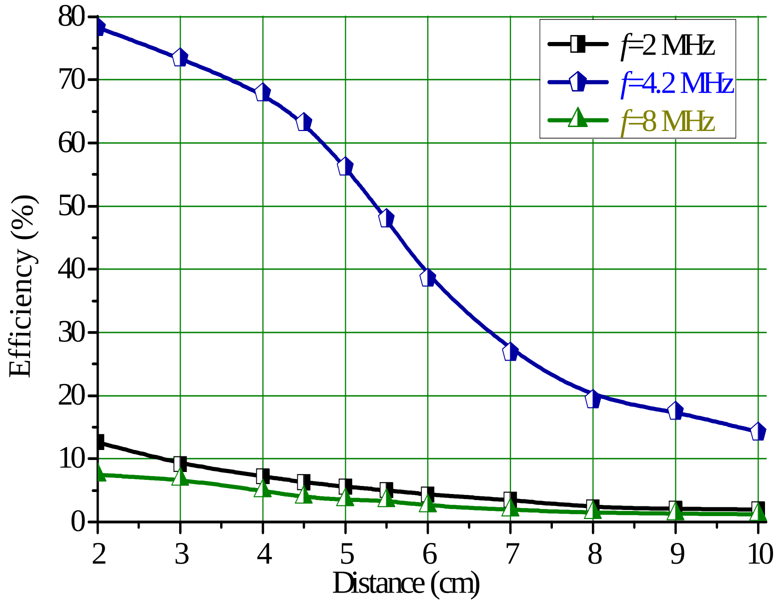

Fig. 4-39 The system efficiency at 2 MHz, 4.2 MHz, and 8 MHz with different distances

The output voltage of the receiver are also recorded at the frequency of 4.2 MHz according to the FEM simulation, when the lateral misalignment is 10 mm and the distance between the transmitter and the receiver is changed from 2 cm to 20 cm. It can be seen from Fig. 4-37(b) that there are large peak when the frequency is at about 4.2 MHz, which are 25.95 V for 5 cm, 12.27 V for 10 cm, 6.425 V for 15 cm and 2.94V for 20 cm. The appearance of these peak values is, once again, because of the resonant condition, which makes the transmitter coil and the receiver coil coupling strongly.

In the angular misalignment case the transmitter and the receiver coils are tilted to form an angle of γ. The x and y components of the magnetic field vector can be ignored due to the circular symmetry at the center of the receiver coil [80].

Fig. 4-38(a) shows the output voltage of the receiver at the frequency range from

0.01 MHz to 8 MHz, when the angular misalignments between the transmitter and the receiver are 10°, 15°, 20°and 30°. The distance between the two coils is also fixed to 5 cm. All the four waves have large peak values when the frequency is at about 4.2 MHz which are 35.2 V for 0°, 29.86 V for 10°, 23.81 V for 20° and 15.07 V for 30°.

When the angular misalignment between the transmitter and the receiver is fixed at 30°, the receiver's output voltage values decrease from its peak value of 15.07 V to 3.42 V at the resonant frequency of 4.2 MHz. From these results, it can be seen Fig. 4-38(b) that the energy being transferred for coils with small angular misalignments is reduced gradually when compared with other models with no misalignments.

The most important parameters among these results are the efficiency against distance as shown in Fig. 4-39. It provides very useful information about the witricity system, based on the resonant magnetic coupling method. It can be seen that even though the efficiency decreases when distance between the transmitter and the receiver increases, this system offers a much more efficient power delivery possibility compared to traditional magnetic inductive coupling transmissions.

4.4 Summary

For many electric charging applications such as in implantable medical devices, mobile phones, and even TVs, usually an average distance of about 5 cm between the transmitter and the receiver is enough. The efficiency at that distance is up to 50%-80% according to the simulation and measurement results of the system. It should be noted that by using traditional magnetic inductive coupling methods, the distance must be kept much shorter, less than 0.5 mm, in order to obtain similar efficiency. The study of the model indicates that if the system can be made to operate at the resonant frequency, satisfactory performances are realized.

A resonant energy transfer system with rectangular spiral inductors for wireless charging electrical devices has been analyzed firstly by employing FEM analysis and the findings are validated experimentally. Output voltage, current, power and the transfer efficiency are studied at different frequencies and distances between the primary coil and the secondary coil.

And then a novel analytical model for witricity has been presented, incorporating misalignment effects. FEM simulations and corresponding experiments for the magnetic field at the receiver with lateral and angular misalignments have been suggested. The analytical model introduced can be used to develop a design procedure for optimum power transfer in low power inductive links. It is the intention of this research to extend the model for square and circular spiral coils.

New interlayers with high relative permittivity, produced by combined TiO_2 nano-powder and $(C_4H_6O_2)_x$ latex, are proposed next to design two novel resonant inductive magnetic coupling wireless chargers. The proposed T-witricity chargers have been analyzed by employing FEM analysis and the findings are validated experimentally. Operating resonant frequency, output voltage, current, power and the transfer efficiency are studied at different frequencies and distances between the primary coil and the secondary coil.

The measured results indicate that if the proposed chargers can be made to operate at the resonant frequency, which is much lower than that of the witricity model without TiO_2 combined interlayers, satisfactory performances can be realized.

And then novel witricity analytical spiral models for charging the electrical devices have been proposed and studied both through simulation and experiments. Also, the study incorporating misalignment effects has been carried out. FEM simulations and corresponding experiments for the magnetic field at the receiver under lateral and angular misalignments have been suggested. The efficiency at that distance is up to 50% according to the analytical and experiment findings of the proposed system. By carefully designing and calibrating the system, a higher efficiency is likely to be achievable. It is the intention of this research to extend the model for the circular spiral coils.

There is a good chance that the proposed scheme can be further improved to result in strong coupling between the two coils for efficient energy transfer over non-trivial distances which are of paramount importance for implant devices in the medical field.

CHAPTER 5 WITRICITY CHARGER FOR IMPLANTED DEEP BRAIN STIMULATION

5.1 Introduction

Based on the study in the above chapters, we have designed two devices as well as a cell phone charger, shown in Appendice I, to verify the feasibility of applying witricity technology to practical applications. For some artificial medical devices like artificial limb, the power might up to several watts. Considering the experiment condition and the complexity, we choose the cell phone in Appendice I as the experiment subject to study its performance for future design, though it is not directly related to the medical devices. The other two ones have been done in Pittsburgh University in U.S., under the guidance of Prof. Mingui Sun. We have designed one platform for rats' implanted coils experiments, which is shown in Appendice II, and one novel charger for charging the DBS device, presented in this chapter. Both of them are analyzed by FEM simulations and corresponding experiments to illustrate their great potential performances.

In the current design of clinical neural implants, electric energy transmission plays a critical role in essentially all intelligent man-made prosthetic devices, from artificial hearts to brain implants. The DBS device is a typical example of a useful device and provides an excellent vehicle for further developments in more general applications

[85-89].

The power source problem is a dominant factor in the high cost of implanting the current DBS devices. Currently, the battery is sealed within the implantable pulse generator so that the entire device must be surgically replaced once the battery's power has been depleted. The period between repeated surgeries ranges from less than one year to several years. The combined cost of a replacement device, accessories, and surgical procedures is approximately HK$200,000 for each replacement.

The primary goal of this part is to develop a charger based on witricity technology for recharging DBS device. The witricity system with the feature of high energy transfer efficiency is based on a new magnetic-resonance principle. A novel simulation model for full-wave 3-dimensional (3-D) electromagnetic (EM) field computation using HFSS will be developed as a powerful tool to analyze the performance of the device efficiently. Corresponding experiments and measurements have been carried out to test the charger.

Wireless power transmission (WET) has been studied for many years. Although biomedical applications of the resonant WET method have not been envisioned in the literature, it could become the most effective method for transmitting electric power into the human body for the following reasons:

- As the previous example shows, in using the resonant WET, energy is selectively delivered to the location where a resonant object is present. Since the intrinsic frequency of biological tissue is normally very low, little energy is absorbed by biological matter. It has been shown that human tissue is essentially transparent to the resonant WET. Clearly, these properties are extremely valuable.

- The resonant WET system can pass energy in the air or tissue over a long distance while traditional methods cannot.
- In either case where the transmitter and receiver are not well aligned or the line of sight is blocked by a non-resonant object, the RWET system can still perform well [90]. This property implies robustness in energy delivery.
- If the strength of the EM field for given frequency is controlled under proper level, the energy transfer system is safe to humans [90].

EM field computation is one of the most important way analyze bioelectric phenomena and design EM devices. The EM field analysis method has been successfully utilized in researches and applications, like magnetic resonance images [91], and in the researches, such as effect of 900 Hz mobile phones signals to human head, and 1-30 MHz transmitter signal to human bodies.

An appropriate model of human body, which has a complicated structure, should be built up while analyzing the EM field. The human body react has been studied when exposed to high frequency ranging from 50-200 MHz [94]. The result shows that apparent electric field is induced in human body. Damage might be brought in the human body reaction, so it is necessary to limit the EM exposure of human body to a safe level. The widely accepted recommendations are made by the ANSI/IEEE guidelines [95].

5.2 Microwave Network Theory for Analytical Calculation

5.2.1 The Concept of Impedance and Parameters [96]

The term impedance was applied to transmission lines, in terms of lumped-element equivalent circuits and the distributed series impedance and shunt admittance of the line.

Characteristic impedance

Characteristic impedance is the ratio of voltage to current for a traveling wave on a transmission line. Since voltage and current are uniquely defined for TEM waves, the characteristic impedance of a TEM wave is unique. The characteristic impedance is defined as below and it is 50 Ω in this project.

$$Z_0 = 1/Y_0 = \sqrt{L/C} \tag{5-1}$$

The Impedance Parameters

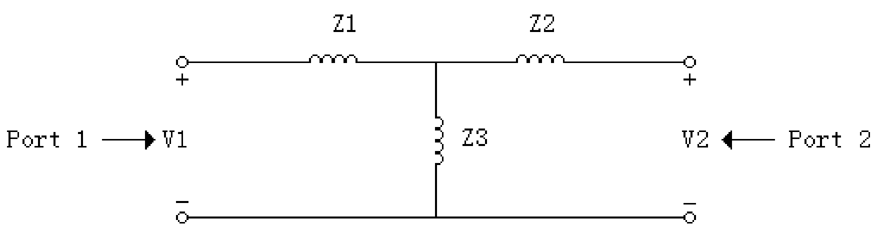

Fig. 5-1 A two-port T-network

The impedance matrix [Z] relates the voltages and the currents:

$$\begin{bmatrix} V_1 \\ V_2 \\ \vdots \\ V_N \end{bmatrix} = \begin{bmatrix} Z_{11} & Z_{12} & \cdots & Z_{1N} \\ Z_{21} & & & \vdots \\ \vdots & & & \vdots \\ Z_{N1} & \cdots & \cdots & Z_{NN} \end{bmatrix} \begin{bmatrix} I_1 \\ I_2 \\ \vdots \\ I_N \end{bmatrix} \tag{5-2}$$

So Z_{ij} can be found as

$$Z_{ij} = \left. \frac{V_i}{I_j} \right|_{I_k = 0 \quad for \quad k \neq j} \tag{5-3}$$

And Y_{ij} can be found as

$$Y_{ij} = \left. \frac{I_i}{V_j} \right|_{V_k = 0 \quad for \quad k \neq j} \tag{5-4}$$

From equation (5-3), we can find that Z_{11} is the input impedance of port 1 when port 2 is open-circuited:

$$Z_{11} = \left. \frac{V_1}{I_1} \right|_{I_2 = 0} = Z_A + Z_C \tag{5-5}$$

The transfer impedance Z_{12} from port 1 to port can be found when a current I_2 is applied at port 2 and we measure the open-circuit voltage at port 1:

$$Z_{12} = \left. \frac{V_1}{I_2} \right|_{I_1 = 0} = Z_C \tag{5-6}$$

It can be verified the $Z_{21} = Z_{12}$ because the circuit is reciprocal. Then we can find Z_{22} as following

$$Z_{22} = \left. \frac{V_2}{I_2} \right|_{I_1=0} = Z_B + Z_C \tag{5-7}$$

The Scattering Parameters

The scattering matrix [S] is defined in relation to the incident and reflected voltages waves as:

$$\begin{bmatrix} V_1^- \\ V_2^- \\ \vdots \\ V_N^- \end{bmatrix} = \begin{bmatrix} S_{11} & S_{12} & \cdots & S_{1N} \\ S_{21} & & & \vdots \\ \vdots & & & \vdots \\ S_{N1} & \cdots & \cdots & S_{NN} \end{bmatrix} \begin{bmatrix} V_1^+ \\ V_2^+ \\ \vdots \\ V_N^+ \end{bmatrix} \tag{5-8}$$

So S_{ij} can be determined as

$$S_{ij} = \left. \frac{V_i^-}{V_j^+} \right|_{V_k^+=0 \quad for \quad k \neq j} \tag{5-9}$$

Then we get S_{11}, S_{12}, S_{21}, and S_{22}

$$\begin{aligned} S_{11} &= \left. \frac{V_1^-}{V_1^+} \right|_{V_2^+=0} \\ S_{12} &= \left. \frac{V_1^-}{V_2^+} \right|_{V_1^+=0} \\ S_{21} &= \left. \frac{V_2^-}{V_1^+} \right|_{V_2^+=0} \\ S_{22} &= \left. \frac{V_{21}^-}{V_2^+} \right|_{V_1^+=0} \end{aligned} \tag{5-10}$$

The Transmission (ABCD) Parameters

In practice some microwave networks are formed of a connection of two or more two-port networks. Under this condition, it is convenient to define a 2×2 transmission *ABCD* matrix for each two-port network.

The *ABCD* matrix is defined in terms of the total voltages and currents

$$\begin{bmatrix} V_1 \\ I_1 \end{bmatrix} = \begin{bmatrix} A & B \\ C & D \end{bmatrix} \begin{bmatrix} V_2 \\ I_2 \end{bmatrix} \tag{5-11}$$

The *ABCD* parameters for the circuit are

$$\begin{aligned} &A = 1 + \frac{Z_1}{Z_3}, \quad B = Z_1 + Z_2 + \frac{Z_1 Z_2}{Z_3} \\ &C = \frac{1}{Z_3}, \qquad D = 1 + \frac{Z_2}{Z_3} \end{aligned} \tag{5-12}$$

5.2.2 Calculated the *Q* Based on *S* Parameters

One of the important parameters for the coil is the unloaded *Q* factor, Q_0. In this part, two methods [97-99] have been used to calculate the Q_0 factor based on the Smithchart measurements.

Calculate the Q_0 factor with the 1-port method

The loaded *Q* factor is defined as

$$Q_L = \frac{Q_o}{1+\kappa} \tag{5-13}$$

So the unloaded Q factor is

$$Q_0 = Q_L(1+\kappa) \qquad (5\text{-}14)$$

The coupling coefficient is computed by (see Fig. 5-3)

$$\kappa = \frac{d}{2-d} \qquad (5\text{-}15)$$

For the choice of Φ_L , the corresponding frequencies are denoted by f_1 and f_2. The formula for computation of Q_L is then

$$Q_L = \frac{f_L}{f_1 - f_2}\tan\phi_L \qquad (5\text{-}16)$$

Here we set Φ_L to be ±45°, then the loaded Q factor is as

$$Q_L = \frac{f_0}{f_3 - f_4} \approx \frac{f_L}{f_3 - f_4} \qquad (5\text{-}17)$$

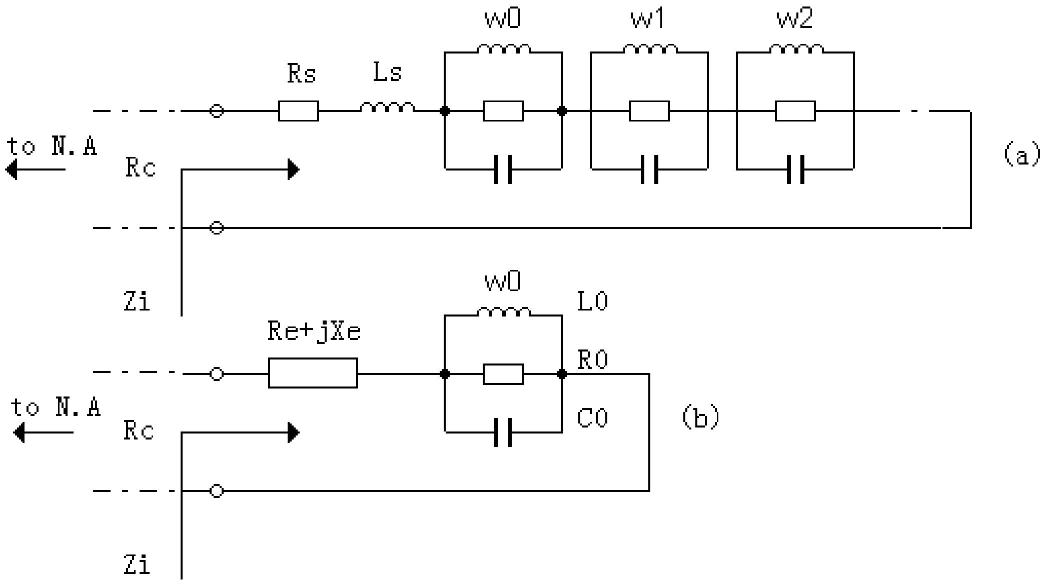

Fig. 5-2 (a) Equivalent circuit for the input impedance of an inductance-coupled cavity. (b) Simplied equivalent circuit for the vicinity of frequency ω_0.

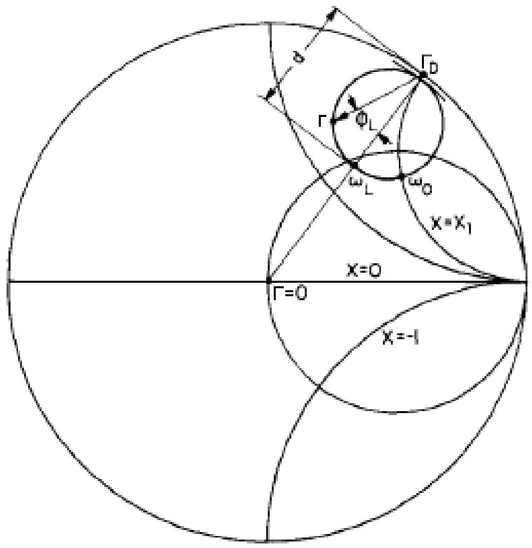

Fig. 5-3 Input reflection coefficient as a function of frequency

Calculate Q_0 factor with the 2-port method

The half power points $2Q_L\delta = \pm 1$ are easily obtained by fixing the frequencies f_1 and f_2 that satisfy

$$\frac{S_{21}(\omega)}{S_{210}} = \frac{1}{\sqrt{2}} \tag{5-18}$$

Then the loaded Q factor is

$$Q_L = \frac{f_0}{f_1 - f_2} \tag{5-19}$$

So the unloaded Q factor is

$$Q_0 = \frac{2}{S_{110} + S_{220}} Q_L \tag{5-20}$$

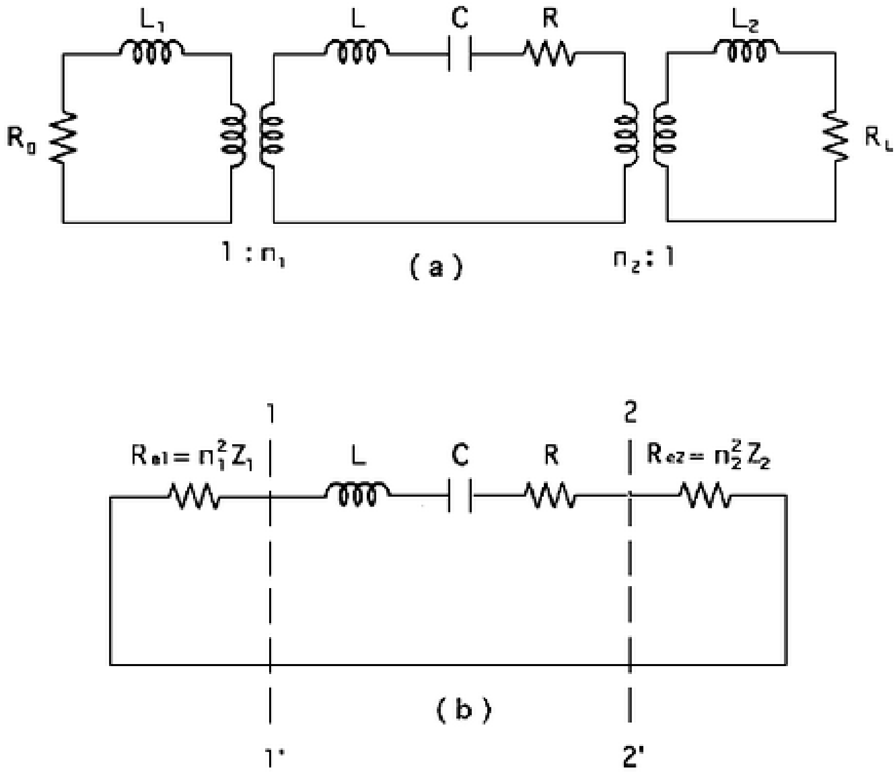

Fig. 5-4 Equivalent circuit (a) of a loop coupled cavity, (b) referred to the middle loop.

5.2.3 Power Gains of General 2-Port System [96, 100-102]

We can use any two-port parameter set, including admittance parameters *Y*, impedance parameters *Z* or others to represent the power gains. These parameters denote a linear relationship between the input, output voltages and currents. Following the *Y* parameters have been employed for discussion.

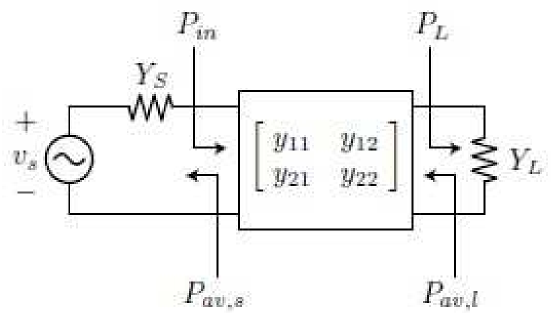

Fig. 5-5 Definitions of different power gains

The power gain G_p is defined as follows

$$G_P = \frac{P_L}{P_{in}} \tag{5-21}$$

And

$$\begin{aligned} P_{in} &= \frac{|V_1|^2}{2}\Re(Y_{in}) \\ P_L &= \frac{|V_2|^2}{2}\Re(Y_L) \end{aligned} \tag{5-22}$$

The power gain G_p becomes

$$G_P = \frac{|V_2|^2}{|V_1|^2}\frac{\Re(Y_L)}{\Re(Y_{in})} \tag{5-23}$$

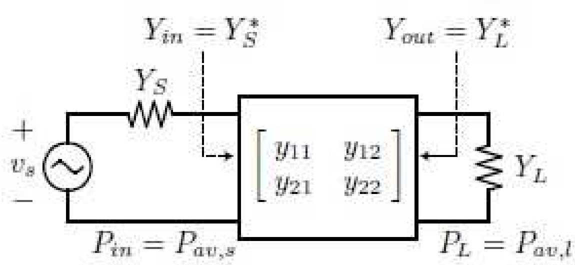

Fig. 5-6 The simultaneous input and output match

If we simultaneously conjugate match both the input and output, we can obtain the maximum possible power gain, shown in Fig. 5-6. Under this condition all three gains are equal

$$G_{\max} = G_p\left(Y_S = Y_{in}^*, Y_L = Y_{out}^*\right) \tag{5-24}$$

The Rollett stability factor K can be defined as

$$K = \frac{1-\left|S_{11}\right|^2 - \left|S_{22}\right|^2 + \left|\Delta\right|}{2\left|S_{12}S_{21}\right|}, \Delta = S_{11}S_{22} - S_{12}S_{21} \tag{5-25}$$

It also can be defined as

$$K = \frac{2\Re(S_{11})\Re(S_{22}) - \Re(S_{12}S_{21})}{\left|S_{12}S_{21}\right|} \tag{5-26}$$

Here, S parameters in the equation (5-26) can be replaced by Z, Y, or $ABCD$ parameters. The optimal source and load impedance is as below

$$\begin{aligned} Y_{S,opt} &= \frac{Y_{12}Y_{21} + \left|Y_{12}Y_{21}\right|\left(K + \sqrt{K^2 - 1}\right)}{2\Re\left(Y_{22}\right)} \\ Y_{L,opt} &= \frac{Y_{12}Y_{21} + \left|Y_{12}Y_{21}\right|\left(K + \sqrt{K^2 - 1}\right)}{2\Re\left(Y_{11}\right)} \end{aligned} \tag{5-27}$$

And we use U to represent the invariant part

$$U = \frac{\left|Y_{21} - Y_{12}\right|^2}{4\left[\Re\left(Y_{11}\right)\Re\left(Y_{22}\right) - \Re\left(Y_{12}\right)\Re\left(Y_{21}\right)\right]} = G_{\max} \tag{5-28}$$

Then K and $G_{\max}$ become

$$K=\frac{2\Re(Y_{11})\Re(Y_{22})-\Re(Y_{12}Y_{21})}{|Y_{12}Y_{21}|}=\frac{2\Re(S_{11})\Re(S_{22})-\Re(S_{12}S_{21})}{|S_{12}S_{21}|}$$
$$G_{\max}=\frac{Y_{21}}{Y_{12}}\frac{1}{K+\sqrt{K^2-1}}=\frac{S_{21}}{S_{12}}\frac{1}{K+\sqrt{K^2-1}}=\frac{S_{21}}{S_{12}}\left(K-\sqrt{K^2-1}\right) \tag{5-29}$$

5.2.4 Relationship between $G_{\max}$ and Q Factor

The necessary and sufficient condition for simultaneous matching is $K \geq 1$. Then the $G_{\max}$ is

$$G_{\max}=\left(K-\sqrt{K^2-1}\right)\frac{|S_{21}|}{|S_{12}|} \quad (K>1) \tag{5-30}$$

If we use Z parameters to replace S parameters, K and $G_{\max}$ become

$$K=\frac{2\Re(Z_{11})\Re(Z_{22})-\Re(Z_{12}Z_{21})}{|Z_{12}Z_{21}|} \tag{5-31}$$

and

$$G_{\max}=\left(K-\sqrt{K^2-1}\right)\frac{|Z_{21}|}{|Z_{12}|} \quad (K>1) \tag{5-32}$$

We know the matrix of Z parameters is

$$Z=\begin{bmatrix} R_2+j\omega L_2 & j\omega M \\ j\omega M & R_S+j\omega L_S \end{bmatrix} \tag{5-33}$$

And the coefficient factor k is

$$k = M \Big/ \sqrt{L_1 L_2} \qquad (5\text{-}34)$$

From (5-33) and (5-34), we get

$$K = \frac{2R_S R_2 + \omega^2 k^2 L_1 L_2}{\omega^2 k^2 L_1 L_2} \qquad (5\text{-}35)$$

The Q factor of an inductor is

$$Q = \frac{X_L}{R_L} = \frac{\omega L}{R_L} \qquad (5\text{-}36)$$

For our project, the source coil and the receiver coil are the same, that means $R_2=R_S$ and $L_2=L_1=L$. Then combining (5-35) and (5-36), The Q factor of each coil is

$$Q = \frac{\omega L}{R_S} \qquad (5\text{-}37)$$

From equations above, we have

$$G_{\max}(Q,k) = 1 + \frac{2}{Q^2 k^2} - 2\sqrt{\frac{1}{Q^4 k^4} + \frac{1}{Q^2 k^2}} \qquad (5\text{-}38)$$

5.2.5 Using *S* Parameters to Calculate L_1, L_2 and k

The *ABCD* parameters for the circuit shown in Fig. 5-1 are

$$A = 1 + \frac{Z_1}{Z_3}, \quad B = Z_1 + Z_2 + \frac{Z_1 Z_2}{Z_3}$$
$$C = \frac{1}{Z_3}, \qquad D = 1 + \frac{Z_2}{Z_3} \tag{5-39}$$

Conversions from *ABCD* parameters to *S* parameters between two-port network parameters are as following

$$\begin{cases} S_{11} = \dfrac{A + B/Z_0 - CZ_0 - D}{A + B/Z_0 + CZ_0 + D} \\ S_{12} = \dfrac{2(AD - BC)}{A + B/Z_0 + CZ_0 + D} \\ S_{21} = \dfrac{2}{A + B/Z_0 + CZ_0 + D} \\ S_{22} = \dfrac{-A + B/Z_0 - CZ_0 + D}{A + B/Z_0 + CZ_0 + D} \end{cases} \tag{5-40}$$

We get

$$\begin{cases} S_{11} = \dfrac{Z_1 - Z_2 + (Z_1Z_2 + Z_1Z_3 + Z_2Z_3)/Z_0 - Z_0}{Z_1 + Z_2 + 2Z_3 + (Z_1Z_2 + Z_1Z_3 + Z_2Z_3)/Z_0 + Z_0} \\ S_{12} = \dfrac{2Z_3}{Z_1 + Z_2 + 2Z_3 + (Z_1Z_2 + Z_1Z_3 + Z_2Z_3)/Z_0 + Z_0} \\ S_{21} = \dfrac{2Z_3}{Z_1 + Z_2 + 2Z_3 + (Z_1Z_2 + Z_1Z_3 + Z_2Z_3)/Z_0 + Z_0} \\ S_{22} = \dfrac{-Z_1 + Z_2 + (Z_1Z_2 + Z_1Z_3 + Z_2Z_3)/Z_0 - Z_0}{Z_1 + Z_2 + 2Z_3 + (Z_1Z_2 + Z_1Z_3 + Z_2Z_3)/Z_0 + Z_0} \end{cases} \tag{5-41}$$

And for Fig. 5-1

$$\begin{cases} Z_1 = j\omega(L_1 - M) \\ Z_2 = j\omega(L_2 - M) \\ Z_3 = j\omega M \end{cases} \tag{5-42}$$

From equations (5-41) and (5-42), the following equation can be obtained

$$\begin{cases} S_{11}/S_{12} = \dfrac{j\omega L_1 - j\omega L_2 + \omega^2\left(-L_1L_2 + M^2\right)/Z_0 - Z_0}{2j\omega M} \\ S_{12} = S_{21} = \dfrac{2j\omega M}{j\omega\left(L_1 + L_2 + 2M\right) + \omega^2\left(-L_1L_2 + M^2\right)/Z_0 + Z_0} \\ S_{22}/S_{21} = \dfrac{-j\omega L_1 + j\omega L_2 + \omega^2\left(-L_1L_2 + M^2\right)/Z_0 - Z_0}{2j\omega M} \end{cases} \tag{5-43}$$

If S_{11}=S_{22}, that means Z_1=Z_2, we can have

$$\begin{cases} S_{11}/S_{12} = \dfrac{\left(Z_1^{\ 2} + 2Z_1Z_3\right)/Z_0 - Z_0}{2Z_3} \\ S_{12} = S_{21} = \dfrac{2Z_3}{2Z_1 + 2Z_3 + \left(Z_1^{\ 2} + 2Z_1Z_3\right)/Z_0 + Z_0} \end{cases} \tag{5-44}$$

And,

$$\begin{cases} S_{11}/S_{12} = \dfrac{\omega^2\left(-L_1^{\ 2} + M^2\right)/Z_0 - Z_0}{2j\omega M} \\ S_{12} = S_{21} = \dfrac{2j\omega M}{j2\omega\left(L_1 + M\right) + \omega^2\left(-L_1^{\ 2} + M^2\right)/Z_0 + Z_0} \end{cases} \tag{5-45}$$

If we know S_{11}, S_{12}, we can calculate L_1, L_2 =L_1 and M. M and k have the relationship below

$$M = k\sqrt{L_1L_2} = kL_1, (L_1 = L_2) \tag{5-46}$$

Therefore, it is easy to calculate k.

Under the normal condition shown in equation (5-43), that means $Z_1 \neq Z_2$, we need to know S_{11}, S_{12} (S_{21}=S_{12}), and S_{22} for the computation. And we may have to measure S parameters at different frequencies.

5.3 System Design for the Charger

Hitherto witricity works at the MHz range; hence some undesirable problems become inevitable. Firstly, high frequency devices are much more expensive than their low frequency counterparts. High-frequency circuits and digital circuits are often sharing the same circuit board, constituting mixed signals or cross talks. High-frequency circuits are sometimes unstable as the digital circuits are starting up because the noise generated by the digital circuit could affect the normal functions of high frequency circuits. Also, realization of inductive charging at high frequencies results in relatively more radiation and heat generation in the vicinity of the electrical device.

5.3.1 The Transmitter Design

TABLE 5-I. DIMENSION PARAMETERS OF THE TRANSMITTER COIL

Shape of winding	Spiral
Number of turns	10
Radius of the spiral (mm)	136.5
Thickness of copper (mm)	0.04
Width of copper (mm)	4
Copper track separation (mm)	1.18
Width of the strip (mm)	18
Length of the strip (mm)	25.4
Number of the strips	20

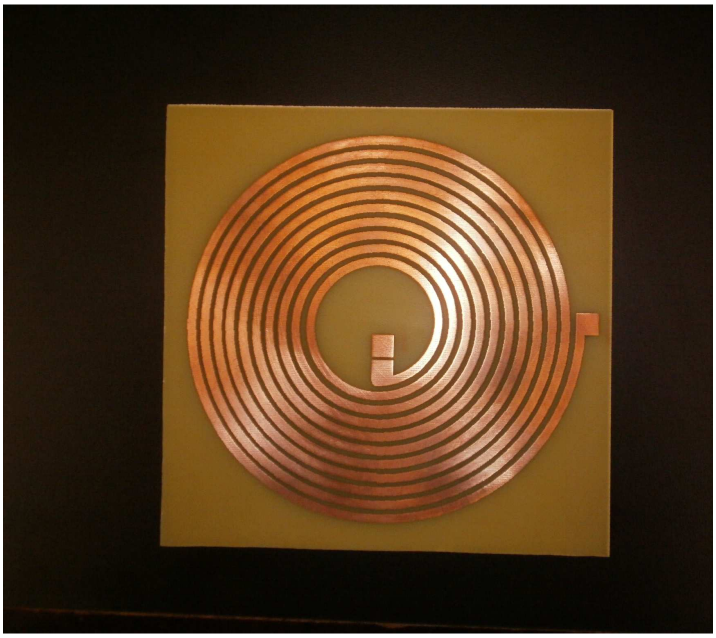

Fig. 5-7 The spiral coil for the transmitter

For the transmitter, we have done some simulations with different copper tape arrangements to compare the performances in order to reduce the resonant frequency. Figs. 5-8 (a)-(e) present the coil, the copper tape arrangements, and the magnetic flux distributions at the position of above 2 cm. And the dimension is shown in Table 5-I.

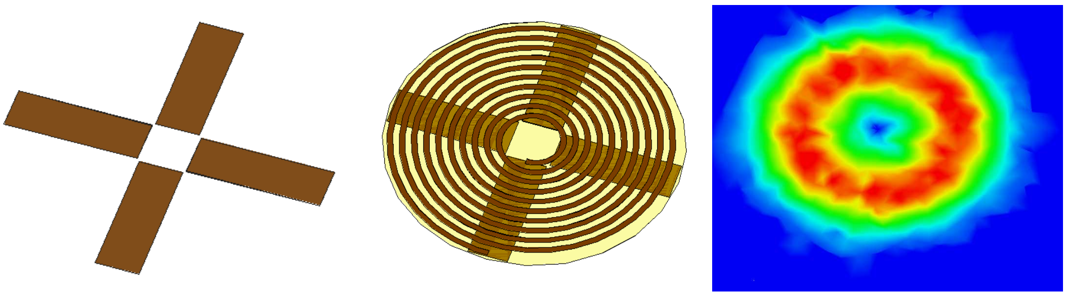

(a) Four copper tapes

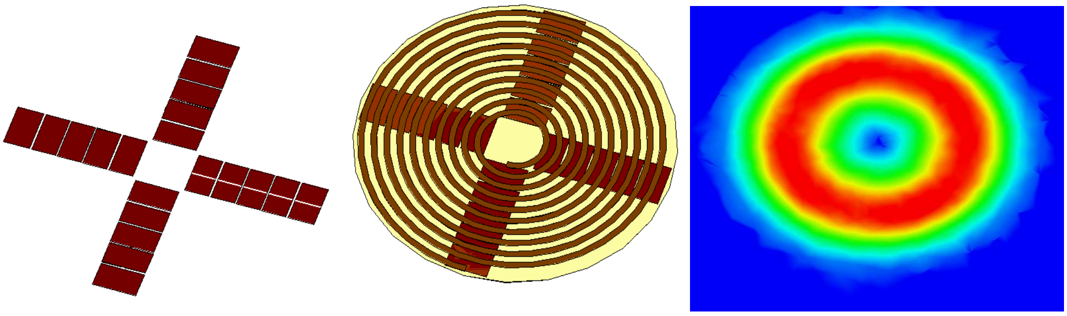

(b) Four separated copper tapes

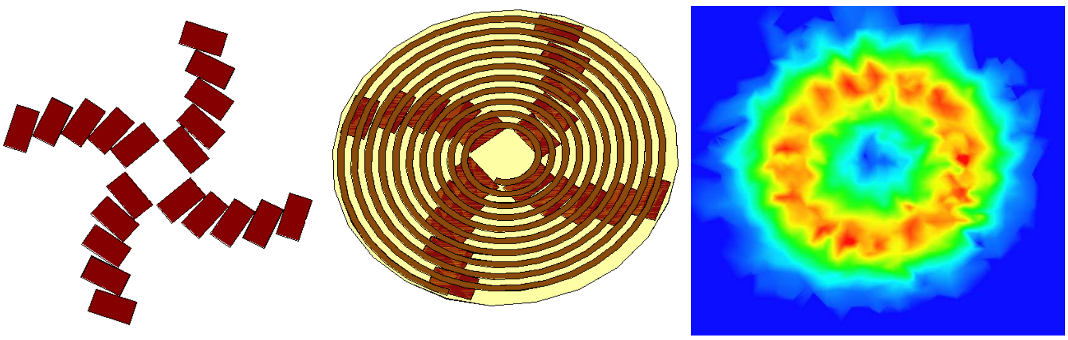

(c) Four separated copper tapes with small angular misalignment

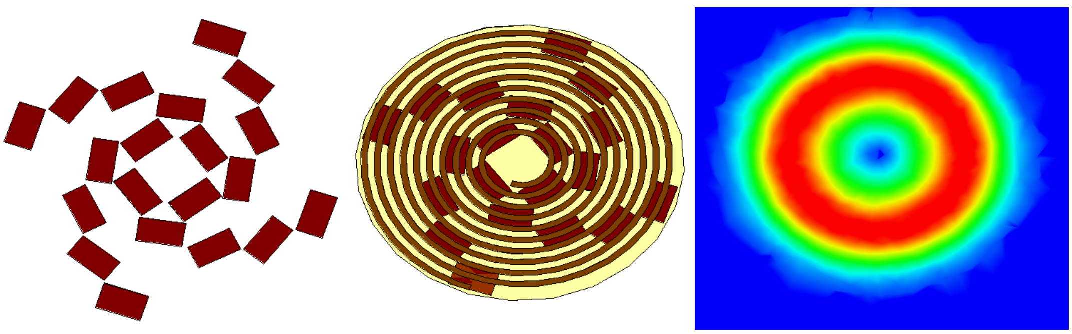

(d) Four copper tapes with large angular misalignment

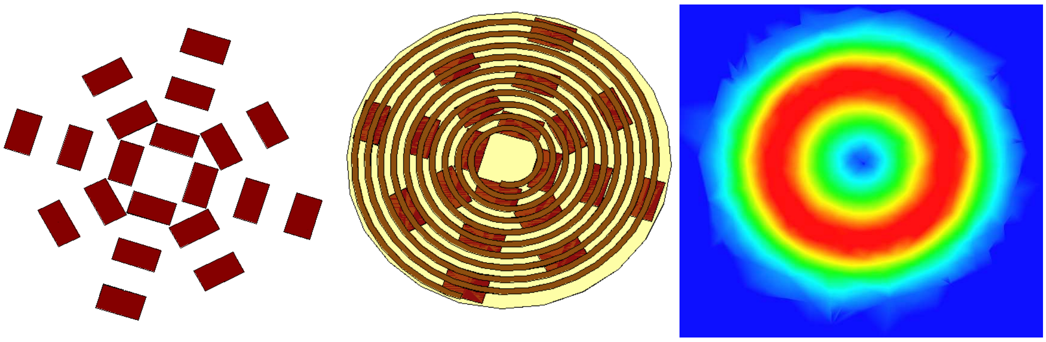

(e) Twenty copper tapes

Fig. 5-8. The coil, the copper tape arrangements, and the magnetic flux distributions

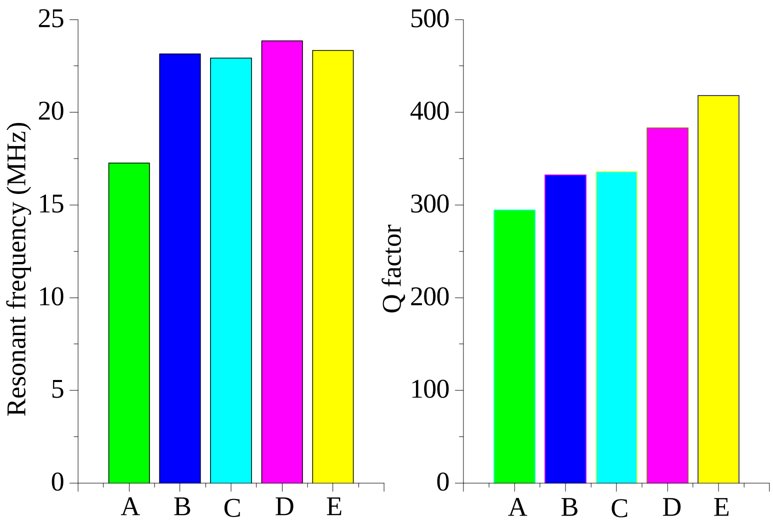

Fig. 5-9 The simulated resonant frequencies and the unloaded *Q* factors of the five coils with different copper tapes (A- Four copper tapes, B- Four separated copper tapes, C- Four separated copper tapes with small angular misalignment, D- Four copper tapes with large angular misalignment, and E- Twenty copper tapes)

The resonant frequencies and the unloaded *Q* factors of the five coils with different copper tapes have been shown in Fig. 5-9. We can see the last one with twenty copper tapes has the similar resonant frequency and magnetic flux distributions with others but the highest unloaded *Q* factor. Its self-inductance is about 2.2*u*H based on the analytical calculation and the simulation results. When using network analyzer, the measured unloaded *Q* factor of the last model is about 356 based on the two methods mentioned in **5.2.2**, slightly different from the simulation results.

5.3.2 The Receiver Box Design

And in order to make the receiver much smaller but with the same resonant frequency of the transmitter, a fabricated small "box" is built and shown in Fig. 5-10, which contains two spiral coils on the two top surfaces and a connected helix between the coils. The simulated and measured resonant frequencies of the "box" are about 7.961 MHz and 8.152 MHz, respectively.

TABLE 5-II. DIMENSION PARAMETERS OF THE RECEIVER BOX

The Helix	Shape of winding	Helix
	Number of turns for Helix	30
	Radius of the Helix (mm)	22
	Radius of the wire (mm)	0.4
	Height of the Helix (mm)	16
The Two Spirals	Shape of winding	Spiral
	Number of turns	36
	Radius of the wire (mm)	0.14
	Copper track separation (mm)	1.18

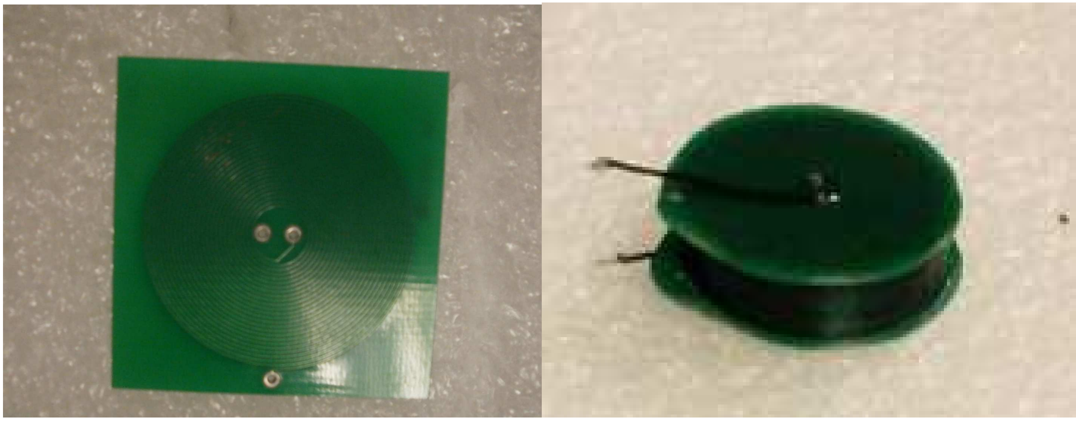

Fig. 5-10 A fabricated small "box" for the receiver

The simulated unloaded Q factor of the receiver box is about 227 and the measured one is near to 200 using the two methods mentioned in **5.2.2**. Its self-inductance is about 11.6 uH.

5.3.3 System Design

Through the discussion above, we can see the transmitter and the receiver box have different resonant frequencies, which will make the system non-resonant. In order to make them work under resonance, the receiver must be revised to make it have the same resonant frequency with the receiver box. Then, external capacitors have been added. Following is the resonant frequencies and the unloaded Q factors with different external capacitors.

When the external capacitor is 160 pF, the resonant frequency of the transmitter is about 8.221 MHz, quite near to the receiver's. Then adjust the position of the copper tapes on the coil to make its resonant frequency to be about 8.152 MHz.

TABLE 5-III. THE RESONANT FREQUENCIES AND THE Q FACTORS WITH DIFFERENT EXTERNAL CAPACITORS

Capacitance (pF)	Resonant frequency (MHz)	Unloaded Q factor
100	18.583	402.60
110	15.884	389.77
120	13.708	375.90
130	11.816	363.48
140	10.357	352.53
150	9.012	342.73
160	8.221	334.49
170	7.570	327.23
180	7.043	322.68
190	6.734	318.80
200	6.472	314.71

Using the transmitter and the receiver box studied above, a simple platform has been built. The network analyzer was employed to measure the S parameters and get the smithchart at resonant frequency of 8.0742 MHz, presented in Fig. 5-11. Matlab fsolve(@) has been implemented to calculate the coupling coefficient k, transmitter's self-inductance L_1 and the receiver's self-inductance L_2 based on equation (5-42) under normal condition. Gmax was also calculated through equation (5-28) and the unloaded Q factor, Q_0, was given in the Table 5-IV below according to the two methods presented in 5.2.2.

TABLE 5-IV. CALCULATED DATA BASED ON THE MEASURED S PARAMETERS

Resonant frequency (MHz)	k	$L_1\,(uH)$	$L_2\,(uH)$	Gmax	Q_0 (System's)
8.0742	0.1783	2.37	13.25	0.3324	117

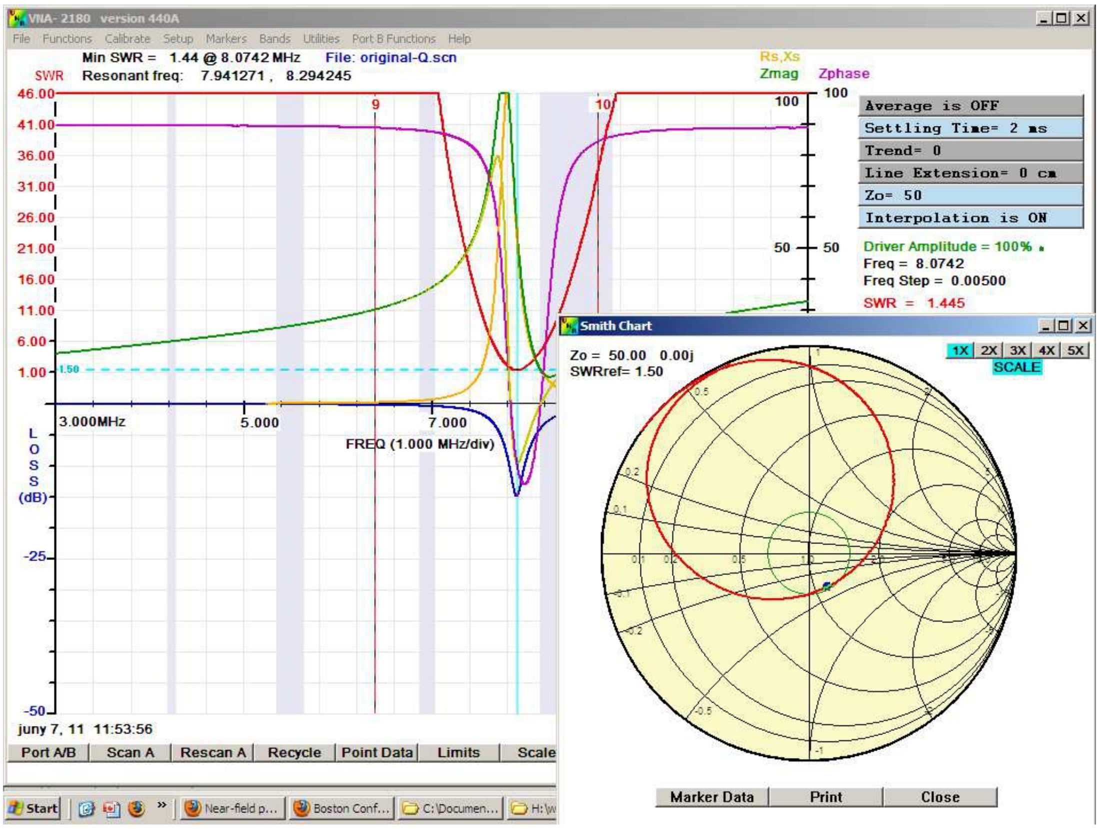

Fig. 5-11 The measured *S* parameters and smithchart for the platform

During the evaluation, the external witricity transmitter is placed at different distances and angles from the head phantom implanted with the witricity cell, and the output voltages have been measured and compared to the results obtained from computer simulation. In order to facilitate measurements, impedance matched RF circuits, cables and probes have been utilized to obtain relevant data.

Fig. 5-12 presents both the measured and the simulation the output voltages when the frequency ranging from 2 MHz to 16 MHz. It is clear that when the operating frequency is at or near the resonant frequency, the output voltage of the receiver reached to the highest value. For the simulation result, it is about 383.8 mV at 7.877 MHz; and for the measured result, that value is up to 327.4 mV at 8.102 MHz.

Output voltages with lateral and angular misalignments have been shown in Fig. 5-13 and Fig. 5-14, respectively. We can see that the output voltages are about 250 mV even with lateral misalignments of 10 mm or angular misalignment of 20˚. That is enough for supplying the DBS.

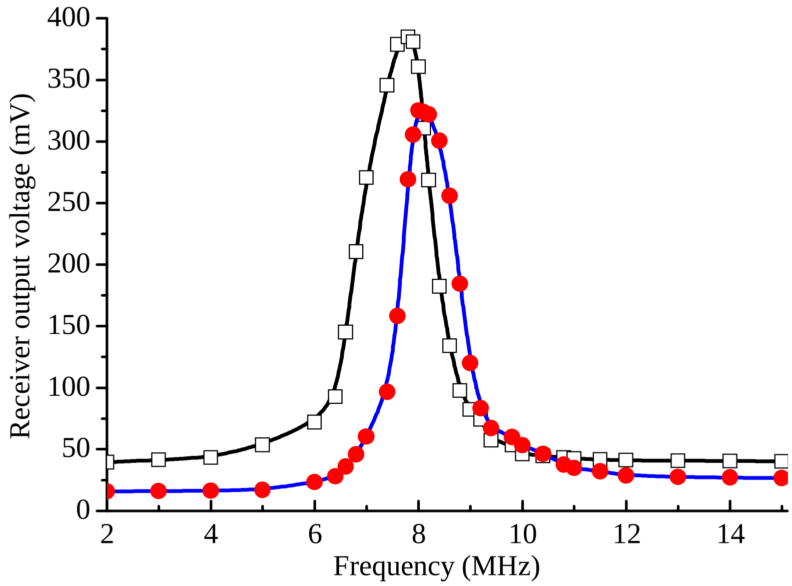

Fig. 5-12 Simulation and measured receiver output voltages vs. frequency with a distance of 20 mm

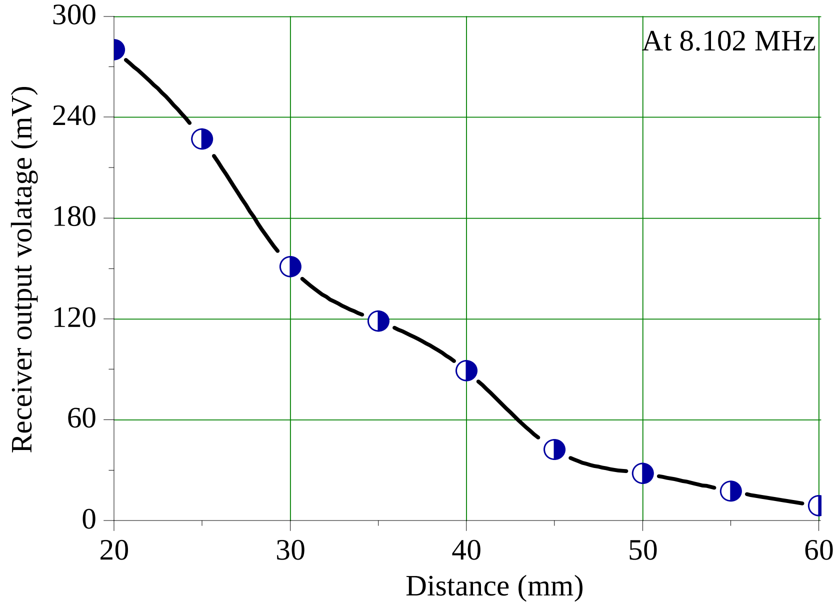

Fig. 5-13 Receiver output voltages with lateral misalignments of 10 mm

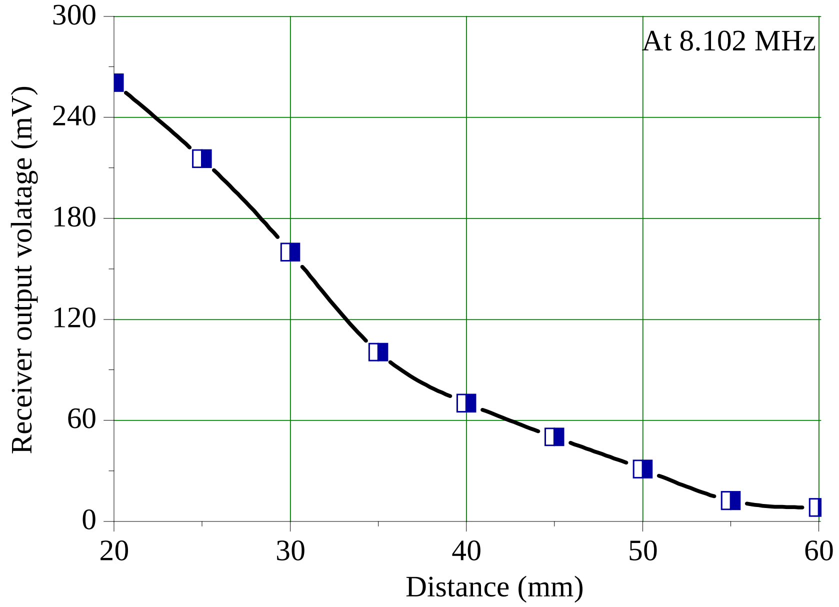

Fig. 5-14 Receiver output voltages vs. distance with angular misalignment of 20˚

In order to make the charger applicable for practical application and getting experiences of device design, a wireless charger was built for demonstration and doing corresponding experiments. The charger is designed to charge the battery, Maxwell ML 2032, for DBS device and the rated voltage, and the rated power capacity are 3 V, 65 mAh, respectively.

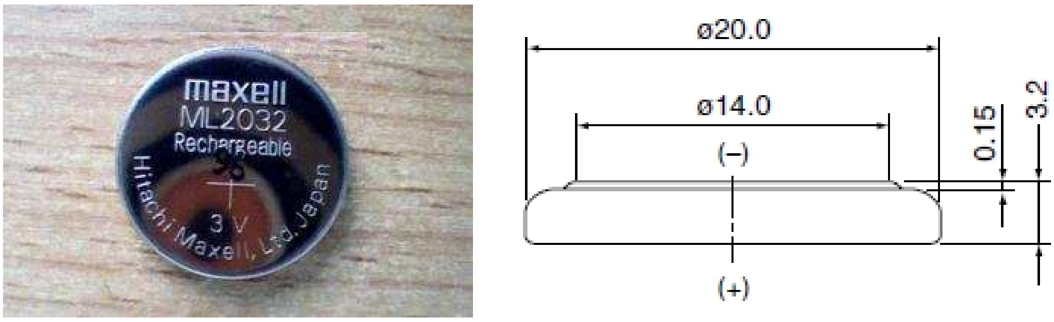

Fig. 5-15 Maxwell ML 2032 rechargeable battery.

Based on the design requirements, the charger provides invariable current to charge the battery. For the witricity study, where the operating frequency is much higher, the model should be constructed considering the material composition to make it for the intended frequency range.

The electrical properties of this model are verified; we have implanted the encapsulated witricity cell with ML 2032 rechargeable battery within the skull and conducted experiments. The construction of the head model was intended to be used at a frequency up to 10 MHz. In order to simplify the experimental setup, a partial scalp model has been used to cover the implant as we did in our previous volume conduction power delivery experiments before.

A head phantom has been constructed for the study of electrical energy delivery between an external transmitter and an internal receiver (Here is the small “box”). This phantom, which geometrically resembles the upper portion of a human head, simulates the geometry and electrical properties of the brain, skull and scalp, which is shown in Fig. 5-16. Both the intracranial contents and scalp of this model were made of agar and conductive agents, and the skull was made from a mixture of carbon black epoxy and barium titanate ($BaTiO_3$). A series of molding procedures was used to accurately construct the head components. Fig. 5-17 presents the completed head phantom.

Fig. 5-16 The phantom for the performance verification of the proposed witricity system

Fig. 5-17 The completed head phantom

Figs. 5-18, 5-19, 5-20 and 5-21 present the curves of input voltage, current from the rectifier bridge, and the charging voltage, current received.

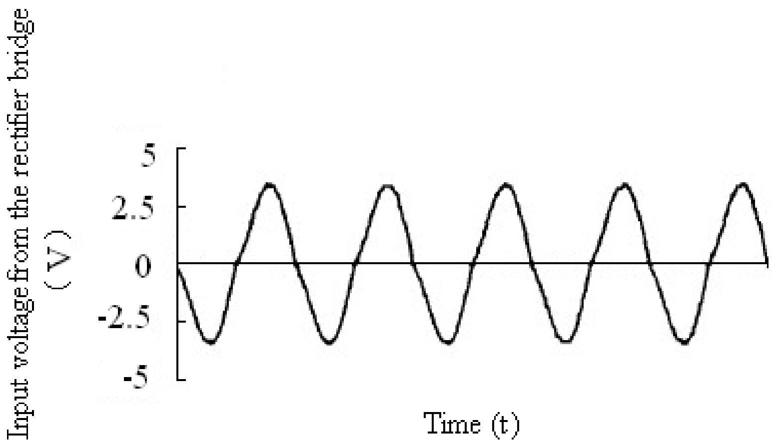

Fig. 5-18 Input voltage from the rectifier bridge

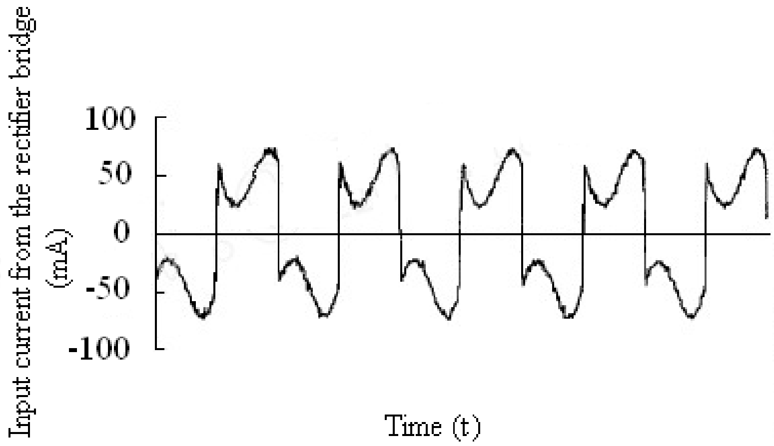

Fig. 5-19 Input current from the rectifier bridge

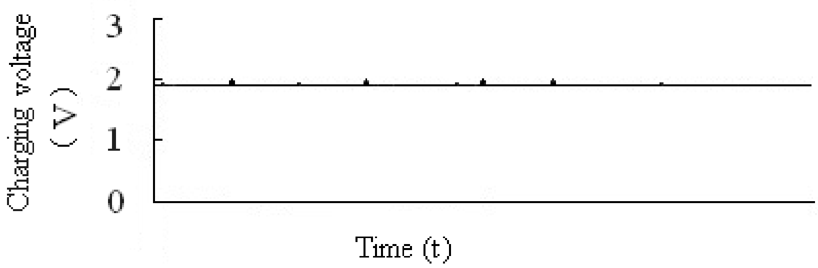

Fig. 5-20 Charging voltage

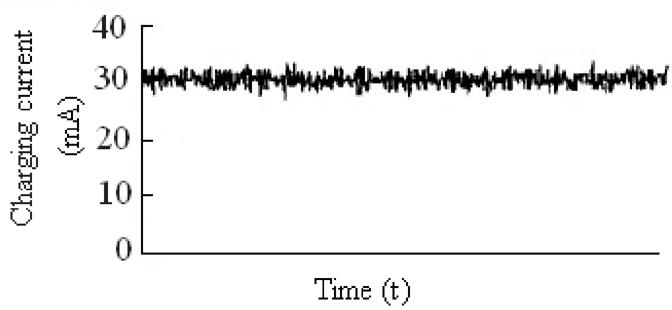

Fig. 5-21 Charging current

5.3.4 Electric Distributions in the Head Phantom

The resonant frequency of the coils in this project is near to 8 MHz. So it is needed to study the electric distribution in the head phantom to make sure whether the method is harmful to the patients or not. Figs. 5-22 are the simulation results of the electric distributions in the phantom.

From the results we can see, the highest density occurred at the center of the receiver box and it is up to 2e-4 V/meter. And the highest value is about 1e-4 V/meter at the distance of 20 mm and 5e-5 V/meter at 30 mm. The electric distribution is only 1e-6 V/meter when the distance is larger than 40 mm. Based on the equation below, we calculated the SAR values and found even the peak SAR values are much lower than the US standard (1.6 W/kg) and the EU standard (2 W/kg). Therefore, it is safe using this resonant method to transfer power for the implanted medical devices like DBS.

$$SAR = \int_{Brain} \frac{\sigma(r)|E(r)|^2}{\rho(r)} dr \tag{5-47}$$

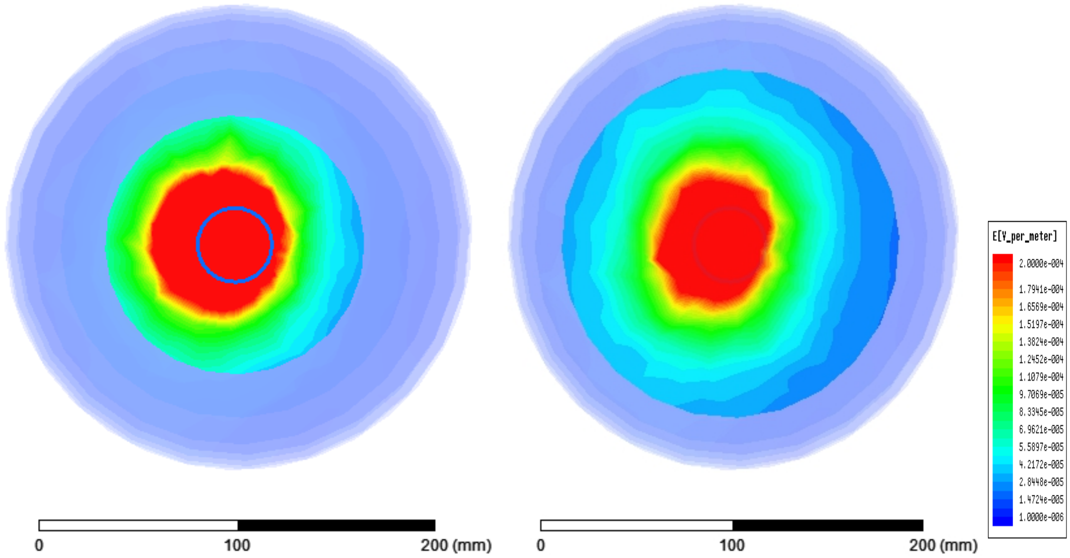

(a) at the center of the receiver box, (b) at the distance of 10 mm below

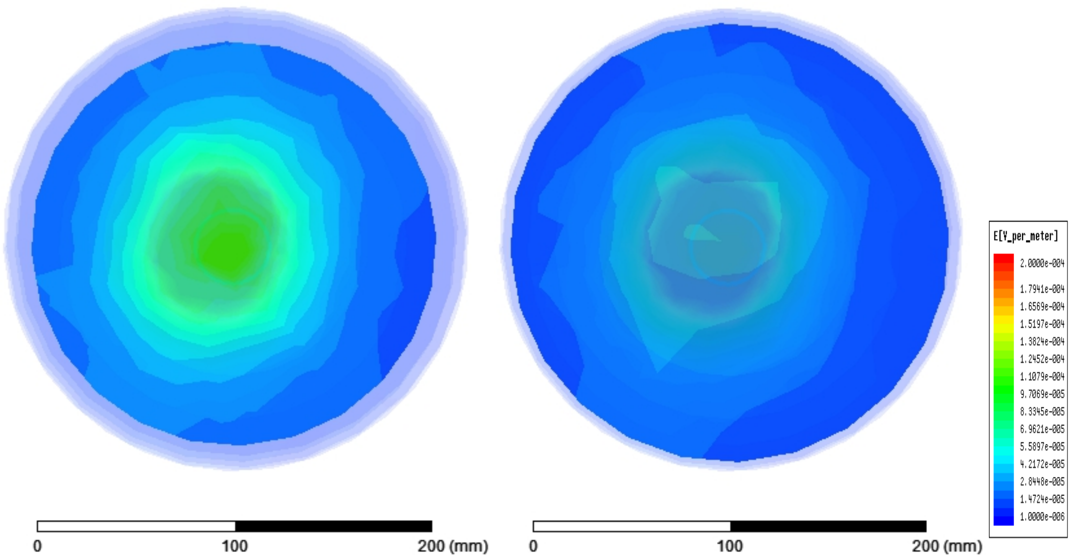

(c) at the distance of 20 mm, (d) at the distance of 30 mm

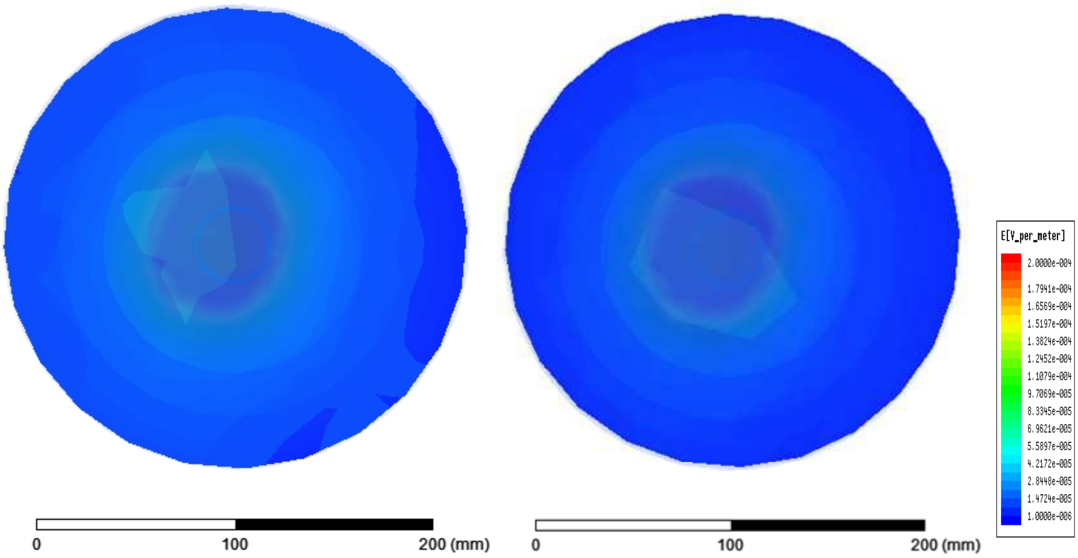

(e) at the distance of 40 mm, (f) at the distance of 50 mm

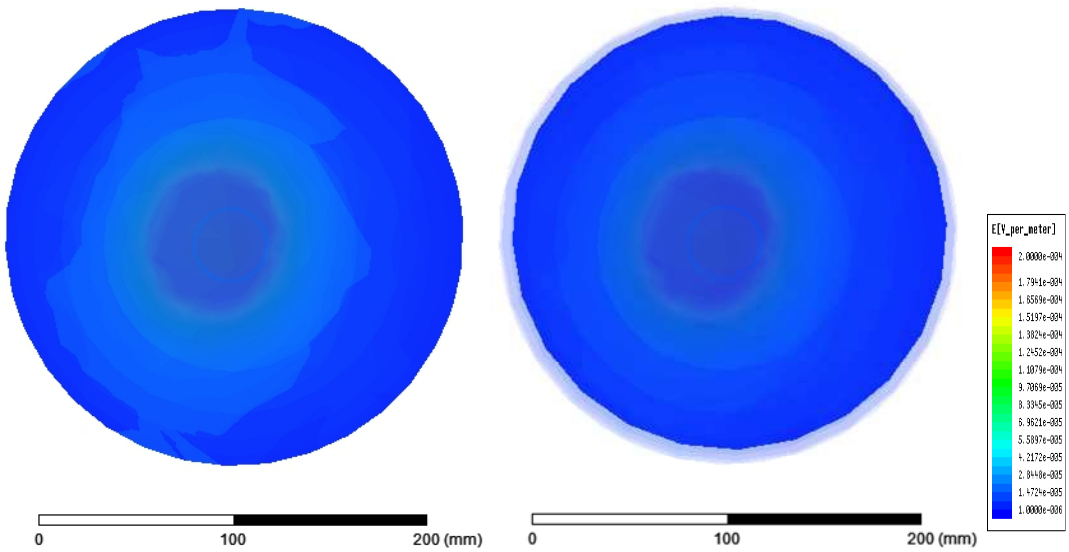

(g) at the distance of 60 mm, (h) at the distance of 70 mm

Fig. 5-22 Electric distributions in the head phantom at different distance between the receiver box and the plane

5.4 Summary

In this chapter, a wireless charger based on the novel witricity technology has been proposed for Implanted DBS. Microwave network theory for analytical calculation has been discussed firstly. Then, the simulation structure and the experiment model have been illustrated, respectively. And the inductance, the resistance, the coupling coefficient have been compared between the simulation results and the measured results. Finally, we proposed the charger for implanted DBS power supply charging. We did the simulation for coils with different copper tape arrangements to select the well matched one. Then a fabricated small "box" for the receiver has been designed and a head phantom has been constructed for the study of electrical energy delivery. The experiments have been carried out and the input voltage, input current, charging voltage and charging current have been measured for verification. At the end the electric distributions have been studied to make sure its safety for human beings.

CHAPTER 6 CONCLUSION AND FUTURE WORK

6.1 Conclusion

Traditional chargers have many disadvantages because the charger must be physically connected to the load and the charging contacts can be broken or easily interrupted. To alleviate the aforementioned drawbacks, interests in wireless charging have reemerged. Traditional method in wireless energy transfer is through magnetic coupling using a transformer which has a primary coil and a secondary coil. When AC power is applied to the primary coil, a voltage is induced in the secondary coil by mutual inductance.

Witricity technology, as a new resonant coupling energy transmission technology, can transmit power wirelessly over a long distance based on strongly coupled magnetic resonance. The source resonator fills the surrounding with lossless non-radiative magnetic fields oscillating at MHz frequencies. The non-radiative fields allow efficient power exchange between the source and the device resonators. The resonant nature of the process ensures that the interaction between the source and device is sufficiently strong and the interaction with non-resonant objects is minimal. And the power loss is mainly the copper loss. The radiation loss is much smaller compared with the copper loss

According to the specifications of energy storage and space available, initial implanted medical systems with different geometry structures including round coil, rectangular coil, and thin film coil have been studied. In this thesis, the self-inductance and mutual-inductance of the spiral and rectangular coils are studied, and the relationship between them and the shape of the coil loops, the permeability of the medium around, the number of windings and the distributions of the current along the lead's cross section has also been presented. The coupling coefficient, which depends on the above factors except the number of windings, is illustrated through related equations.

We have constructed several prototypes of the witricity cell with different coil dimention. As the fundamental witricity theory requires identical resonant frequencies of the transmitter and the receiver, it would therefore be easy for design if the physical sizes of them are comparable. However, for implanted medical devices, the receiver has a much smaller physical size than the transmitter and hence some design studies need to be carried out.

We utilized several methods to increase the product of the inductance and the capacitance values in the LC tank. We used the entire circumference of the ring-structure to maximize the capacitance value. A gap is intentionally formed within each of the two conductors to break the harmful loop current. Here we did not use ferrite core to make the system to be a completely wireless power transfer application.

For the convenience of evaluating the resonant frequency, the capacitance of the transmitter coil needs to be adjustable. The resonant frequency of the transmitter can also be adjusted by changing the inductance value of the coil. In order to reduce the resistance within the LC tank of the receiver, a solid copper and/or silver wire are used to construct the coil and a thicker copper and/or silver strip have been also used to form the conductors within the capacitor. As in the transmitter case, the LC loop resistance can be reduced by eliminating the wiring connections.

To make the system operate at its highest efficiency, many factors, such as the distributed parameters, geometric shapes and dimensions, material properties, and physical arrangements of the components need to be determined precisely. And the efficiency in our project is the transfer efficiency without considering the copper loss.

Numerical models for the EM field computation have been developed. Since the study of the witricity requires high-frequency analysis involving displacement current and skin conduction effects, full-wave 3-D EM fields in the transmitter, the receiver and the regions around them need to be computed. Then the CMT has been applied to build the analytical framework for modeling this resonant wireless power transfer. And corresponding formulations have been deduced for study. In the last part, the theory about the resonant power transmission system is shown for the further simulations and experiments.

We used commercial Ansoft HFSS (High Frequency Structure Simulator). It can solve 3-D high-frequency electromagnetic field in frequency domain using FEM. It supports parameterized geometry so the dimensions can be swept or optimized. It can compute the s-parameters and resonant frequency directly. According to the s-parameters of the input port of the transmitter coil and the output port of the receiver coil, an equivalent impedance matrix is obtained. Then an equivalent circuit has been established and the currents in the transmitter coil and the receiver coil can be computed. The simulation has been repeated to study the effects on different dimensional and structural parameters to evaluate and compare different design schemes, different physical sizes, different components and materials in order to optimize the system performance further.

For many electric charging applications such as in implantable medical devices, mobile phones, and even TVs, usually an average distance of about 5 cm between the transmitter and the receiver is enough. The efficiency at that distance is up to 50%-80% according to the simulation and measurement results of the system. And the distances only affect the resonant frequencies slightly when the values changed. It should be noted that by using traditional magnetic inductive coupling methods, the distance must be kept much shorter, less than 0.5 mm, in order to obtain similar efficiency.

Resonant energy transfer systems with rectangular spiral and circular spiral inductors for wireless charging electrical devices has been analyzed firstly by employing FEM analysis and the findings are validated experimentally. Output voltage, current, power and the transfer efficiency are studied at different frequencies and distances between the primary coil and the secondary coil.

And then a novel analytical model for witricity has been presented, incorporating misalignment effects. FEM simulations and corresponding experiments for the magnetic field at the receiver with lateral and angular misalignments have been suggested. The analytical model introduced can be used to develop a design procedure for optimum power transfer in low power inductive links. By carefully designing and calibrating the system, a higher efficiency is likely to be achievable. It is the intention of this research to extend the model for the circular spiral coils.

New interlayers with high relative permittivity, produced by combined TiO_2 nano-powder and $(C_4H_6O_2)_x$ latex, is proposed next to design two novel resonant inductive magnetic coupling wireless chargers. The proposed T-witricity chargers have been analyzed by employing FEM analysis and the findings are validated experimentally. Operating resonant frequency, output voltage, current, power and the transfer efficiency are studied at different frequencies and distances between the primary coil and the secondary coil.

The measured results indicate that if the proposed chargers can be made to operate at the resonant frequency, which is much lower than that of the witricity model without TiO_2 combined interlayers, satisfactory performances can be realized.

There is a good chance that the proposed scheme can be further improved to result in strong coupling between the two coils for efficient energy transfer over non-trivial distances which are of paramount importance for implant devices in the medical field.

Three wireless devices based on the novel witricity technology have been proposed based on the study in the above chapters. The first one is cell phone charging Then the experiments have been carried out and the open circuit output voltages at different frequencies of the amplifier have been analyzed. The second one is a playground for rats' experiments. The three most common wireless approaches today are shown at the beginning. The simulation structure and the experiment model have been illustrated, respectively. Finally, we proposed a charger for implanted DBS power supply charging. We first did the simulation for coils with different copper tape arrangements to select the well matched one. Then a fabricated small “box” for the receiver has been designed and a head phantom has been constructed for the study of electrical energy delivery. Related figures have been presented to showcase its performance.

The final stage of the project involves the collection of results, report on the findings and dissemination of this knowledge to the outside world. The findings of this project, including the modeling, simulation of the implanted medical energy system, the design program of the transmitters and receivers, the construction and manufacturing of the devices, and the overall performance of the device. Details of the design have been made freely available to the industry.

6.2 Future Work

The witricity technology has solid theoretical support in physics and the basic concepts have been successfully proven for power transfer by both the literature and our preliminary experiments. We believe that turning this significant discovery in physics into a working witricity cell implanted within the biological body will have strong impact not only on the DBS device, but also on a variety of other implantable devices as well. However, the history of innovation has shown that the transformation from a new physical concept to an actual engineering system is not always straightforward. Therefore, in anticipation of engineering challenges, we have: 1) proposed two different designs with different structures to increase our chance of success; 2) planned finite element simulation to gain insights into the workings of the system and allow rapid design verification and modification, especially to study how to determain the optimal operating frequency; and 3) proposed both a physical model and an animal model to initiate an evaluation of the witricity approach in both the engineering and biological perspectives. We believe that these designs will provide enhanced insurance of the success of this project.

We will propose the next-stage research in the form of a competitive renewal or a supplemental support. The most important task during this period will be the study of data communication using a modified witricity system in order to provide a complete platform to support DBS devices, a variety of other medical implants, and body networks. We will approach the communication problem by using amplitude modulation of the resonant signal, on-off keying, and/or modifying the frequency tuning circuit described previously which will effectively modulate the Q-factor. The secondary task will be the construction of a working prototype of the new DBS device with complete functionalities of pulse generation, system control, and user interface. A more extensive animal study will be carried out involving both acute and chronic tests on a larger number of animals. We will also seek an industrial partner (e.g., through a joint adventure or technology transfer) who will actively bring the results of this research to the market place.

The two witricity cell designs (thin-film horizontal design and vertically layered design) will both be evaluated further. During the procedure to switch between the two designs, we will carefully reopen the surgical site and replace the neural implant with a different design. Then, we will repeat the above measurement procedures. In each live pig experiment, we will perform measurements twice for each design, following the 1st-2nd- 1st-2nd order.

The acquired data will be utilized to assess the energy transmission performance. The mean values and standard deviations of the transmitted energy, received energy, efficiency, and especially the copper loss will be tabulated, plotted and analyzed with respect to distances and orientation angles and compared between the two designs. The magnetic field measurements will be numerically interpolated and plotted. The deviation between the computed and measured results will be studied.

In addition to the evaluation of system performance in the engineering perspective, we will also study possible biological effects of witricity transmission on tissue. Although it is impossible to obtain any long-term effects using our acute experiments, we will, at this exploratory stage, look carefully any immediate effects of witricity on tissue. The tissue samples surrounding the implanted device will be visually and histologically inspected to determine if any changes or damages occurred when tissues were exposed to magnetic and electric fields. If necessary, more sophisticated biochemical analysis will be performed. The primary goal of this research is to prove the feasibility of using the witricity technology for recharging implanted devices, especially for the DBS devices.

We have been active in publishing the results of our research studies and findings. We will continue to do so with the technology developed in this proposed research. Our system designs, software programs, and evaluation results will be shared among research community.

APPENDICE I: Cell phone charging

I have completed this part with Mr. Cheung Tsz Kit. Because of the lower power rate, we redesigned the amplifier for this specific experiment, not using the one as described before.

Appendice I -1. Design of Mid-high Frequency Amplifier

The specification of our amplifier is as following: the input voltage is 2.0Vp-p, the expected output is above 8 Vp-p, the output power is about 3 W, and the frequency response is 0.5 MHz – 4.5 MHz.

For many video amplifiers, it is often used LM7805 as the positive voltage regulator. Its maximum voltage is 5V, so it is possible to increase the output voltage and output power by replacing another positive voltage regulator with higher output voltage. Thus, LM7818 was chosen, it is also a positive voltage regulator but with a higher output voltage of 18V. The corresponding supply voltage circuit was illustrated in Fig. Appendice I -1.

In order to increase the range of frequency response of the amplifier, both transistors have to support a high frequency. The commonly use transistor for video amplifier is BC545, which the waveform will saturate and distorted when the frequency is higher than 4.5 MHz. Thus, transistor BC545 was replaced by C945. C945 can support a much higher frequency up to 30MHz. Then the following power amplifier was built, which is shown in Figs. Appendice I -2, Appendice I -3 and Appendice I -4.

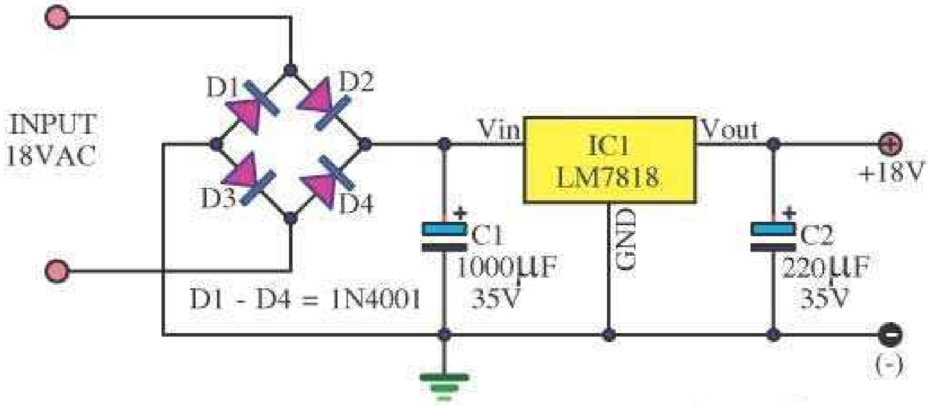

Fig. Appendice I -1 Supply voltage circuit

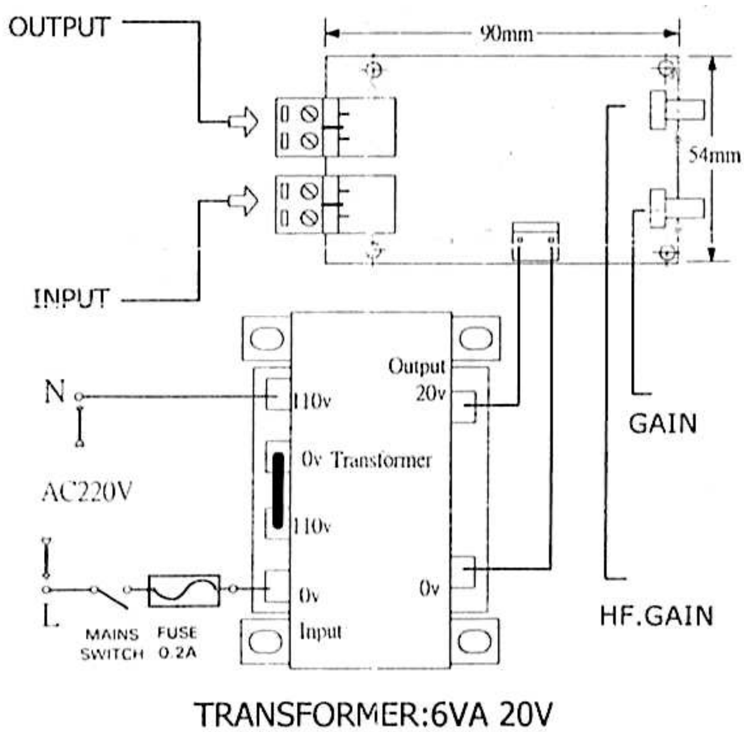

Fig. Appendice I -2 The circuit of the designed amplifier

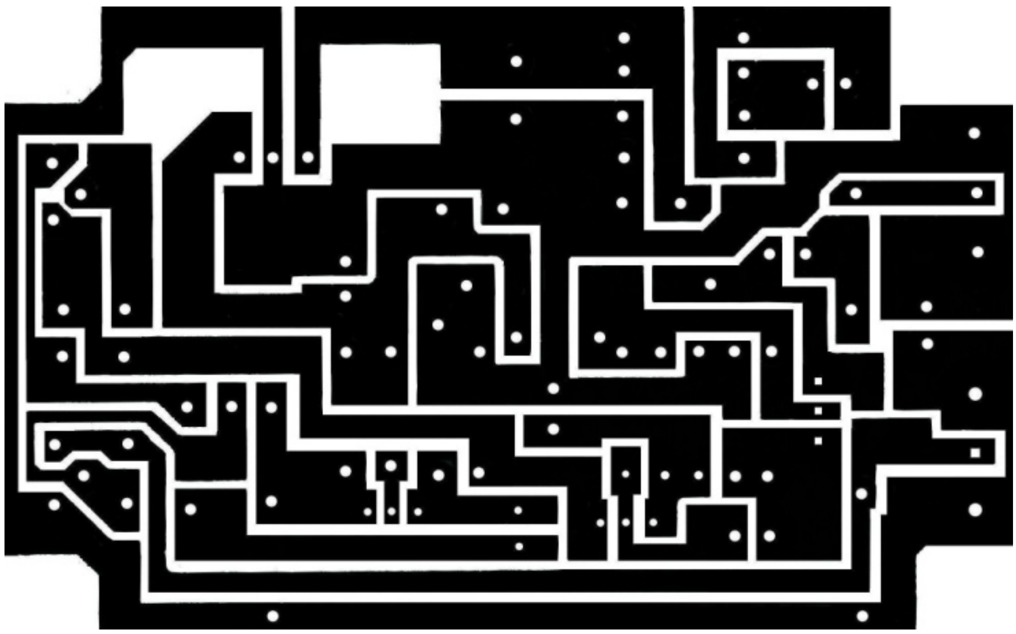

Fig. Appendice I -3 The PCB circuit of the designed amplifier

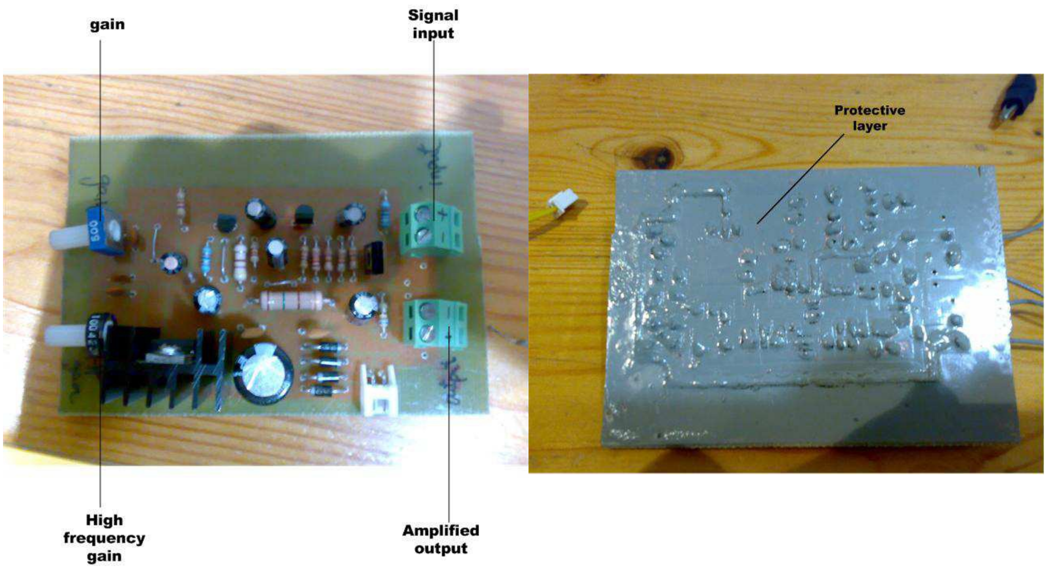

Fig. Appendice I -4 Photos of the designed amplifier

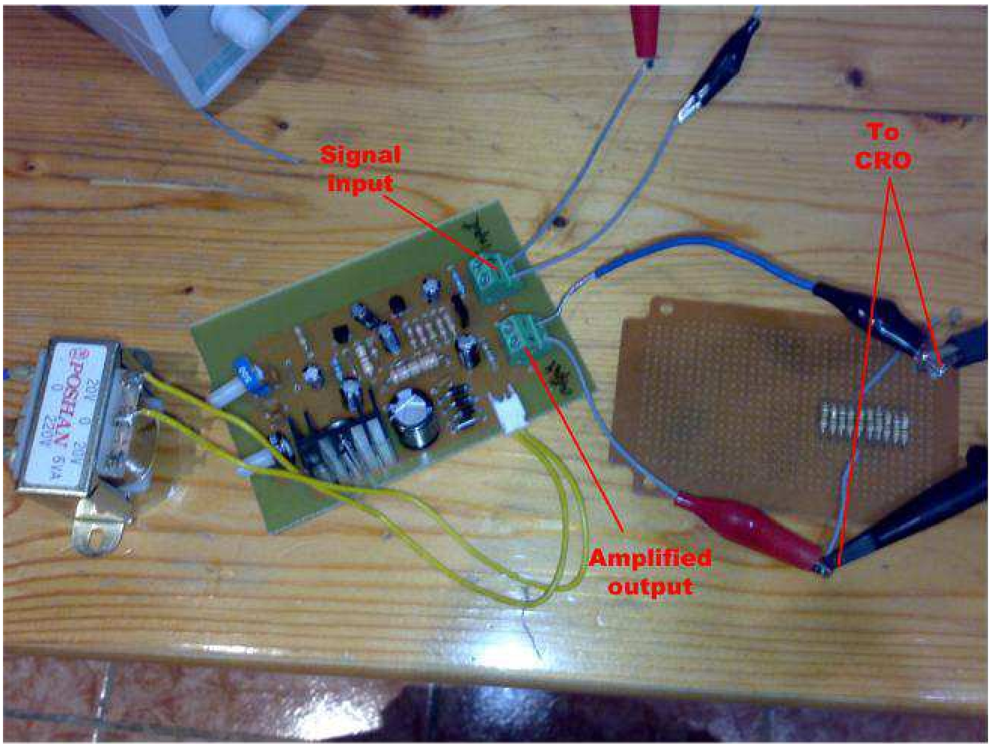

Fig. Appendice I -5 Experimental setup for measuring voltage across 0.1Ω resistor at 4 MHz

Fig. Appendice I -5 is the experimental setup for measuring voltage at 5MHz across a 0.1Ω resistor. The measured voltage is 0.773Vrms, so the output power is 5.98W.

The following Fig. Appendice I -6 shows different open circuit output voltages with 5 Vp-p input at different frequencies from 500 kHz to 5 MHz. It is found that when the frequency reaches over 1.5 MHz, the output waveform has a little distortion. Furthermore, once the input is over 3 Vp-p, the voltage of the output signal is no longer amplified. This shows that the maximum input voltage is around 3 Vp-p.

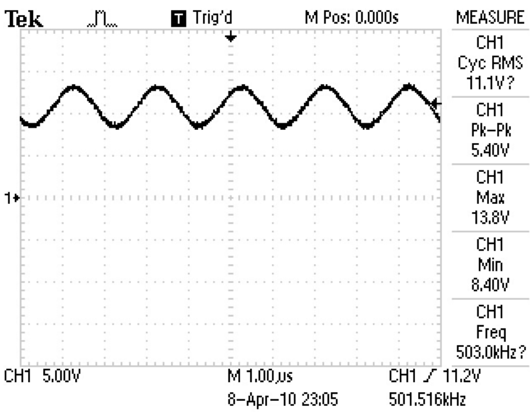
Tek
Trig'd
M Pos: 0.000s
MEASURE
CH1 Cyc RMS 11.1V?
CH1 Pk-Pk 5.40V
CH1 Max 13.8V
CH1 Min 8.40V
CH1 Freq 503.0kHz?
CH1 5.00V
M 1.00µs
CH1 ⁄ 11.2V
8-Apr-10 23:05
501.516kHz

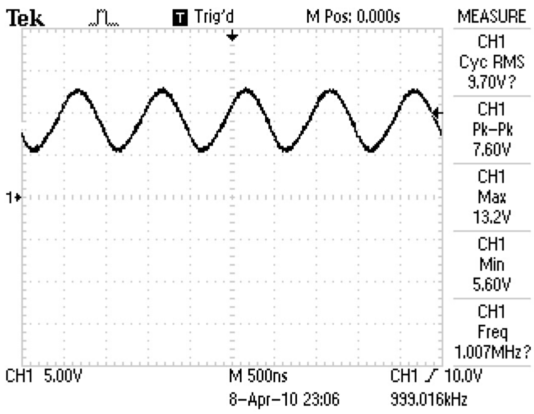
Tek
Trig'd
M Pos: 0.000s
MEASURE
CH1 Cyc RMS 9.70V?
CH1 Pk-Pk 7.60V
CH1 Max 13.2V
CH1 Min 5.60V
CH1 Freq 1.007MHz?
CH1 5.00V
M 500ns
CH1 ⁄ 10.0V
8-Apr-10 23:06
999.016kHz

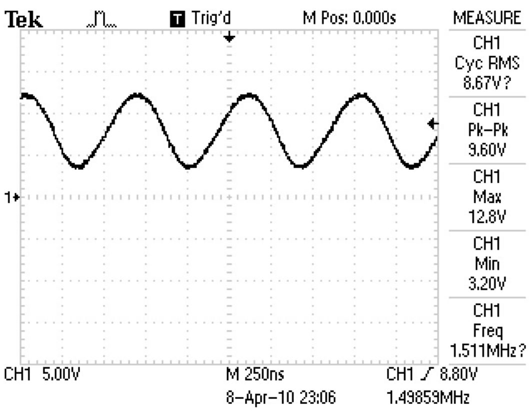
Tek
Trig'd
M Pos: 0.000s
MEASURE
CH1 Cyc RMS 8.67V?
CH1 Pk-Pk 9.60V
CH1 Max 12.8V
CH1 Min 3.20V
CH1 Freq 1.511MHz?
CH1 5.00V
M 250ns
CH1 ⁄ 8.80V
8-Apr-10 23:06
1.49859MHz

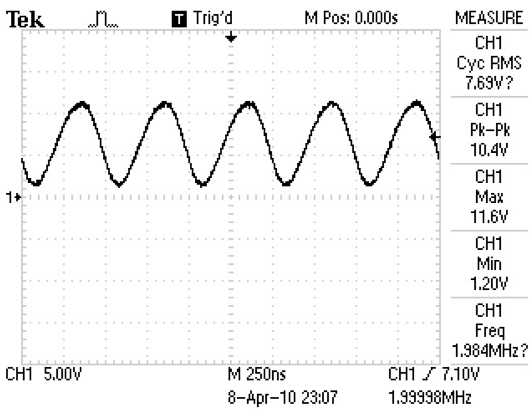
Tek
Trig'd
M Pos: 0.000s
MEASURE
CH1 Cyc RMS 7.69V?
CH1 Pk-Pk 10.4V
CH1 Max 11.6V
CH1 Min 1.20V
CH1 Freq 1.984MHz?
CH1 5.00V
M 250ns
CH1 ⁄ 7.10V
8-Apr-10 23:07
1.99998MHz

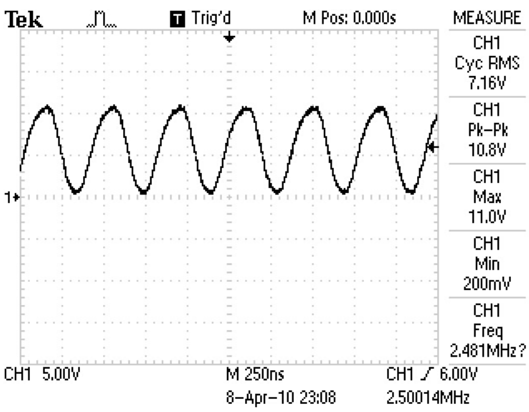
Tek
Trig'd
M Pos: 0.000s
MEASURE
CH1 Cyc RMS 7.16V?
CH1 Pk-Pk 10.8V
CH1 Max 11.0V
CH1 Min 200mV
CH1 Freq 2.481MHz?
CH1 5.00V
M 250ns
CH1 ⁄ 6.00V
8-Apr-10 23:08
2.50014MHz

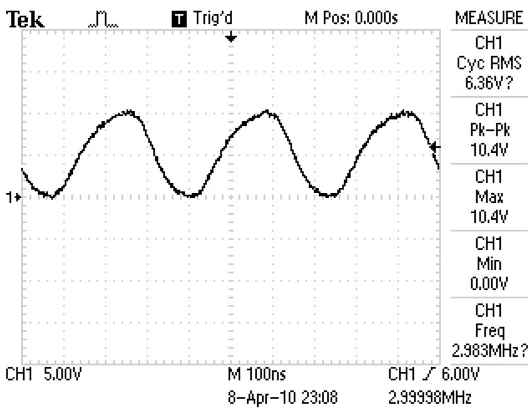
Tek
Trig'd
M Pos: 0.000s
MEASURE
CH1 Cyc RMS 6.36V?
CH1 Pk-Pk 10.4V
CH1 Max 10.4V
CH1 Min 0.00V
CH1 Freq 2.983MHz?
CH1 5.00V
M 100ns
CH1 ⁄ 6.00V
8-Apr-10 23:08
2.99998MHz

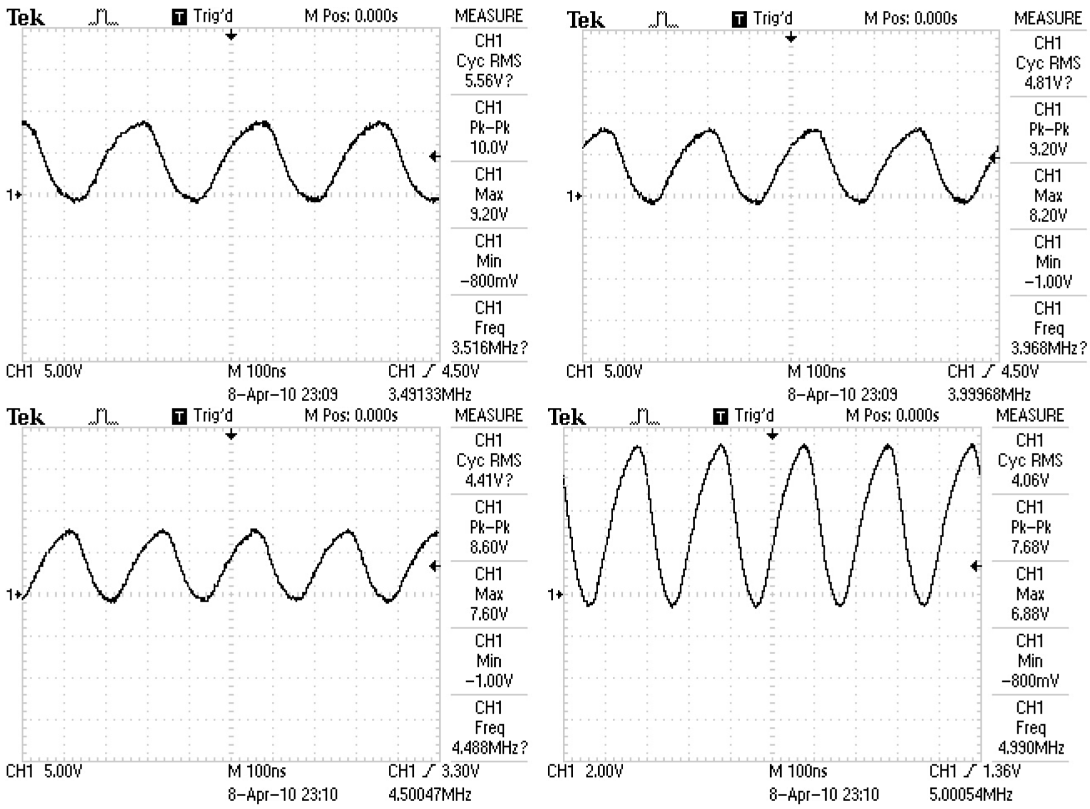

Fig. Appendice I -6 Output open circuit output voltages with 5 Vp-p input

The resonant frequency for both transmitter and receiver is 5.5 MHz, so the following experiments will mainly operating at 4-6 MHz. In addition, as the ultimate goal of the project is to develop implant medical devices, so the separating distance is critical. Thus, the following experiments will also mainly focus on the performance of the system with 5-7 cm separating distance.

Appendice I -2. Charging the Cell Phone

The following Fig. Appendice I -7 shows the experimental setup of the device to charge the cell phone.

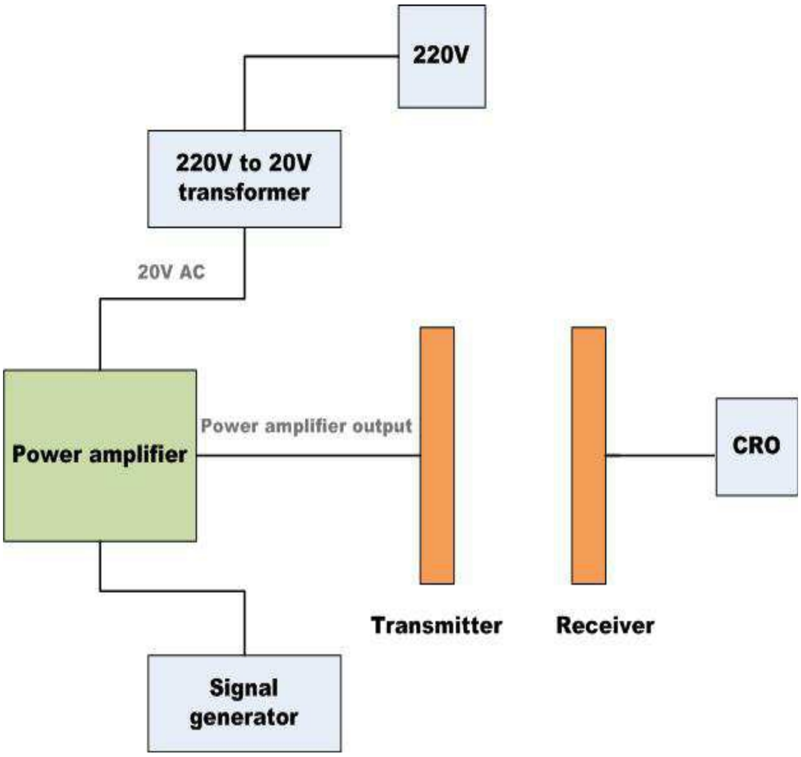

Fig. Appendice I -7 The flow chart of the experimental setup

Then we did measurements to obtain the output waveform at the receiver side at different distance for verification. The results' figures with different distances are shown in Fig. Appendice I -8.

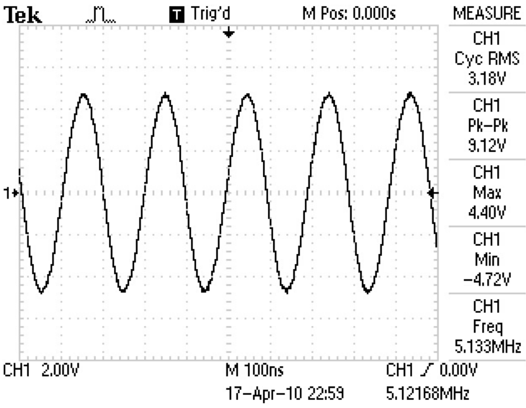

(a) at distance of 4 cm

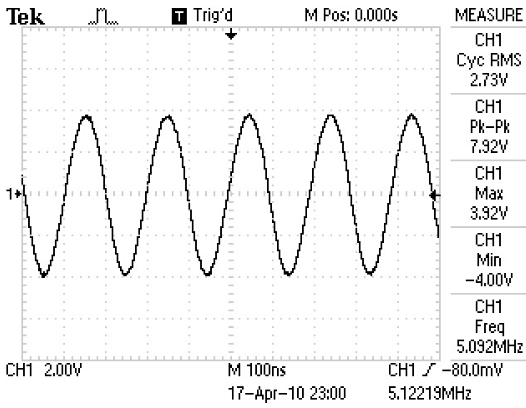

(b) at distance of 5 cm

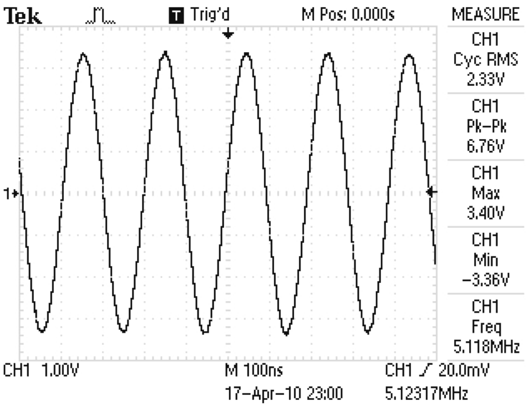

(c) at distance of 6 cm

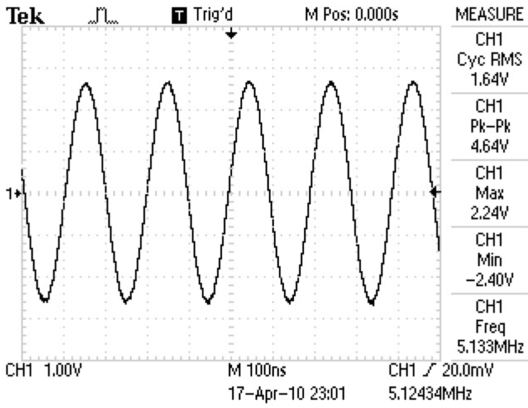

(d) at distance of 7 cm

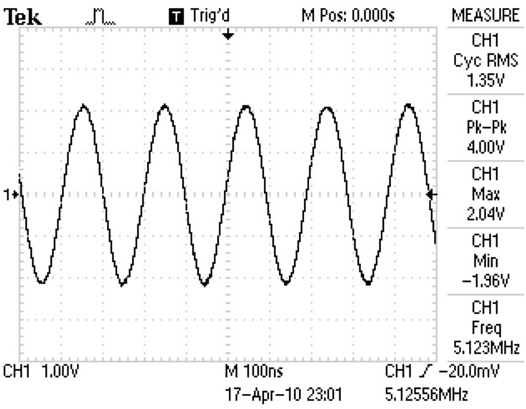

(e) at distance of 8 cm

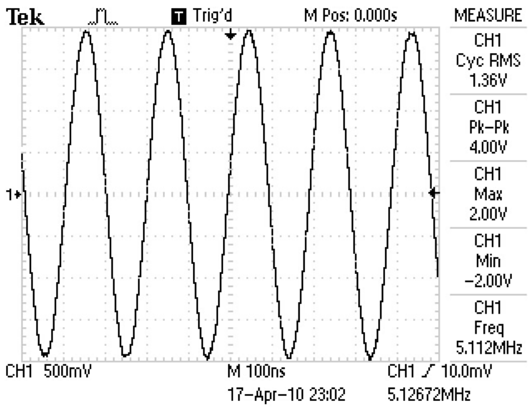

(f) at distance of 9 cm

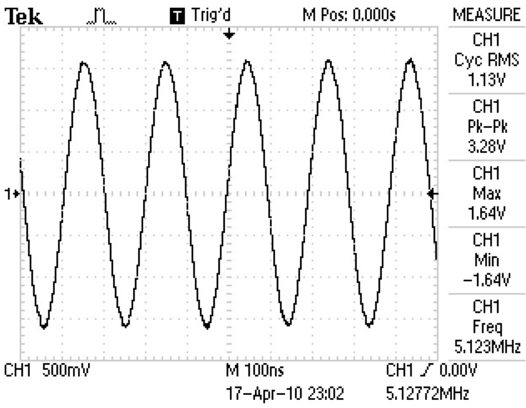

(g) at distance of 10 cm

Fig. Appendice I -8.Output voltages with different distances

It is clear that as the separating distance of transmitter and the receiver increases, the output voltage at the receiver side decreases significantly.

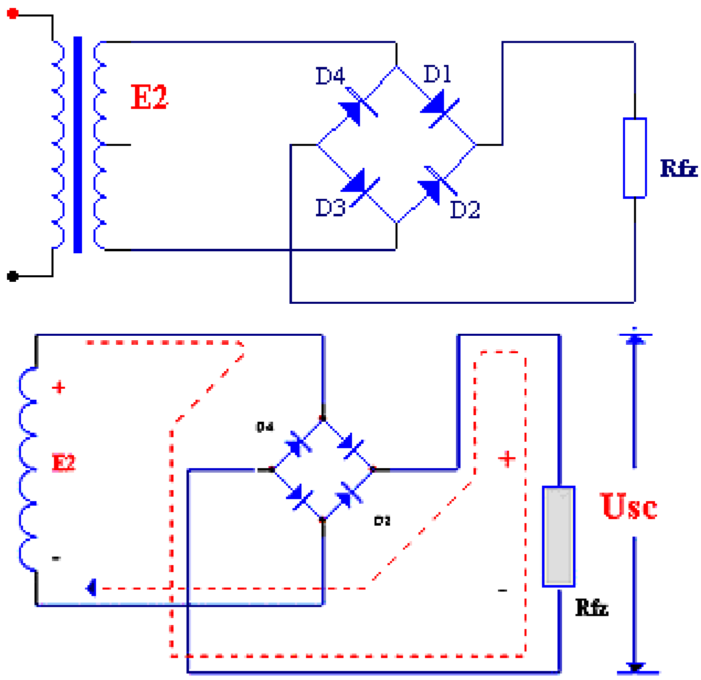

Fig. Appendice I -9 Full bridge rectifier for measuring the output voltages

Fig. Appendice I -9 shows the full bridge rectifier for measuring the receiver's output power. Requirements for charging the cell phone battery and the outputs of the designed device are shown in Table Appendice I -I.

TABLE APPENDICE I -I COMPARISON BETWEEN THE STANDARD REQUIREMENTS AND THE OUTPUTS OF OUR CHARGER

	Requirements	Outputs	Comments
Input voltage	4.2V	5V	Can satisfy the requirements.
Input current	350-450mA	0.45A – 0.5A	Can satisfy the requirements.

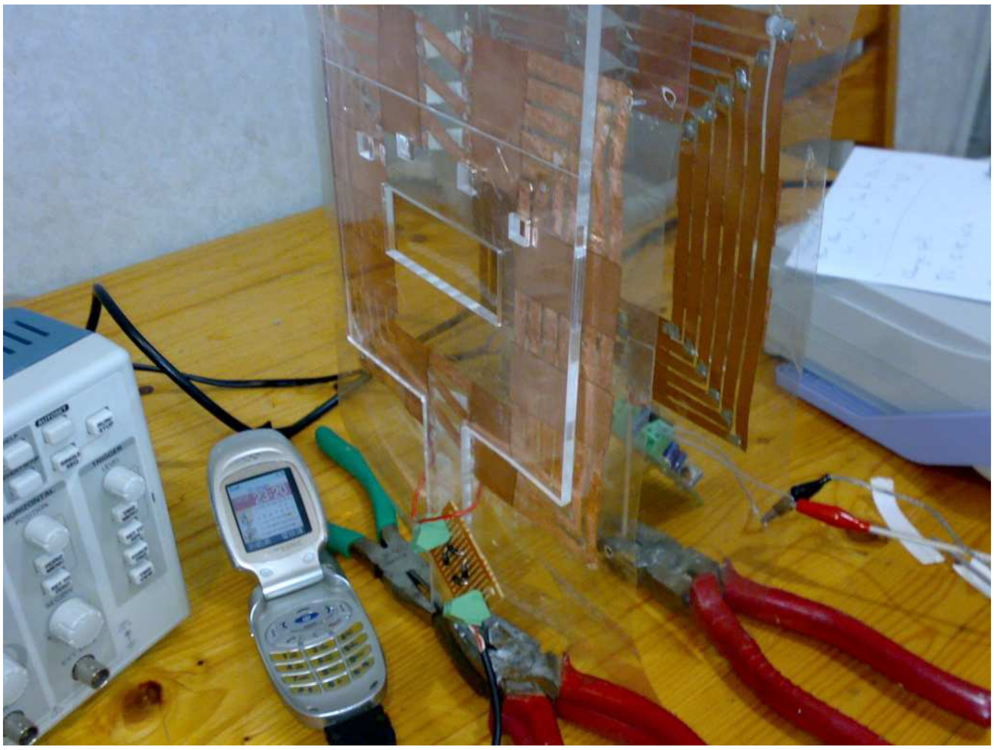

First step: Setup for charging a cell phone

Second step: Start to charge the cell phone

Third step: After 16 minutes, the phone has been charged to additional grid

Fig. Appendice I -10 Cell phone charging process

TABLE APPENDICE I -II. EXPERIMENTS FOR MEASURING THE OUTPUT POWER AND THE EFFICIENCY

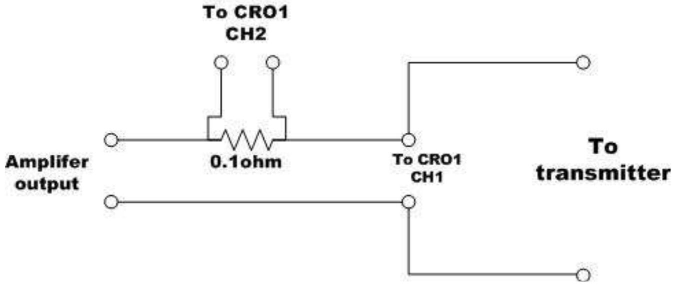 	$V_{0.1\Omega}$	67mV
	$I_{0.1\Omega rms}$	0.67A
	V_{CH1rms}	13V
	S	8.71VA
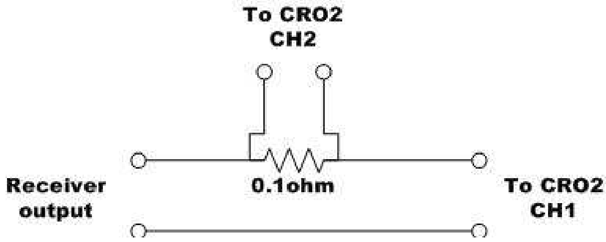 	$V_{0.1\Omega rms}$	47mV
	$I_{0.1\Omega rms}$	0.47A
	V_{CH1rms}	10V
	S	4.7VA
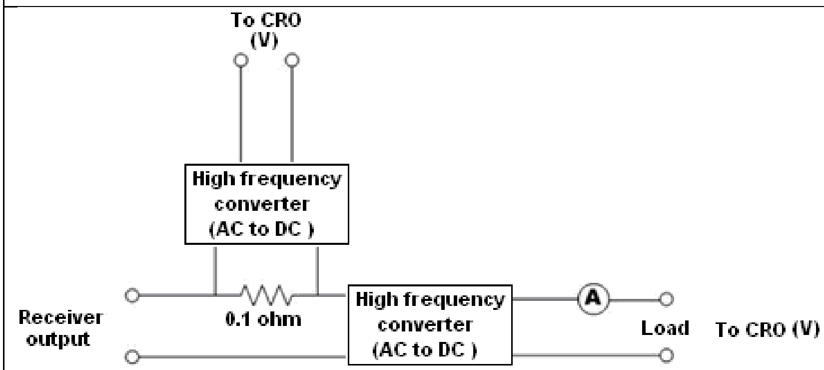 	V_{DC}	9V
	V_{CRO}	30mV
	I_{DC}	0.3A
	P	2.7W

$\textbf{Efficiency} = \frac{S_{output} \cdot \cos\varphi_R}{S_{input} \cdot \cos\varphi_T} \times \mathbf{100\%} = \frac{\mathbf{4.7}}{\mathbf{8.71}} \times \mathbf{100\%} = \mathbf{53.96\%}$, because we used resistors as the load to measure the circuit, $\varphi_R \approx \varphi_T$.

Cell phone was charged successfully. At 1-5 cm, the transmission system was able to charge the cell phone. The output power and efficiency should be further investigated, and which will be done in the following experiments shown in Table Appendice I -II.

In order to find out the efficiency of the transmission system, we have measured the input voltage, input current, output voltage and output current at distance of 5cm, and then do corresponding calculations.

APPENDICE II: Playground For Rats Experiments

Animal experiments can be employed to test a wide range of stimulation protocols, to identify effective interventions, and to study the basic biological mechanisms of the cellular and tissue response to various protocols. Animal studies in parallel with clinical studies enhance overall understanding of the medical devices for human beings. In this part, we proposed a playground for rats experiments based on the novel witricity technology.

The promising way to satisfy the requirements of implanted medical devices is the wireless charging technology which has the potential of unifying the charging protocol for a wide range of portable electronic products. There are three main approaches today as described below, and shown in Figs. Appendice II-1 (a), (b) and (c) [84].

Fig. Appendice II-1 (a) presents a standard fixed-positioning method that has been applied to some existing electric products such as electric tooth brushes. The loads must be set to a fixed location, and features 'fixed-positioning' charging. The mutual coupling and energy transfer efficiency will be very low if the load or the receiver is not fixed directly above the primary coil. So it is essential to make sure that the primary coil and the secondary coil are directly overlapped for maximum mutual coupling.

Fig. Appendice II-1 (b) shows a one-to-one charging method with a mechanically movable primary coil. This approach needs a component to search the secondary coils and tell the device to move the primary coil in order to ensure it underneath the charging surface. Though a device can be placed anywhere on the charging surface, it is quite similar to the 'fixed-positioning' approach as described. The control and the feedback for the primary coil will be very complex and costly for multiple-load charging.

For the system illustrated in Fig. Appendice II-1 (c), we can place one or more portable electronic devices on the charging surface regardless of their positions and orientations. The device can utilize the entire charging surface for energy transfer and it is no need to consider the orientation of the receiver coils. But that method requires much more complicated structure and control topology, which increase the design difficulty and the whole cost [84].

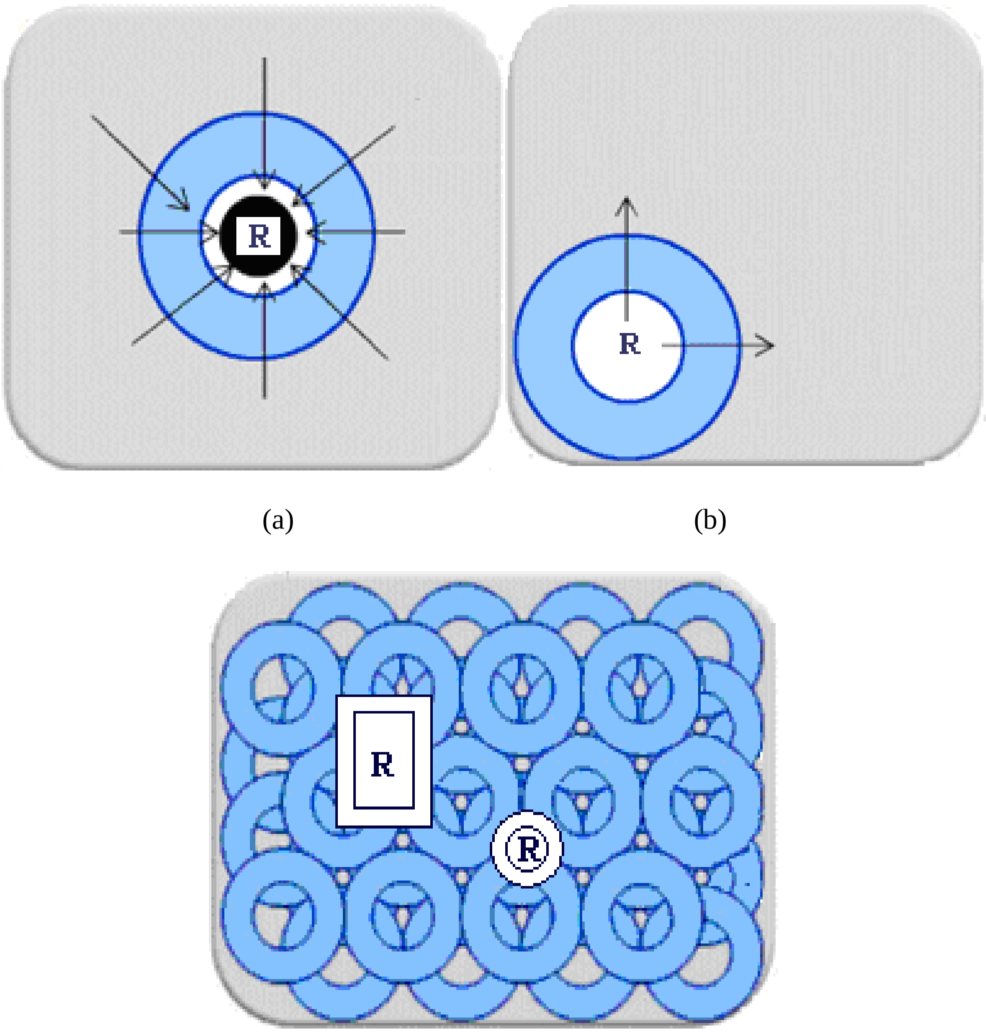

(a) (b)

(c)

Fig. Appendice II-1 Three main approaches for charging portable electronic products [84]

Compared with the traditional magnetic coupling inductive systems discussed above, a witricity transfer based on magnetic resonance wireless transmission technology can attain the strong magnetic coupling between the two resonators regardless of arrangement of the two coils. A simple but efficient structure has been proposed with witricity techonology for rats' experiments, which is shown in Fig. Appendice II-2. The out diameter of the seven-coil transmitter is 30 cm. And the receiver's maximum out diameter is 2.2 cm

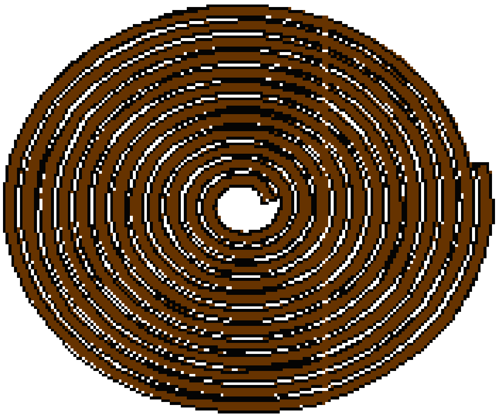

(a) One single coil for transmitter;

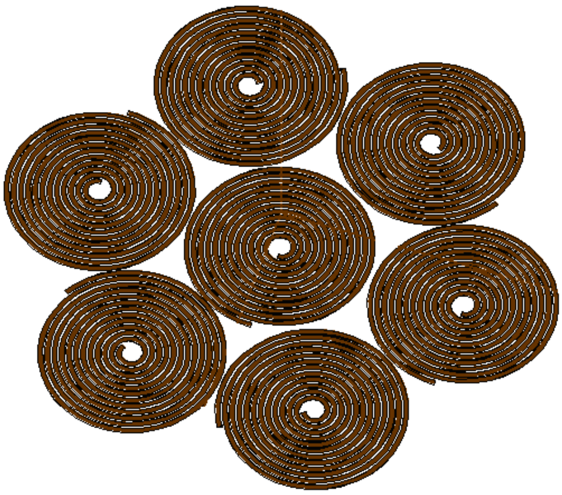

(b) The structure with seven coils for transmitter.

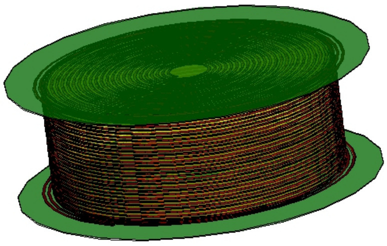

(c) The small “box” acting as a receiver

Fig. Appendice II-2 Simulation structure of the proposed charging platform

And the experiment structure of the proposed platform has been shown in Fig. Appendice II-3. It has the exact same dimension with the simulation model. Based on the models we designed, corresponding simulations and the experiments have been carried out to verify the operation of the platform and to study the witricity system’s performance.

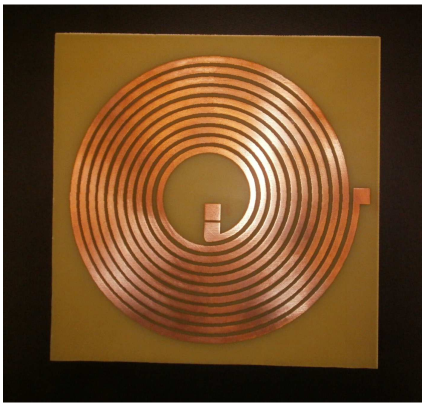

(a) One single coil (b) The structure with seven coils

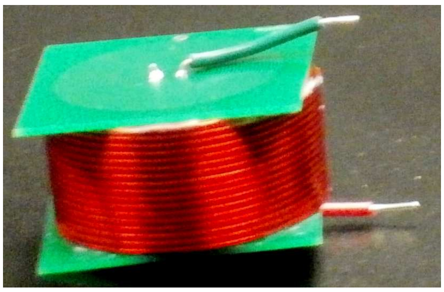

(c) The receiver box

Fig. Appendice II-3 Experiment structure of the proposed charging platform

Fig. Appendice II-3 (c) shows the receiver, which is much smaller than the transmitter's coil but with the same resonant frequency. The standing wave ratio (SWR) has been presented in Figs. Appendice II-4 (a) and (b). Through the figures we can find the resonant frequency of the proposed transmitter platform and also that of the whole system with the receiver.

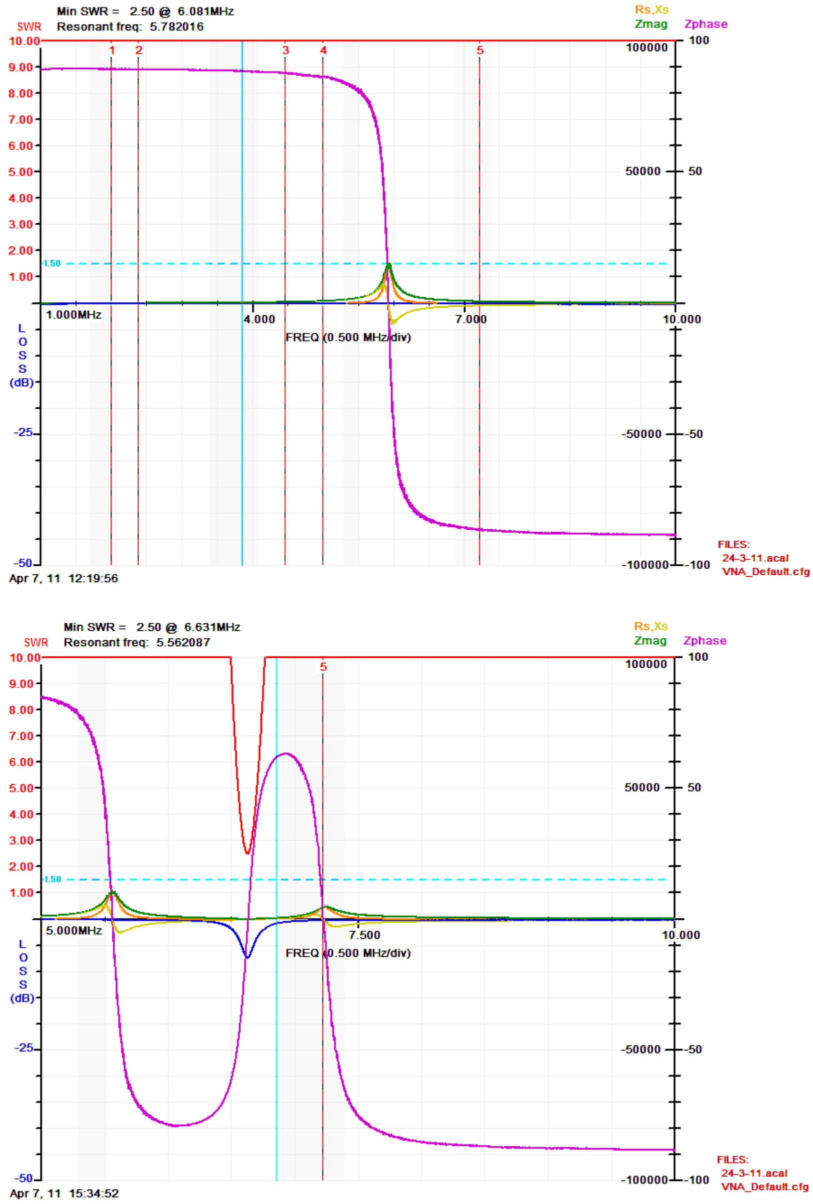

Figs. Appendice II-4 The standing wave ratio (SWR) for the platform

The system efficiency has been shown in Fig. Appendice II-5 at 3 MHz, 5.56 MHz, 5.50 MHz and 8 MHz with different distances. We can see the efficiency reaches the highest value at the resonant frequency 5.56 MHz and even near to this frequency, at 5.50 MHz, the efficiency is relatively higher compared with the other two non-resonance conditions.

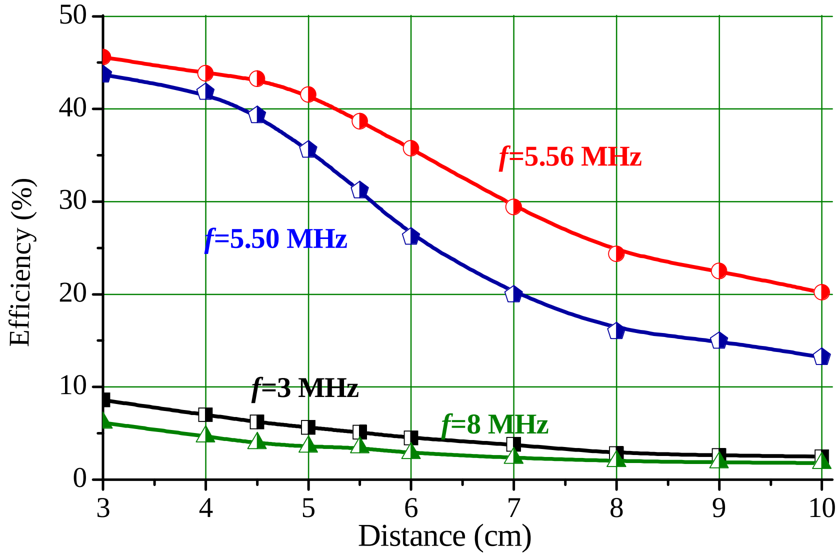

Fig. Appendice II-5 The system efficiency at 3 MHz, 5.56 MHz, 5.50 MHz and 8 MHz with different distances

REFERENCES

[1] A. Esser and H. Skudelny, "A new approach to power supplies for robots," *IEEE Trans. Ind. Applicat.*, vol. 27, pp. 872-875, 1991.

[2] K. W. Klontz, D. M. Divan et al, "Contactless power delivery system for mining applications," *IEEE Trans. Ind. Applicat.*, vol. 31, no. 1, pp. 27-35, 1995.

[3] G. Elliott, J. Boys, and A. Green, "Magnetically coupled systems for power transfer to electric vehicles," *Proceedings of 1995 International Conference on Power Electronics and Drive Systems*, vol. 2, pp. 797-801, 1995.

[4] T. B. John, "Inductive power pick-up coils," U. S. Patent, 5, 528, 113, Jun 1996.

[5] J. Hirai, T. W. Kim, A. Kawamura, "Wireless transmission of power and information and information for cableless linear motor drive," *IEEE Trans. Power Electron*, vol. 15, pp. 21-27, 2000.

[6] Y. Wu, L. G. Yan, S. G. Xu et al, "Transmission performance analysis of new non-contact power transmission system," *Electrical power of new technologies*, vol. 22, no. 4, pp. 10-13, 2003.

[7] A. Kurs, A. Karalis, R. Moffatt, J. D. Joannopoulos, P. Fisher, and M. Soljacic, "Wireless power transfer via strongly coupled magnetic resonances," *Science*, vol. 317, pp. 83-86, July 2007.

[8] A. Karalis, J. D. Joannopoulos, M. Soljacic, “Efficient Wireless Non-radiative Mid-range Energy Transfer,” *Annals of Physics,* vol. 323, pp. 34-48, January 2008.

[9] Barnes, Jr., Arnold A. Berthel, Robert O. “A survey of laser lightning rod techniques,” http://handle.dtic.mil/100.2/ADA239988.

[10] “What is LIPC? ,” Ionatron directed-energy weapons.

[11] “Frequently Asked Questions,” HSV Technologies.

[12] Peter A. Schlesinger, (President, HSV Technologies, Inc.), “Vehicle disabling weapon,” http://www.dtic.mil/ndia/nld4/schles.pdf, March 2000.

[13] Nikola Tesla, “The transmission of electrical energy without eires,” *Electrical World and Engineer*, 21st Century Books, March 1904.

[14] Leland I. Anderson, “Nikola Tesla on his work with alternating currents and their application to wireless telegraphy, telephony and transmission of power”, *Twenty Century Books,* pp. 129-130, 1992.

[15] “In-1825-William-Sturgeon-Invented-the-Electromagnet-A,” http://www.scribd.com.

[16] R. Schmitt, “Electromagnetics explained: A handbook for wireless/RF, EMC, and high-speed electronics,” *EDN Series for Design Engineers,* The Netherlands: Newnes, 2002.

[17] L. Collins, “Cut the cord,” *Electron. Syst. Softw.*, vol. 5, no. 6, pp. 42–46, Jan.–Dec. 2007.

[18] J. J. Casanova, Z. N. Low, J. Lin, and R. Tseng, “Transmitting coil achieving uniform magnetic field distribution for planar wireless power transfer system,” *Proc. IEEE Radio Wireless Symp.*, Jan. 18–22, 2009, pp. 530–533.

[19] Y. Jang and M. M. Jovanovic, “A contactless electrical energy transmission system for portable-telephone battery chargers,” *IEEE Trans. Ind. Electron.*, vol. 50, no. 3, pp. 520–527, Jun. 2003.

[20] C. Wang, G. A. Covic, and O. H. Stielau, “Power transfer capability and bifurcation phenomena of loosely coupled inductive power transfer systems,” *IEEE Trans. Ind. Electron.*, vol. 51, no. 1, pp. 148–157, Feb. 2004.

[21] H. Abe, H. Sakamoto, and K. Harada, “A non-contact charger using a resonant converter with parallel capacitor of the secondary coil,” *Proc. IEEE Appl. Power Electron. Conf. Expo.*, Feb. 15–19, 1998, vol. 1, pp. 136–141.

[22] C. Wang, O. Stielau, and G. A. Covic, “Design considerations for a contactless electric vehicle battery charger,” *IEEE Trans. Ind. Electron.*, vol. 52, no. 5, pp. 1308–1314, Oct. 2005.

[23] U. Joe and M. Hgovanloo, “Design and optimization of printed spiral coils for efficient transcutaneous inductive power transmission,” *IEEE Trans. Biomed. Circuits Syst.*, vol. 1, no. 3, pp. 193–202, Sep. 2007.

[24] Dell Latitude 2600, http://en.wikipedia.org/wiki/Inductive_charging.

[25] M. Soljacic, "Wireless Non-Radiative Energy Transfer," presentation archived at the website of American Institute of Physics, http://www.aip.org/ca/2006/soljacic.pdf.

[26] A. Karalis, J.D. Joannopoulos, and M. Soljacic, "Efficient wireless non-radiative mid-range energy transfer," *Annals of Physics*, vol. 323, pp. 34-48, Jan. 2008.

[27] C. E. Greene, D. W. Harrist, J. G. Shearer, M. Migliuolo, and G. W. Puschnigg, "Implementation of an RF power transmission and network," International Patent Application WO/2007/095267, Aug. 23, 2007.

[28] W. C. Brown, "The history of power transmission by radio waves," *IEEE Trans. Microw. Theory Tech.*, vol. MTT-32, no. 9, pp. 1230–1242, Sep. 1984.

[29] Komerath, N.M., Boechler N., Wanis S., "Space power grid-evolutionary approach to space solar power," *Proceedings of the ASCE Earth and Space 2006 conference*, League City, Texas, April 2006.

[30] "Electrical conductivity," http://en.wikipedia.org/wiki/Electrical_conductivity.

[31] Koen J. van Vlaenderen, "A generalization of classical electrodynamics for the prediction of scalar field effects," *Institute for Basic Research*, 2008.

[32] C. Monstein and J. P Wesley, "Observation of scalar longitudinal electrodynamic waves", *Europhysics Letters*, vol. 59, no. 4, pp. 514-520, 2002.

[33] Chubykalo, Andrew E., Rumen I. Tzontchev and Juan M. Rivera-Juárez, “Coulomb interaction does not spread instantaniously”, *Hadrionic Journal*, vol. 23, pp. 401-424, 2000.

[34] John T. Ratzlaff, “Solutions to Tesla's secrets and the Soviet Tesla weapons”, Tesla Book Co. (Millbrae, Calif), 1981.

[35] Tesla Nikola, “Art of transmitting electrical energy through the natural mediums,” Canadian Patent No. 142352, Filed Date: April 1906, Issued Date: August 1912.

[36] Henry Bradford and Gary Peterson, “Nikola Tesla on wireless energy transmission,” The Schumann Cavity Resonance Hypothesis.

[37] K. L. Corum, J. F. Corum, Ph.D., and J. F. X. Daum, Ph.D. “An analysis of Tesla's experimentally determined propagation model,” *Spherical Transmission Lines and Global Propagation,* 1996, p. 10.

[38] Gary L. Peterson, “Comparing the Hertz-wave and Tesla wireless systems,” Twenty-First Century Books, http://www.tfcbooks.com/articles/tws09.htm, May 2008.

[39] "How can an electric toothbrush recharge its batteries when there are no metal contacts between the toothbrush and the base?" (Commercial website). How Stuff Works, Inc., via howstuffworks.com. Retrieved on 2007-08-23.

[40] Brannon P. Wells, San Jose, “Series resonant inductive charging circuit,” U.S. patent 6972543, 2003.

[41] David Pogue, “Another Pre Innovation: The touchstone charging stand,” http://pogue.blogs.nytimes.com, June 2009.

[42] D.A.G. Pedder, A. D. Brown, and J. A. Skinner, “A contactless electrical energy transmission system,” *IEEE Trans. Ind. Elec.*, vol. 46, pp. 23-30, Feb. 1999.

[43] Roszyk L., Barnas L., “Hand held battery operated device and charging means therefore,” U. S. Patent 3, 840, 795, October 1974.

[44] Giuliani D, McMahon R, Engel D, “Pacing toothbrush,” U. S. Patent 5, 544 382, August 13, 1996.

[45] Hiroki Yomogita, “Non-contact charging system simultaneously charges multiple mobile devices,” http://techon.nikkeibp.co.jp/english/, November 2008.

[46] Boys J T, “Supply of power to primary conductors,” International Patent, WO 99/30402.

[47] John T B, “Inductive power pick-up coils,” U. S. Patent, 5, 528, 113, Jun 1996.

[48] Boys J T, “ Inductive power transfer across an extended gap,” International Patent, WO 98/50993.

[49] Elliott G A J, Boys J T, Green A W, “Magnetically coupled systems for power transformer to electric vehicles,” *IEEE Catalogue 95th*, pp: 797-801.

[50] WM7200, “Inductive charger owner’s manual. GM Advanced Technology Vehicles”, Torrance, California 90509-2923, 1-800-482-6644. 1998. p. 15.

[51] George Bellino, “GM pulls the plug on inductive charging: Letter from General Motors Advanced Technology Vehicles,” http://ev1-club.power.net/archive/020315/index.htm, March 15, 2002.

[52] Franklin Hadley, “MIT team experimentally demonstrates wireless power transfer, potentially useful for powering laptops, cell phones without cords,” *MIT News*, Massachusetts Institute of Technology, June 7, 2007.

[53] Davide Castelvecchi, “Wireless energy may power electronics: Dead cell phone inspired research innovation,” *TechTalk*, Massachusetts Institute of Technology, vol. 51, no. 9, November 2006.

[54] Scott Lowe, “Energizer induction charger for Wii preview,” http://gear.ign.com/articles, April 28, 2009.

[55] Miller, Paul, “Palm Pre's wireless charger, the Touchstone,” *Engadget*, Janunary 8, 2009.

[56] Chris Brandrick, “Wireless electricity specification nearing completion,” *PC World*, August 18, 2009.

[57] "TX40 and CX40, Ex-approved torch and charger". http://www.hernis.com.

[58] Charych Arthur (Setauket, NY), “System and method for wireless electrical power transmission”, Patent No. 6,798,716, September 28, 2004.

[59] Komadina, Ana Poljak, Dragan, “Analytical model of human body when exposed to high frequency EM fields,” *Software in Telecommunications and Computer Networks,* 2006. Sept. 29 2006-Oct. 1, pp. 32-36.

[60] A. Kurs, A. Karalis, R. Moffatt, J. D. Joannopoulos, P. Fisher, and M. Soljacic, “Wireless power transfer via strongly coupled magnetic resonances,” *Science*, vol. 317, July 2007, pp. 83-86.

[61] C.M. Collins, M.B. Smith, “RF fields induced during MRI in a heterogeneous human head model,” *Proceedings of the IEEE 24th Annual Northeast Bioengineering Conference,* 1998. 29- 31.

[62] O.E. Gouda, E.M.A. Zein, G.Amer, “Effect of high frequency electromagnetic fields on homogenous and inhomogeneous human head models,” *6th International Multi-Conference on Systems, Signals and Devices 2009*, pp. 1-5, 23-26 March 2009.

[63] R. W. P. King, “The electric field induced in human body when exposed to EM fields at 1 to 30 MHz range on shipboard,” *IEEE Trans. Biomed. Eng.,* vol. 46, June 1999.

[64] P. A. Starr, R. Turner, G. Rau, N. Lindsey, S. Heath, M. Volz, J. L. Ostrem and W. Marks, “Microelectrode-guided implantation of deep brain stimulators into

the globus pallidus internus for dystonia: techniques, electrode locations and outcomes," *J Neurosurg.*, 2006, 104:488-501.

[65] D. Kondziolka, D. Whiting, A. Germanwala, M. Oh, "Hardware-related complications after placement of thalamic deep brain stimulator systems," *Stereotact Funct Neurosurg.*, 2002, 79(3-4):228-33.

[66] M. Y. Oh, A. Abosch, S. H. Kim, A. E. Lang, A. M. Lozano, "Long-term hardware-related complications of deep brain stimulation," *Neurosurgery*, June 2002, 50(6):1268-1274.

[67] J. Volkmann, "Deep brain stimulation for the treatment of Parkinson's disease," *J Clin Neurophysiol.*, Jan-Feb 2004, 21(1):6-17.

[68] M. I. Hariz, "Complications of deep brain stimulation surgery," *Mov Disord.*, 2002, 17, Suppl. 3:S162-S166.

[69] C. Joint,D. Nandi, S. Parkin, R. Gregory, T. Aziz, "Hardware-related problems of deep brain stimulation," *Mov Disord.*, 2002, 17, Suppl. 3:S175-S180.

[70] J.D. Joannopoulos, A.Karalis, and M. Soljacic, "Wireless non-radiative energy transfer," US patent application No. 60/698,442.

[71] Frederick W. Grover, Inductance Calculations: Working Formulas and Tables, Dover Publications, Inc., New York, 1946.

[72] Department of Electrical Engineering, Magnetic circuits and transformers, The MIT Press, November, 1977.

[73] Nathan R. Grossner. Transformers for Electronic Circuits. McGraw-Hill, Inc. 1967.

[74] H. A. Haus and W.-P. Huang, "Coupled-mode theory," in *Proc. IEEE 79*, 1505-1518, 1991.

[75] H. A. Haus, W. P. Huang and A. W. Snyder, "Coupled-mode formulations," *Opt. Lett. 14*, 1222-1224, 1989.

[76] H. A. Haus, B. E. Little, M. A. Popović, S. T. Chu, M. R. Watts and C. Manolatou, "Optical resonators and filters," in Optical Microcavities, K. Vahala, ed. (World Scientific, Singapore, 2004).

[77] H. A. Haus, "Microwaves and Photonics," in OSA TOPS 23 Symposium on Electro-Optics: Present and Future, H.A. Haus, ed., (Optical Society of America, Washington, DC, 1998), pp. 2-8.

[78] M. J. Khan, C. Manolatou, S. Fan, P. R. Villeneuve, H. A. Haus and J. D. Joannopoulos, "Mode-coupling analysis of multipole symmetric resonant add/drop filters," *IEEE J. Quantum Electron.* 35, 1451-1460, 1999.

[79] Y. Wu, L. G. Yan, S. G. Xu et al, "Transmission performance analysis of new non-contact power transmission system," *Electrical power of new technologies*, vol. 22, no. 4, pp. 10-13, 2003.

[80] Kyriaki Fotopoulou and Brian W. Flynn, “Wireless powering of implanted sensors using RF inductive coupling, ” *IEEE Sensors 2006, EXCO*, Daegu Korea, pp. 765-768, Oct. 22-25, 2006.

[81] CERAM Research Ltd, Instruction Book, Jan 11, 2002.

[82] J. Okumu, D. Köhl, A. Sprafke, etc., “The role of energetic ion bombardment during growth of TiO_2 thin films by reactive sputtering,” *Appl. Phys. Lett.* 97, 112905 (2010).

[83] Yuanhao Wang, Hongxing Yang, and Lin Lu, “Three-dimensional double deck meshlike dye-sensitized solar cells,” *J. Appl. Phys.* 108, 064510 (2010).

[84] W. X. Zhong, X. Liu, S. Y. R. Hui, “A novel single-layer winding array and receiver coil structure for contactless battery charging systems with free-positioning and localized charging features, ” *IEEE Trans. Ind. Elec.*, vol. 58 (9), pp. 4136-4144, 2011.

[85] D. Kondziolka, D. Whiting, A. Germanwala, M. Oh, “Hardware-related complications after placement of thalamic deep brain stimulator systems,” *Stereotact Funct Neurosurg.*, 2002, 79(3-4), pp. 228-33.

[86] M. Y. Oh, A. Abosch, S. H. Kim, A. E. Lang, A. M. Lozano, “Long-term hardware-related complications of deep brain stimulation,” *Neurosurgery*, Jun 2002, 50(6), pp.1268-1274; discussion pp. 1274-1276.

[87] J. Volkmann, “Deep brain stimulation for the treatment of Parkinson’s disease,” *J. Clin. Neurophysiol.*, Jan-Feb 2004, 21(1), pp. 6-17.

[88] M. I. Hariz, “Complications of deep brain stimulation surgery,” *Mov. Disord.*, 2002, 17 Suppl 3:S162-S166.

[89] C. Joint,D. Nandi, S. Parkin, R. Gregory, T. Aziz, “Hardware-related problems of deep brain stimulation,” *Mov. Disord.*, 2002, 17 Suppl 3, pp. S175-S180.

[90] Bing Keong Li, Feng Liu, and Stuart Crozier, “High-field magnetic resonance imaging with reduced field/tissue RF artefacts—a modeling study using hybrid MoM/FEM and FDTD technique,” *IEEE Trans. EM Compatibility*, vol. 48, no. 4, November 2006, pp. 628-633.

[91] Komadina, Ana Poljak, Dragan, “Analytical model of human body when exposed to high frequency EM fields,” *Software in Telecommunications and Computer Networks, 2006.* Sept. 29 2006-Oct. 1, pp. 32-36.

[92] R. W. P. King, “The electric field induced in human body when exposed to EM fields at 1 to 30 MHz range on shipboard,” *IEEE Trans. Biomed. Eng.*, vol. 46, June 1999.

[93] Lidija Ololoska, Ljuben Janev and Suzana Loskovska, “A method for determination, analysis and visualization of high frequency EM field influence on human,” *Proceedings of the 3rd International Conference on Computational EMs and Its Applications*, 2004, pp. 442-445.

[94] Patrick Mason, "IEEE EMF health & safety standards," *Asian and Oceanian Regional EMF Scientific Meeting*, 2001.

[95] André Barka, "Assessment of spectral basis functions in BEM/FEM/GSM domain decomposition methods for scattering and radiation applications," *Proceedings of International Symposium on Antennas and Propagation Society*, 5-11 July 2008, pp. 1-4.

[96] E. L. Ginzton, Microwave Measurements. *New York: McGraw-Hill*, 1957. See Chapter 9.

[97] G. L. Matthaei, L. Young and E. M. T. Jones, Microwave Filters, Impedance-Matching Networks, and Coupling Structures. *New York: McGraw-Hill*, 1964. See Chapter 11.

[98] A. Podcameni, L. F. M. Conrado, and M. M. Russo, "Unloaded quality factor measurement for MIC dielectric resonator application," *Electronics Letters*, vol. 17, pp. 656-658, 1981.

[99] W. P. Wheless and D. Kajfez, "Microwave resonator circuit model from measured data fitting," *1986 IEEE MTT-S Symposium Digest*, pp. 681-684, Baltimore, June 1986.

[100] Wen H. Ko. Sheau P.Liang, and Cliff D. F. Fung, "Design of radio-freeuency powered coils for implant instruments," *Med. & Biol. Eng. & Comput.*, vol 15, pp. 634-640, 1977.

[101] Lar Rindorf, Lars Lading, and Olav Breinbjerg, “Resonant coupled antennas for passive sensors,” *IEEE Sensors 2008 Conference, 2008,* pp. 1611–1614.

[102] R.J. Smialowicz, “Immunologic effects of nonionizing electromagnetic radiation,” *IEEE Eng. Med. Biol.* 6 (1) (1987) 47–51.